A FINITE ELEMENT, NAVIER-STOKES STUDY OF THE CONFINED, LAMINAR FLOW OVER A DOWNSTREAM FACING STEP

by

Philip A. Treventi

Dissertation submitted to the Graduate Faculty of the
Virginia Polytechnic Institute and State University
in partial fulfillment of the requirements for the degree of
DOCTOR OF PHILOSOPHY
in
Mechanical Engineering

APPROVED:

F. J. Pierce, Chairman

W. C. Thomas

J. A. Burns

S. B. Thomason

H. P. Marshall

September 1984

Blacksburg, Virginia

ACKNOWLEDGEMENTS

I wish to express my gratitude to the members of my advisory committee: Professor F. J. Pierce, Chairman, and Professors, J. A. Burns, W. C. Thomas, S. B. Thomason and H. P. Marshall. Their advice and suggestions have been most helpful. I would also like to thank Dominique H. Pelletier of the Aerospace and Ocean Engineering Department, a fellow doctoral student, for the use of his mesh generator and the many enlightening conversations over the past few years.

TABLE OF CONTENTS

Page

ACKNOWLEDGMENTS ii

LIST OF FIGURES v

LIST OF TABLES ix

NOMENCLATURE x

1. INTRODUCTION 1

2. THE COMPUTATIONAL METHOD 4

2.1 Governing Equations 4

2.2 Derivation of the Weak Form 6

2.3 Boundary Conditions 13

2.4 Spatial Discretization and Matrix Formulation 14

2.5 Selection of the Basis Functions 22

2.6 Isoparametric Transformation 31

2.7 Evaluation of the Coefficient Matrices . . 36

2.8 Solution Method 43

2.8.1 Iterative Method 44

2.8.2 Matrix Inversion Procedure 50

3. RESULTS AND DISCUSSION 60

3.1 Analysis of the Downstream Facing Step Flow 63

3.2 Analysis of the Initial Plane of Experimental Data 95

TABLE OF CONTENTS (continued)

Page

3.2.1 Analysis of the Denham and Patrick Working Section 95

3.2.2 Analysis of an Alternative Working Section Design 101

3.2.3 Sensitivity Studies 130

3.2.3.1 Inlet Velocity Profile 130

3.2.3.2 Geometry of the Fairing 134

4. SUMMARY 146

REFERENCES 149

APPENDICES

A. Tabulated Results of the Analysis of the Denham and Patrick (7) Step 153

A.1 Results of the Analysis at Re = 73 (Run 201) 154

A.2 Results of the Analysis at Re = 125 (Run 301) 159

A.3 Results of the Analysis at Re = 191 (Run 302) 163

A.4 Results of the Analysis at Re = 229 (Run 303) 167

VITA 171

ABSTRACT

LIST OF FIGURES

Figure		Page
2.1	Local coordinate system and nodal point numbering scheme	27
2.2	Isoparametric coordinate transformation . . .	32
2.3	Typical structure of an assembled coefficient matrix	56
2.4	Compact storage modes for the coefficient matrix in Fig. 2.3	57
3.1	Denham and Patrick (7) step	64
3.2	Finite element mesh with 50 elements and 231 nodal points for run 101	67
3.3	Finite element mesh with 64 elements and 291 nodal points for run 102	68
3.4	Finite element mesh with 78 elements and 351 nodal points for run 103	69
3.5	Finite element mesh with 312 elements and 1325 nodal points for run 201	70
3.6	Velocity-vectors and comparison of experimental and computed (run 101) u-velocity profiles for Re = 73 with the mixed downstream boundary conditions applied at x/h = 8.	72
3.7	Velocity-vectors and comparison of experimental and computed (run 102) u-velocity profiles for Re = 73 with the mixed downstream boundary conditions applied at x/h = 12.0	73
3.8	Velocity-vector and comparison of experimental and computed (run 103) u-velocity profiles for Re = 73 with the mixed downstream boundary conditions applied at x/h = 16.0	74
3.9	Lines of constant pressure coefficient for run 101. Re = 73, with the mixed downstream boundary conditions applied at x/h = 8.0 . . .	77
3.10	Lines of constant pressure coefficient for run 102. Re = 73, with the mixed downstream boundary conditions applied at x/h = 12.0 . .	78

LIST OF FIGURES (continued)

Figure		Page
3.11	Lines of constant pressure coefficient for run 103. Re = 73, with the mixed downstream boundary conditions applied at x/h = 16.0 . .	79
3.12	Velocity-vectors and comparison of experimental and computed (run 201) u-velocity profiles for Re = 73 on the refined mesh (Fig. 3.5) with the outflow boundary conditions applied at x/h = 16.0	80
3.13	Computed (run 201) lines of constant pressure coefficient for Re = 73 on the refined mesh (Fig. 3.5) with 312 elements and 1325 nodal points	83
3.14	Finite element mesh with 411 elements and 1749 nodal points for runs 301-303	84
3.15	Velocity-vectors and comparison of experiments and computed (run 301) u-velocity profiles for Re = 125 on the mesh depicted in Fig. 3.14 . .	86
3.16	Velocity-vectors and comparison of experiments and computed (run 302) u-velocity profiles for Re = 191 on the mesh depicted in Fig. 3.14 . .	88
3.17	Velocity-vectors and comparison of experiments and computed (run 303) u-velocity profiles for Re = 229 on the mesh depicted in Fig. 3.14 . .	90
3.18	Computed (run 301) lines of constant pressure coefficient for the Re = 125 case	92
3.19	Computed (run 302) lines of constant pressure coefficient for the Re = 191 case	93
3.20	Computed (run 303) lines of constant pressure coefficient for the Re = 229 case	94
3.21	The Denham and Patrick (7) working section . .	96
3.22	Assumed inlet velocity profile for the analysis of the Denham and Patrick (7) working section (runs 401 through 404)	98

LIST OF FIGURES (continued)

Figure		Page
3.23	Finite element mesh with 326 elements and 1401 nodal points for the analysis of the Denham and Patrick (7) working section at Re = 73 (run 401)	99
3.24	Finite element mesh with 516 elements and 2199 nodal points for the analysis of the Denham and Patrick (7) working section at the higher Reynolds numbers (runs 402-404)	100
3.25	Velocity-vectors and computed (run 401) u-velocity profiles for the Denham and Patrick (7) working section at Re = 73	102
3.26	Velocity-vectors and computed (run 402) u-velocity profiles for the Denham and Patrick (7) working section at Re = 125	104
3.27	Velocity-vectors and computed (run 403) u-velocity profiles for the Denham and Patrick (7) working section at Re = 191	106
3.28	Velocity-vectors and computed (run 404) u-velo-city profiles for the Denham and Patrick (7) working section at Re = 229	108
3.29	Alterntive working section design	111
3.30	Finite element mesh with 551 elements and 2349 nodes used in the analysis of the alternative working section design at all Reynolds numbers (run 501-504)	112
3.31	Velocity-vectors and computed (run 501) u-velocity profiles for the alternative working section design at Re = 73	114
3.32	Velocity-vectors and computed (run 502) u-velocity profiles for the alternative working section design at Re = 125	117
3.33	Velocity-vectors and computed (run 503) u-velocity profiles for the alternative working section design at Re = 191	120

LIST OF FIGURES (continued)

Figure		Page
3.34	Velocity-vectors and computed (run 504) u-velocity profiles for the alternative working section design at Re = 229	123
3.35	Variation of separation length with Reynolds number	129
3.36	Alternative inlet profiles	132
3.37	Finite element mesh with 516 elements and 2199 nodal points for run 603	133
3.38	U-velocity profiles from run 601. Inlet mass flow shifted towards tunnel floor	135
3.39	U-velocity profiles from run 602. Inlet mass flow shifted towards top of tunnel	136
3.40	U-velocity profile from run 603. Thinner boundary layers at the inlet	137
3.41	Alternative transitions to the step	140
3.42	Finite element mesh with 516 elements and 2199 nodal points for run 701. Lengthened transition to the step	141
3.43	Finite element mesh with 516 elements and 2199 nodal points for run 702. Shortened transition to the step	142
3.44	U-velocity profiles from run 701. Effects of lenghtening the transition to the step	143
3.45	U-velocity profiles from run 702. Effects of shortening the transition to the step	144

LIST OF TABLES

Table		Page
2.1	Biquadratic Lagrange interpolating polynominals used to construct the velocity basis functions	26
2.2	Summary of Lagrangian element configurations considered	29
2.3	Sampling points and weights in the Gauss-Legendranumerical integration formulas	41
3.1	Summary of the cases run	61
3.2	Computed (run 103) v-velocity components at x/h = 8.0.	75
3.3	Comparison of the results of runs 103 and 201 at x/h = 5.0	82
3.4	Comparison of the results of the original (run 404) and modified (run 504) working section analyses at x/h = - 1.333	127
3.5	Comparison of the results of the orginial (run 404) and modified (run 504) working section analyses in the plane eight step-heights down-stream of the sudden expansion	128
3.6	Comparison of u-velocities from runs 404, 601, 602 and 603 at x/h = - 1.333	138
3.7	Comparison of computed u-velocity components from runs 404, 701 and 702 at x/h = - 1.333	145

NOMENCLATURE

Algebraic combinations of the symbols M(mass), L(length) and T(time) are used to indicate the units of the quantities defined below.

h	step height, L
M_i	pressure basis functions
N_i	velocity basis functions
P	dimensionless pressure coefficient, $(P^*-P_o^*) / \rho U_o^2$
P^*	pressure, $ML^{-1}T^2$
P_o^*	reference pressure, $ML^{-1}T^2$
Re	Reynolds number, $(\rho U_o h)/\mu$
u	dimensionless velocity component in the x-direction, u^*/U_o
u^*	velocity component in the x-direction, LT^{-1}
U_o	reference velocity, LT^{-1}
v	dimensionless velocity component in the y-direction, v^*/U_o
v^*	velocity component in the y-direction, LT^{-1}
x	dimensionless global coordinate, x^*/h
x^*	global coordinate, L
y	dimensionless global coordinate, y^*/h
y^*	global coordinate, L

Greek Symbols

μ	dimensionless absolute viscosity, μ^*/μ_o
μ^*	absolute viscosity, $ML^{-1}T^1$
μ_o	reference absolute viscosity, $ML^{-1}T^{-1}$
η	dimensionless local coordinate corresponding to x

ξ dimensionless local coordinate corresponding to y

ρ dimensionless density, ρ^*/ρ_o

ρ^* density, ML^{-3}

ρ_o reference density, ML^{-3}

1. INTRODUCTION

Great strides have been made in the past sixteen years in the application of the finite element method to problems in fluid mechanics. As noted by Shen (1), the first application appears to have been made by Martin (2), who in 1968 generated a rather crude solution of the potential flow over a circular cylinder. Today the literature abounds with reports of finite element solutions to fully viscous problems in both two and, more recently, three dimensions. This remarkable progress is due not only to the rapid evolutionary development of more efficient computational algorithms, but also to the large strides made by the computer industry.

One of the problems often solved to demonstrate the effectiveness of a given method of computation is the confined, laminar flow over a downstream facing step. This problem is chosen not only for its geometric simplicity and obvious practical value, but also because it provides a good test of the ability of a computational algorithm to track the growth of a free shear layer and resolve secondary flows.

Among those who have reported the results of finite element solutions to this problem are Bredif (3), Ecer (4) and Thomas (5). Bredif started with the stationary (time independent) Navier-Stokes equations written in stream function-vorticity form and generated weak or integral

forms using both conventional and unconventional (upwind) Galerkin methods. In each case the finite dimensional subspace of approximate solutions was generated by a set of basis functions constructed from biquadratic Lagrange interpolating functions. Ecer, on the other hand, used a variational formulation derived from a transformed, time-dependent vorticity transport equation, where the spatial variation of the independent variables was represented in terms of piecewise-bilinear Lagrange polynomials. Like Bredif, Thomas also experimented with the use of unconventional Galerkin weighting functions to artificially dampen oscillatory "solutions" at high Reynolds numbers. However, the variational form used by Thomas was expressed in terms of the primitive variables u, v and p, and utilized biquadratic and bilinear Lagrange interpolating functions to construct the velocity and pressure approximation subspaces, respectively.

The objective of the present effort was to investigate the laminar flow over a backward facing step using an alternative finite element method which, like the primitive variable formulation by Thomas (5), could be readily extended in the future to study three-dimensional flows, but which did not require the a priori infusion of artificial dissipation to admit solutions at high Reynolds numbers. To this end a scheme recommended by Fortin (6) based on its superior theoretical convergence properties

was utilized. Specifically, the computational algorithm is based upon a conventional Galerkin formulation in the primitive variables u, v and p, where the subspace of approximations to the velocity field consists of piecewise biquadratic Lagrange polynomials, and the pressure field is represented by a discontinuous, piecewise linear approximation. The details of the derivation of the weak or variational form, the introduction of the spatial discretization, and the procedures used to construct and solve the resulting set of nonlinear, algebraic equations are presented in the next chapter.

The results of the present computations are presented in Chapter 3, where they are also compared to both the prior calculations by Ecer (4) and Taylor (5), and to the experimental data obtained by Denham and Patrick (7). The results of a study to determine the causes and effects of the noticeable lack of development and skewness that characterized the Denham and Patrick data both at and upstream of the step are also reported in Chapter 3. The conclusions drawn from the results presented in Chapter 3 are summarized in Chapter 4.

2. THE COMPUTATIONAL METHOD

The purpose of this chapter is to present the derivation of the set of equations used to generate approximate solutions to the governing equations, and to discuss the method used to effect their solution.

2.1 Governing Equations

The system of equations which is presumed to govern the motion of a steady, constant property incompressible Newtonian fluid can be written in stress-divergence form as

$$\rho^* (\underline{u}^* \cdot \nabla^* \underline{u}^*) = \nabla^* \cdot \underline{\underline{\tau}}^* \qquad (2.1)$$

$$\nabla^* \cdot \underline{u}^* = 0 \qquad (2.2)$$

where the velocity vector $\underline{u}^* = (u^*, v^*)$ in two dimensions, and

$$\tau_{ij}^* = - P^* \delta_{ij} + \mu^* \left(\frac{\partial u_i^*}{\partial x_j^*} + \frac{\partial u_j^*}{\partial x_i^*} \right) \qquad (2.3)$$

is the symmetric stress tensor. The asterisk (*) are used to denote dimensional quantities.

In the discussions that follow, it is tacitly assumed that solutions to the above set of equations exist and are unique. These assumptions are not altogether unreasonable

however, as several rigorous proofs of these and other properties of equations (2.1) through (2.3) have been offered in recent years. For the details of these proofs and the underlying assumptions, refer to References 8 through 10.

To facilitate both the solution of the governing equations and the interpretation of the results, equations (2.1) through (2.3) are recast in a nondimensional form. This is done by dividing the dependent and independent variables in the equations by constant reference properties appropriate to the flow. The reference properties, and hence dimensionless variables, chosen in the present work are those suggested by White (11):

$$x_i = \frac{x_i^*}{L}$$

$$\underline{u} = \frac{\underline{u}^*}{U_o}$$

$$P = \frac{P^* - P_o^*}{\rho_o U_o^2} \qquad (2.4)$$

$$\rho = \frac{\rho^*}{\rho_o}$$

$$\mu = \frac{\mu^*}{\mu_o}$$

$$\nabla = L \nabla^* .$$

Substitution of these new variables into equations (2.1) through (2.3) and rearrangement of some of the terms yields the following set of nondimensional equations:

$$\rho(\underline{u} \cdot \nabla \underline{u}) = \nabla \cdot \underline{\underline{\tau}} \tag{2.5}$$

$$\nabla \cdot \underline{u} = 0 \tag{2.6}$$

$$\tau_{ij} = - P \delta_{ij} + \mu \left(\frac{1}{Re}\right) \left(\frac{\partial u_i}{\partial x_j} + \frac{\partial u_j}{\partial x_i}\right) \tag{2.7}$$

where the Reynolds number, Re, is defined as

$$Re = \frac{\rho_o u_o L}{\mu_o} . \tag{2.8}$$

The boundary data needed to complete the mathematical statement of the problem will be described in section 2.3.

2.2 Derivation of the Weak Form

In finite element analyses, the spatial discretization is carried out on a weak form of the governing equations. This is in contrast to finite difference methods where the approximations for the derivatives are substituted directly into the governing

equations. Loosely speaking, a "weak" form of an equation is a reformulation that is more "permissive" than the original equation. Weak forms, for example, typically admit solutions that do not satisfy the differentiability requirements of the original equation. They can also be constructed so that the requirements placed on the smoothness of the boundary and the boundary data to ensure unique solutions can be relaxed. These and other properties of weak (or variational) formulations are very useful from a practical standpoint, since they enlarge the class of data for which a given problem makes sense. Those motivated by physical rather than purely mathematical arguments should refer to the interesting discussion by Becker, Carey and Oden in Chapter 1 of Reference 12.

The weak form of the governing equations used in the present work is obtained using the standard Galerkin method for mixed problems (13, 14). In this method the motion equations are multiplied by any of the n velocity basis functions, N_i, that generate the n-dimensional space from which the velocity approximations are chosen, and then integrated over the domain Ω. Thus, equation 2.5 becomes:

$$\int_{\Omega} \rho \, (\underline{u} \cdot \nabla \underline{u}) N_i \, d\Omega = \int_{\Omega} (\nabla \cdot \underline{\underline{\tau}}) N_i \, d\Omega \, . \qquad (2.9)$$

An even weaker form of equation (2.5) can be obtained if it is recognized that the right hand side of equation (2.9) can be rewritten as

$$\int_{\Omega} (\nabla \cdot N_i \underline{\underline{\tau}}) d\Omega - \int_{\Omega} (\underline{\underline{\tau}} \cdot \nabla N_i) d\Omega , \qquad (2.10)$$

and that the divergence theorem can be applied to the first of these integrals to yield

$$\int_{\Omega} (\nabla \cdot \underline{\underline{\tau}}) N_i d\Omega = \int_{\Gamma} \hat{n} \cdot (N_i \underline{\underline{\tau}}) d\Gamma - \int_{\Omega} (\underline{\underline{\tau}} \cdot \nabla N_i) d\Omega, \qquad (2.11)$$

where Γ denotes the boundary of Ω and $\hat{n}$ is its outward directed unit normal. Finally, substitution of equation (2.11) into equation (2.9) yields the following weak form of equation (2.5) used in the present work:

$$\int_{\Omega} \rho(\underline{u} \cdot \nabla \underline{u}) N_i d\Omega = \int_{\Gamma} \hat{n} \cdot (N_i \underline{\underline{\tau}}) d\Gamma - \int_{\Omega} (\underline{\underline{\tau}} \cdot \nabla N_i) d\Omega. \qquad (2.12)$$

The weak form (2.12) is preferred over that given by equation (2.9) because it both relaxes the differentiability requirements on $\underline{\underline{\tau}}$, and hence on the approximations for $\underline{u}$ and P, and introduces the so-called "natural" boundary conditions. To complete the weak

formulation of the governing equations, equation (2.6), which, as noted by Gresho in Ref. 13 implicity defines the pressure, is first multiplied by any of the m pressure basis functions M_ℓ, where m is the dimension of the pressure approximation space, and then it too is integrated over the spatial domain Ω:

$$\int_\Omega (\nabla \cdot \underline{u}) M_\ell \, d\Omega = 0 \, . \tag{2.13}$$

As noted by Temam (9), solutions to equations (2.12) and (2.13) are also solutions to equations (2.1) and (2.2) provided the data for the problem is sufficiently regular (smooth).

Two alternative categories of weak formulations of equations (2.5) and (2.6) also in widespread use are the "penalty" and "upwind" formulations. In penalty formulations, the continuity equation (2.6) is dropped in favor of representing the pressure by

$$P = - \lambda(\nabla \cdot \underline{u}) \, , \tag{2.14}$$

where λ is a large positive number specified a priori. The rational behind this approach is explained in detail in the paper by Reddy (15), and other pertinent

discussions can be found in References 16 through 18 and in the literature cited therein. The principal advantage of this method is that the pressure variable is eliminated and thus the overall number of equations to be solved simultaneously is substantially reduced. The pressure field is subsequently recovered in a relatively inexpensive post-processing operation using equation (2.14). The obvious disadvantage of this method is that the computed results depend directly on the a priori choice of the penality parameter, λ. If the selected value of λ is too low, the incompressibility constraint will not be satisfied and the resulting solution will be erroneous. If on the other hand λ is chosen too high, numerical stability problems develop owing to the fact that the computations are performed with finite precision arithmetic. As for the "upwind" or "Petrov-Galerkin" formulations, e.g., References 5, 16, 19 and 20, these methods are the same as that used to generate equations (2.12) and (2.13) except that the functions N_i are not the velocity basis functions; rather they are functions chosen to introduce a certain amount of artificial damping so as to yield oscillatory-free "solutions" on coarse grids. As pointed out by Gresho (21), the theory behind the vast majority of such formulations is not well founded and the

results of computations using these techniques have been shown to be grossly in error in certain circumstances. In the present work both of these categories of alternative formulations were passed over in favor of the more conservative conventional Galerkin formulation, equations (2.12) and (2.13).

To facilitate both the interpretation of the various terms and the introduction of the spatial discretization and subsequent recasting into matrix form, equations (2.12), (2.13) and (2.7) are expanded in terms of two-dimensional, rectangular, Cartesian coordinates:

$$\int_{\Omega} \rho\left[u \frac{\partial u}{\partial x} + v \frac{\partial u}{\partial y}\right] N_i \, d\Omega = \int_{\Gamma} N_i \, f_x \, d\Gamma - \int_{\Omega} \left(\tau_{xx} \frac{\partial N_i}{\partial x} + \tau_{xy} \frac{\partial N_i}{\partial y}\right) d\Omega \quad (2.15)$$

$$\int_{\Omega} \rho\left[u \frac{\partial v}{\partial x} + v \frac{\partial v}{\partial y}\right] N_i \, d\Omega = \int_{\Gamma} N_i \, f_y \, d\Gamma - \int_{\Omega} \left(\tau_{yx} \frac{\partial N_i}{\partial x} + \tau_{yy} \frac{\partial N_i}{\partial y}\right) d\Omega \quad (2.16)$$

and

$$- \int_{\Omega} \left(\frac{\partial u}{\partial x} + \frac{\partial v}{\partial y}\right) M_{\ell} \, d\Omega = 0 \quad (2.17)$$

where, as suggested by Gresho, the minus sign in equation (2.17) is introduced to preserve symmetry,

$$\tau_{xx} = - P + 2\left(\frac{\mu}{Re}\right) \frac{\partial u}{\partial x} \tag{2.18}$$

$$\tau_{xy} = \tau_{yx} = \left(\frac{\mu}{Re}\right) \left[\frac{\partial u}{\partial y} + \frac{\partial v}{\partial x}\right] \tag{2.19}$$

$$\tau_{yy} = -P + 2\left(\frac{\mu}{Re}\right) \frac{\partial v}{\partial y} \tag{2.20}$$

$$f_x \equiv n_x \tau_{xx} + n_y \tau_{xy} = n_x\left(-P + 2 \left(\frac{\mu}{Re}\right) \frac{\partial u}{\partial x}\right)$$

$$+ n_y \left(\frac{\mu}{Re}\right) \left(\frac{\partial u}{\partial y} + \frac{\partial v}{\partial x}\right) \tag{2.21}$$

and

$$f_y \equiv n_x \tau_{yx} + n_y \tau_{yy} = n_x \left(\frac{\mu}{Re}\right) \left(\frac{\partial u}{\partial y} + \frac{\partial v}{\partial x}\right)$$

$$+ n_y \left(-P + 2\left(\frac{\mu}{Re}\right) \frac{\partial v}{\partial y}\right) . \tag{2.22}$$

The last two equations give the x- and y- components, respectively, of the surface traction force on the boundary Γ, and are referred to as the "natural" boundary conditions. These boundary conditions are very useful in many practical problems and will be discussed in more detail in the next section.

2.3 Boundary Conditions

As noted by Gresho (13), the following boundary conditions on Γ are consistent with the weak form used in the present work and are thus permissible:

$$u \quad \text{or} \quad f_x$$

and

$$v \quad \text{or} \quad f_y .$$

If the portions of Γ along which surface tractions are specified are aligned with the x- and y-directions, then f_x and f_y can be immediately identified with the normal and tangential tractions

$$f_n = -P + 2\left(\frac{\mu}{Re}\right) \frac{\partial u_n}{\partial n} \tag{2.23}$$

and

$$f_\tau = \left(\frac{\mu}{Re}\right) \left(\frac{\partial u_n}{\partial \tau} + \frac{\partial u_\tau}{\partial n}\right) , \tag{2.24}$$

where n is the outward directed unit normal and τ is the unit vector tangent to Γ. The traction-free form of these boundary conditions, f_n and/or $f_\tau = 0$, has proven to be quite useful in obtaining solutions to problems of an

engineering nature and are far more flexible than their Neumann counterparts ($\frac{\partial u}{\partial x}$, $\frac{\partial u}{\partial y}$, $\frac{\partial v}{\partial x}$ or $\frac{\partial v}{\partial y} = 0$) used in most finite difference and some finite element methods such as the one described in Reference 22. This is because the zero-traction boundary conditions do not force the streamlines to have zero slopes at the boundaries where they are imposed, and as such permit mass to leave and re-enter the domain across these boundaries. This is very useful from a practical standpoint, because in engineering computations the positions of the surfaces outside which the flow field is unaffected by the presence of a body, or for internal flows, the location of the plane at which the flow becomes fully developed, are generally unknown a priori. Several excellent examples illustrating the use of traction-free boundary conditions are contained in References 13 and 21.

In the next section, the spatial discretization of equations (2.15) through (2.17) is introduced, and the resulting set of simultaneous, nonlinear, algebraic equations is rewritten in matrix form.

2.4 Spatial Discretization and Matrix Formulation

As in the classical variational methods, e.g. Rayleigh-Ritz, least squares, collocation or Galerkin, the

spatial discretization is accomplished by replacing each of the field variables by a linear combination of functions and unknown coefficients:

$$z^h = \sum_{i=1}^{p} c_i \phi_i \ .$$

The set of basis functions $\{\phi_i\}_{i=1,2,\ldots,p}$ must be linearly independent and span the finite dimensional subspace Z_p of the space Z in which solutions to the weak form of the governing equations lie. That is, the $\{\phi_i\}$ must form a basis for the p-dimensional linear space Z_p containing the approximation $z^h \varepsilon Z_p$ to the true solution $z \varepsilon Z$ of the equations. Additional restrictions on the basis functions, ϕ_i, to ensure that $z^h \to z$ as $p \to \infty$ will be presented in section 2.5.

The term spatial "discretization" stems from the fact that in many cases the basis functions are chosen such that

$$\phi_i(x_j, y_j) = \delta_{ij} \ , \tag{2.25}$$

and thus

$$z_i^h \equiv z^h(x_i, y_i) = c_i \ . \tag{2.26}$$

That is, in these instances the unknown coefficients to be solved for turn out to be values of the approximate solution at the p "discrete" points (x_i, y_i). It should be noted that while it is usually desirable to utilize basis functions that satisfy equation (2.25) to avoid having to post-process the computed results, it is not necessary to do so. In the present work, for example, while the velocity basis functions satisfy this property, the pressure basis functions do not. This topic will be taken up again in greater detail in section 2.5, where the basis functions used here will be presented.

For the present, let $\{N_i\}_{i=1,2,\ldots,n}$ denote the set of n basis functions used in the velocity approximation and $\{M_\ell\}_{\ell=1,2,\ldots,m}$ the basis for the m-dimensional pressure approximation space. Thus, approximate solutions (u^h, v^h, P^h) to the true solution (u, v, P) of equations (2.15) through (2.17) take the form

$$u^h = \sum_{i=1}^{n} u_i N_i , \qquad (2.27)$$

$$v^h = \sum_{i=1}^{n} v_i N_i , \qquad (2.28)$$

and

$$P^h = \sum_{\ell=1}^{m} p_\ell M_\ell , \qquad (2.29)$$

so that the discretized form of equations (2.15) through (2.17) becomes, upon substitution of equations (2.27) through (2.29) into equations (2.15) through (2.22) and the rearrangement and grouping of like terms:

$$\left[\int_{\Omega} (\mu/Re)\left(2\frac{\partial N_i}{\partial x}\frac{\partial N_j}{\partial x} + \frac{\partial N_i}{\partial y}\frac{\partial N_j}{\partial y}\right)d\Omega\right]u_j$$

$$+ \left[\int_{\Omega} (\mu/Re)\left(\frac{\partial N_i}{\partial y}\frac{\partial N_j}{\partial x}\right)d\Omega\right]v_j$$

$$+ \left[u_k \int_{\Omega} \left(\rho N_k N_i \frac{\partial N_j}{\partial x}\right)d\Omega\right.$$

$$\left. + v_k \int_{\Omega} \left(\rho N_k N_i \frac{\partial N_j}{\partial y}\right)d\Omega\right] u_j$$

$$- \left[\int_{\Omega} \left(\frac{\partial N_i}{\partial x} M_\ell\right) d\Omega\right]P_\ell = \int_{\Gamma} (N_i f_x)d\Gamma , \qquad (2.30)$$

$$\left[\int_{\Omega} (\mu/Re)\left(\frac{\partial N_i}{\partial x}\frac{\partial N_j}{\partial y}\right)d\Omega\right]u_j$$

$$+ \left[(\mu/Re)\left(\frac{\partial N_i}{\partial x}\frac{\partial N_j}{\partial x} + 2\frac{\partial N_i}{\partial y}\frac{\partial N_j}{\partial y}\right)d\Omega\right]v_j$$

$$+ \left[u_k \int_{\Omega} \left(\rho N_k N_i \frac{\partial N_j}{\partial x}\right)d\Omega\right.$$

$$\left. + v_k \int_{\Omega} \left(\rho N_k N_i \frac{\partial N_j}{\partial y}\right)d\Omega\right]v_j$$

$$- \left[\int_{\Omega} \left(\frac{\partial N_i}{\partial y} M_\ell\right)d\Omega\right]P_\ell = \int_{\Gamma} (N_i f_y)d\Gamma , \qquad (2.31)$$

and

$$- \left[\int_{\Omega} \left(M_{\ell} \frac{\partial N_i}{\partial x} \right) d\Omega \right] u_j - \left[\int_{\Omega} \left(M_{\ell} \frac{\partial N_i}{\partial y} \right) d\Omega \right] v_j = 0, \qquad (2.32)$$

where i and j = 1,2,...,n, ℓ = 1,2,...,m and repeated indices imply summation. As noted by Gresho (13), these equations can be written in the partitioned matrix form as

$$\begin{aligned} &[\underline{\underline{K}} + \underline{\underline{N}}(\underline{u}^h)]\underline{u}^h + [C]\,\underline{P}^h = [F] \\ &[C]^T\,\underline{u}^h = 0 \end{aligned} \qquad (2.33)$$

or

$$\left[\begin{array}{c|c} \underline{\underline{K}} + \underline{\underline{N}}(\underline{u}^h) & \underline{\underline{C}} \\ \hline \underline{\underline{C}}^T & 0 \end{array}\right] \left[\begin{array}{c} \underline{u}^h \\ \hline \underline{P}^h \end{array}\right] = \left[\begin{array}{c} \underline{F} \\ \hline \underline{0} \end{array}\right] \qquad (2.34)$$

where the underscores "=" and "-" indicate that these quantities are themselves matrices or vectors, respectively. Specifically,

$$\underline{u}^h = \begin{bmatrix} u_1^h \\ u_2^h \\ \vdots \\ u_n^h \\ v_1^h \\ v_2^h \\ \vdots \\ v_n^h \end{bmatrix}, \qquad (2.35)$$

$$\underline{p}^h = \begin{bmatrix} p_1^h \\ p_2^h \\ \vdots \\ p_m^h \end{bmatrix}, \qquad (2.36)$$

[F] is the 2nx1 vector containing all the imposed traction boundary conditions (refer to section 2.3), [K] and $[N(\underline{u}^h)]$ are the 2nx2n viscous stress and advection matrices, respectively, [C] is the 2nxm pressure gradient matrix and its transpose $[C]^T$ is the mx2n divergence matrix. To isolate groupings of like terms, these matrices can in turn be partitioned into submatrices as follows:

$$[K] = \left[\begin{array}{c|c} 2\,\underline{\underline{K}}_a + \underline{\underline{K}}_b & \underline{\underline{K}}_c \\ \hline \underline{\underline{K}}_c^T & \underline{\underline{K}}_a + 2\underline{\underline{K}}_b \end{array}\right], \tag{2.37}$$

$$[N(\underline{u}^h)] = \left[\begin{array}{c|c} \underline{\underline{N}}_u(\underline{u}^h) + \underline{\underline{N}}_v(\underline{u}^h) & 0 \\ \hline 0 & \underline{\underline{N}}_u(\underline{u}^h) + \underline{\underline{N}}_v(\underline{u}^h) \end{array}\right], \tag{2.38}$$

$$[C] = \left[\begin{array}{c} \underline{\underline{C}}_x \\ \hline \underline{\underline{C}}_y \end{array}\right], \tag{2.39}$$

and finally

$$[F] = \left[\begin{array}{c} \underline{F}_x \\ \hline \underline{F}_y \end{array}\right], \tag{2.40}$$

where,

$$[K_a]_{ij} = \int_\Omega (\mu/Re)\left(\frac{\partial N_i}{\partial x}\,\frac{\partial N_j}{\partial x}\right) d\Omega\,, \tag{2.41}$$

$$[K_b]_{ij} = \int_\Omega (\mu/Re) \left(\frac{\partial N_i}{\partial y} \frac{\partial N_j}{\partial y}\right) d\Omega \ , \tag{2.42}$$

$$[K_c]_{ij} = \int_\Omega (\mu/Re) \left(\frac{\partial N_i}{\partial y} \frac{\partial N_j}{\partial x}\right) d\Omega \ , \tag{2.43}$$

$$[N_u(\underline{u}^h)]_{ij} = u_k \int_\Omega \left(\rho \ N_k \ N_i \ \frac{\partial N_j}{\partial x}\right) d\Omega \ , \tag{2.44}$$

$$[N_v(\underline{u}^h)]_{ij} = v_k \int_\Omega \left(\rho \ N_k \ N_i \ \frac{\partial N_j}{\partial y}\right) d\Omega \ , \tag{2.45}$$

$$[C_x]_{i\ell} = \int_\Omega \left(\frac{\partial N_i}{\partial x} \ M_\ell\right) d\Omega \ , \tag{2.46}$$

$$[C_y]_{i\ell} = \int_\Omega \left(\frac{\partial N_i}{\partial y} \ M_\ell\right) d\Omega \ , \tag{2.47}$$

$$[F_x]_i = \int_\Gamma (N_i \ f_x) d\Gamma \ , \tag{2.48}$$

and

$$[F_y]_i = \int_\Gamma (N_i f_y) d\Gamma \ . \tag{2.49}$$

The problem of choosing combinations of velocity and pressure basis functions suitable for use with equation 2.34 is discussed in the next section, while that of obtaining solutions to this system of simultaneous, nonlinear equations is taken up in section 2.8.

2.5 Selection of the Basis Functions

As pointed out by Prenter (23), the difference between the finite element method and the other variational-based techniques mentioned earlier in section 2.4 lies in the nature of the space of approximate solutions, and hence in the basis functions used to construct them. In the classical variational methods, the basis functions are chosen so as to generate a space of approximate solutions consisting of polynominals on the entire computational domain. Finite element approximate solutions, on the other hand, are constructed from basis functions that generate spaces of spline functions - low order polynominal segments on portions or "elements" of the computational domain that are "pieced" together to give the spatial variation of a field variable over the entire domain.

The basis functions used to construct spline functions have two properties that are very desirable from a computational viewpoint: (1) they automatically lead to coefficient matrices that are sparse and banded; and (2) they can be built up from "interpolating functions" defined on a local (typical spline segment) basis. The first of these features is important because banded matrices can be manipulated so as to require far less

storage and can be inverted with far fewer arithmetical operations. This is a direct consequence of the fact that the basis functions used to construct splines have regions of small compact support, i.e. they are zero everywhere outside at most a few segments of the spline function. The latter characteristic is very desirable as it paves the way for the construction of algorithms for evaluating the coefficient matrices in equation (2.34) that take full advantage of their sparseness.

In general, the basis functions for a given problem are chosen such that: (1) the domains of the outer-most spline segments in the physical plane conform as closely as possible to the shape of the boundary, Γ ; and (2) they ensure that $(\underline{u}^h, \underline{v}^h, \underline{p}^h) \rightarrow (\underline{u}, \underline{v}, \underline{p})$ in the limit as the number of elements, and hence the dimension of the finite dimensional subspace of approximate solutions, approaches infinity. In the present work, the first criterion was addressed with the aid of the isoparametric transformation described in the next section, and the second by demonstrating compliance with certain mathematical guidelines that will now be discussed.

As noted by several authors, e.g. References (24) through (28), one cannot mix together just any sets of velocity and pressure basis functions and expect to obtain

a sequence of approximate solutions that converges to the true solution of the weak form in the limit as the dimension of the subspaces of approximate solutions approaches infinity. Some authors, e.g. Babuska (24), Brezzi (25), Fix, et al. (26) and Gunzburger and Peterson (27) have proposed rather abstract guidelines regarding the choice of basis functions to assure such behavior. Others, such as Fortin (6) and Sani (14, 29), have presented practical schemes for determining whether or not a given combination of solution subspaces meet these guidelines.

The consensus of opinion among these authors appears to be that to obtain a convergent sequence of solutions: (1) the auxiliary data must be sufficiently smooth; (2) the solution subspaces (and hence the basis functions) must satisfy a stability or compatability condition such as proposed by Babuska (24), Brezzi (25), Fix, et al. (26) or Gunzeburger and Peterson (27); and (3) $V^h \subset H^1(\Omega)$ and $S^h \subset L^2(\Omega)$, where V^h and S^h are the finite dimensional velocity and pressure solution subspaces, respectively, $L^2(\Omega)$ is the set of all Lesbegue square integrable functions on Ω, and H^1 is defined as

$$H^1(\Omega) \equiv \{Z(r,s) \in L^2(\Omega): \frac{\partial Z}{\partial r} \text{ and } \frac{\partial Z}{\partial s} \in L^2(\Omega)\} .$$

The velocity basis functions used in the present work are constructed from the piecewise biquadratic Lagrange interpolating functions given in Table 2.1. These basis functions lead to a continuous (C^o) representation of the velocity field on Ω that is biquadratic on each element. Note that the interpolating functions in Table 2.1 are defined in terms of the normalized local coordinate system depicted in Fig. 2.1. This is done to : (1) facilitate the evaluation of the various integrals that comprise the coefficient matrix in equation (2.34); and (2) take better advantage of the repetitive nature of the calculations.

The pressure field, on the other hand, is represented by a discontinuous (C^{-1}) approximation on Ω that is linear on each segment of the spline function approximation. That is, on each element

$$p^h(x,y) = p_1 + p_2 x + p_3 y \ , \qquad (2.50)$$

where the constants p_1, p_2 and p_3 are not values of p^h at specified nodal points, as is the case for their counterparts in the velocity expansion as discussed in section 2.4, rather they should be thought of as just three unknown coefficients associated with a given segment

Table 2.1. Biquadratic Lagrange interpolating polynomials used to construct the velocity basis functions

i	$\bar{N}_i(\xi,\eta)$
1	$(\frac{1}{4})\ [(\xi)(\xi - 1)(\eta)(\eta - 1)]$
2	$(-\frac{1}{2})[(\xi + 1)(\xi - 1)(\eta)(\eta - 1)]$
3	$(\frac{1}{4})\ [(\xi)(\xi + 1)(\eta)(\eta - 1)]$
4	$(-\frac{1}{2})\ [(\xi)(\xi + 1)(\eta + 1)(\eta - 1)]$
5	$(\frac{1}{4})\ [(\xi)(\xi + 1)(\eta)(\eta + 1)]$
6	$(-\frac{1}{2})\ [(\xi + 1)(\xi - 1)(\eta)(\eta + 1)]$
7	$(\frac{1}{4})\ [(\xi)(\xi - 1)(\eta)(\eta + 1)]$
8	$(-\frac{1}{2})\ [(\xi)(\xi - 1)(\eta + 1)(\eta - 1)]$
9	$[(\xi + 1)(\xi - 1)(\eta + 1)(\eta - 1)]$

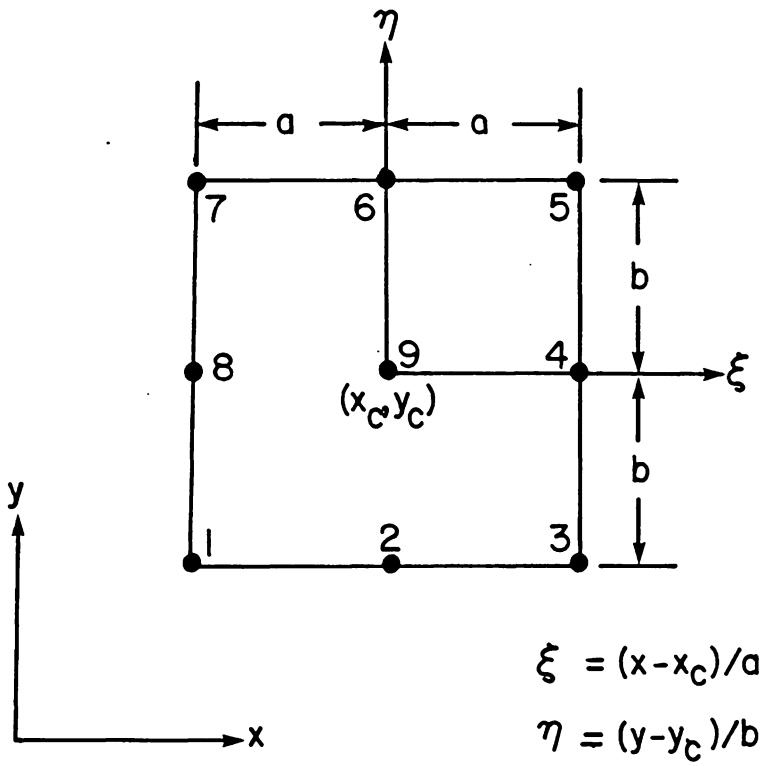

Fig. 2.1. Local coordinate system and nodal point numbering scheme.

of the spline function approximation to P on Ω.

The exact origin of this particular combination of basis functions could not be ascertained. It was previously used by Engleman and Sani (17) in conjunction with a penalty formation of the equations, and Fortin concluded that it "is probably the best one known for two-dimensional incompressible computations" in his 1981 paper (6) in which he compared the convergence and stability properties of several combinations of basis functions in use at that time.

The combinations of basis functions (element type) reviewed by Fortin (6) are given in Table 2.2 along with other combinations commonly referred to in the open literature and reviewed during the course of the present investigation. It is easily shown that all the combinations presented in this table including the one used here satisfy the conditions $V^h \subset H^1$ and $S^h \subset L^2$. However only the first seven entries in this table have been shown to satisfy one of the aforementioned compatibility or stability conditions. The remaining entries have been shown by Fortin (6) and Sani, (14,29) to fail such conditions and have been observed by Gresho (13) and others to yield physically unrealistic pressure distributions under certain flow conditions. Thus, only

Table 2.2. Summary of Lagrangian element configurations considered.

Designation	Description	Reference(s)
$T_1 - P_o^1$		28
$T_1 - P_o^4$		28
$Q_1 - P_o^1$	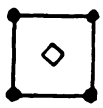	28
$T_2 - P_o^2$		28,30
$Q_2^{(s)} - P_o^1$	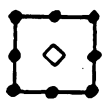	6
$Q_2^{(r)} - P_o^1$	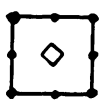	6
$Q_2^{(f)} - P_o^3$	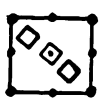	6,17
$Q_2^{(s)} - P_1^4$	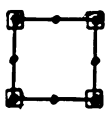	5,13,22,31
$Q_2^{(f)} - P_1^4$	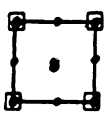	13,32,33

Table 2.2. (continued)

Designation	Description	Reference(s)
$Q_1 - P_o^1$	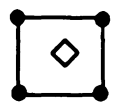	13,34
$Q_2^{(f)} - P_o^4$	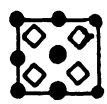	13,34

Symbols:

● velocity degrees of freedom
◇ pressure degree of freedom

P - pressure approximation
Q - quadrilateral velocity element
T - triangular velocity element

Subscripts:

o - discontinuous approximation
1 - bilinear approximation
2 - biquadratic approximation

Superscripts:

f - full Lagrangian element
r - reduced approximation (6)
s - serendipity element
Integer - number of pressure degrees of freedom

the first seven entries in Table 2.2 received serious consideration in the present work. The second order method used here (entry 7) was chosen over the three linear entries in this table because it was felt that it would be better able to take advantage of the inherent "quadratic" nature of the laminar flow velocity fields to be investigated. It was used in lieu of the other quadratic elements presented because of its superior convergence properties.

2.6 Isoparametric Transformation

Perhaps the most common way of attempting to ensure that the union of the domains of the individual spline segments adequately approximates the shape of the physical domain is to use a transformation that maps the geometrically simple domains on which the interpolating functions are defined into distorted shapes in the physical plane. Refer to Fig. 2.2. For the sake of convenience, these transformations are usually defined by equations of the form:

$$x(\xi,\eta) = \sum_{i=1}^{n} F_i^{(e)}(\xi,\eta)\, x_i^{(e)} \qquad (2.51)$$

and

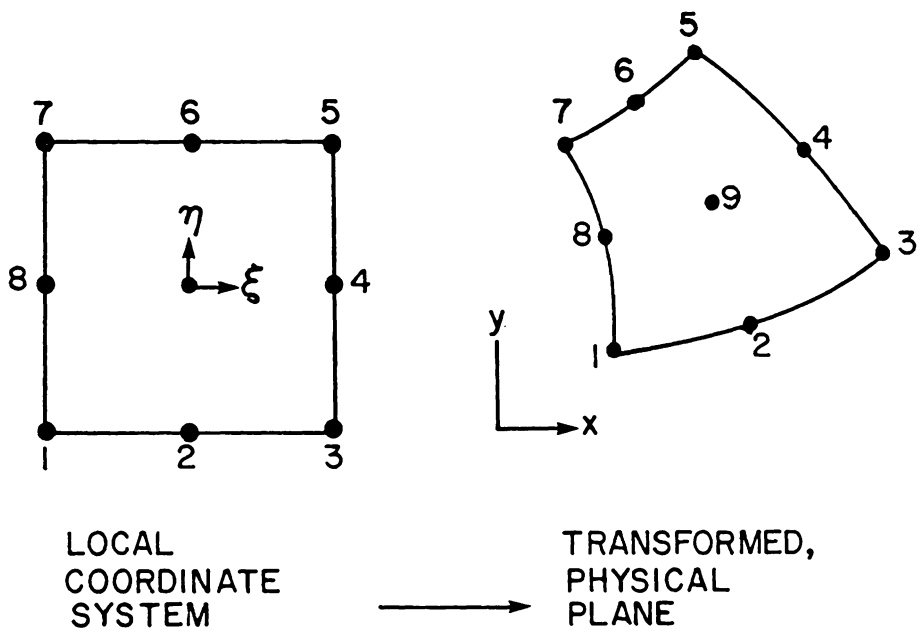

Fig. 2.2. Isoparametric coordinate transformation.

$$y(\xi,\eta) = \sum_{i=1}^{n} F_i^{(e)}(\xi,\eta)\, y_i^{(e)} \qquad (2.52)$$

where ξ and η are the normalized coordinates in the geometrically simple transformed plane, x and y the corresponding coordinates in the distorted physical plane, and $x_i^{(e)}$ and $y_i^{(e)}$ are the coordinates of the n nodal points associated with element (spline segment) e in the physical plane. If the functions $F_i^{(e)}(\xi,\eta)$, i = 1, 2, ..., n are chosen to be the same as the basis functions used to represent the spatial variation of the main field variables, u and v in the present case, then the mapping expressed by equations (2.51) and (2.52) is referred to as an "isoparametric" transformation. Such a transformation is used in the present work, so that equations (2.51) and (2.52) become, respectively:

$$x(\xi,\eta) = \sum_{i=1}^{9} \bar{N}_i^{(e)}(\xi,\eta)\, x_i^{(e)} , \qquad (2.53)$$

and

$$y(\xi,\eta) = \sum_{i=1}^{9} \bar{N}_i^{(e)}(\xi,\eta)\, y_i^{(e)} , \qquad (2.54)$$

where the $\bar{N}_i^{(e)}(\xi,\eta)$ are the interpolating functions given in the aforementioned Table 2.1 and the remaining

variables are as defined above.

As will be shown in the next section, terms like

$$\frac{\partial \overline{N}_i^{(e)}(\xi,\eta)}{\partial x(\xi,\eta)}$$

and

$$\frac{\partial \overline{N}_i^{(e)}(\xi_m,\eta)}{\partial y(\xi,\eta)}$$

arise when equations (2.41) through (2.49) are transformed so as to enable the use of locally defined interpolating functions. When this transformation is of the form of equations (2.53) and (2.54), these derivatives are evaluated using the following expressions which are derived from a straightforward application of the chain rule as shown, for example, in References 18, 35 and 36:

$$\begin{bmatrix} \dfrac{\partial \overline{N}_i^{(e)}(\xi,\eta)}{\partial x(\xi,\eta)} \\ \dfrac{\partial \overline{N}_i^{(e)}(\xi,\eta)}{\partial y(\xi,\eta)} \end{bmatrix} = \frac{1}{\det \underline{\underline{J}}^{(e)}(\xi,\eta)} \begin{bmatrix} \dfrac{\partial y(\xi,\eta)}{\partial \eta} & \dfrac{-\partial y(\xi,\eta)}{\partial \xi} \\ \dfrac{-\partial x(\xi,\eta)}{\partial \eta} & \dfrac{\partial x(\xi,\eta)}{\partial \xi} \end{bmatrix} \begin{bmatrix} \dfrac{\partial \overline{N}_i^{(e)}(\xi,\eta)}{\partial \xi} \\ \dfrac{\partial \overline{N}_i^{(e)}(\xi,\eta)}{\partial \eta} \end{bmatrix} \tag{2.55}$$

where $\underline{\underline{J}}^{(e)}(\xi,\eta)$ is the Jacobian matrix associated with the

transformation,

$$\det J^{(e)}(\xi,\eta) = \left(\frac{\partial x(\xi,\eta)}{\xi\eta}\ \frac{\partial y(\xi,\eta)}{\partial\eta}\right) - \left(\frac{\partial y(\xi,\eta)}{\partial\xi}\ \frac{\partial x(\xi,\eta)}{\partial\eta}\right), \tag{2.56}$$

$$\frac{\partial x(\xi,\eta)}{\partial\xi} = \sum_{i=1}^{9} \frac{\partial \bar{N}_i^{(e)}(\xi,\eta)}{\partial\xi}\, x_i^{(e)}, \tag{2.57}$$

$$\frac{\partial x(\xi,\eta)}{\partial\eta} = \sum_{i=1}^{9} \frac{\partial \bar{N}_i^{(e)}(\xi,\eta)}{\partial\eta}\, x_i^{(e)}, \tag{2.58}$$

$$\frac{\partial y(\xi,\eta)}{\partial\xi} = \sum_{i=1}^{9} \frac{\partial \bar{N}_i^{(e)}(\xi,\eta)}{\partial\xi}\, y_i^{(e)}, \tag{2.59}$$

and

$$\frac{\partial y(\xi,\eta)}{\partial\eta} = \sum_{i=1}^{9} \frac{\partial \bar{N}_i^{(e)}(\xi,\eta)}{\partial\eta}\, y_i^{(e)}. \tag{2.60}$$

It is also shown in these same references that the incremental area $d\Omega$ in the physical plane is related to

the incremental area $d\xi\, d\eta$ in the normalized local coordinate system by

$$d\Omega = \det \underline{\underline{J}}^{(e)}(\xi,\eta)\, d\xi\, d\eta \,. \qquad (2.61)$$

2.7 Evaluation of the Coefficient Matrices

The procedure followed in the present work to evaluate the coefficient matrices in equation (2.34) parallels that presented in any basic text on the subject of finite elements, e.g. References 18, 35 and 36. Basically, it involves:

1. Partitioning the domain Ω into a set of subdomains or elements, $\{\Omega^{(e)}\}$, where e runs from one contiguously through the number of elements. Each element corresponds to the domain of a single segment of the spline function approximation.
2. Evaluating the element-level coefficient matrices one at a time. These matrices are formed and evaluated as described below.
3. Assembling the element-level coefficient matrices to form the global coefficient matrices in equation (2.34). The coupling between the individual elements, which is ignored during the

formation of the element-level matrices, is introduced in this step.

The element-level coefficient matrices are formed by simply restricting equation (2.34) to the domain of the element under consideration. That is, the element-level matrices retain the same form as their global equivalents, however the domain of the integrals in the component equations is re-interpreted as being $\Omega^{(e)}$. As noted earlier in secton 2.4, the process of evaluating the components of the various coefficient matrices is facilitated if the component equations are recast in a normalized coordinate system and the basis functions are replaced by the interpolating functions from which they are constructed. Thus the element-level equivalents of equations (2.41) through (2.47) become:

$$[K_a]_{ij} = \int_{-1}^{+1} \int_{-1}^{+1} (\mu/Re) \frac{\partial \bar{N}_i(\xi,\eta)}{\partial x} \frac{\partial \bar{N}_j(\xi,\eta)}{\partial x} \det \underline{\underline{J}}(\xi,\eta)\, d\xi\delta\eta, \tag{2.62}$$

$$[K_b]_{ij} = \int_{-1}^{+1} \int_{-1}^{+1} (\mu/Re) \frac{\partial \bar{N}_i(\xi,\eta)}{\partial y} \frac{\partial \bar{N}_j(\xi,\eta)}{\partial y} \det \underline{\underline{J}}(\xi,\eta)\, d\xi d\eta\,, \tag{2.63}$$

$$[K_c]_{ij} = \int_{-1}^{+1}\int_{-1}^{+1} (\mu/Re)\, \frac{\partial \bar{N}_i(\xi,\eta)}{\partial y}\, \frac{\partial \bar{N}_j(\xi,\eta)}{\partial x}$$

$$\det \underline{\underline{J}}(\xi,\eta)\, d\xi d\eta\,, \qquad (2.64)$$

$$[N_u(\underline{u}^h)]_{ij} = \int_{-1}^{+1}\int_{-1}^{+1} \rho\, u_k\, \bar{N}_k(\xi,\eta)\, \bar{N}_i(\xi,\eta)\, \frac{\partial \bar{N}_j(\xi,\eta)}{\partial x}$$

$$\det \underline{\underline{J}}(\xi,\eta)\, d\xi d\eta\,, \qquad (2.65)$$

$$[N_v(\underline{u}^h)]_{ij} = \int_{-1}^{+1}\int_{-1}^{+1} \rho\, v_k \bar{N}_k(\xi,\eta)\, \bar{N}_i(\xi,\eta)\, \frac{\partial \bar{N}_j(\xi,\eta)}{\partial y}$$

$$\det \underline{\underline{J}}(\xi,\eta)\, d\xi d\eta\,, \qquad (2.66)$$

$$[C_x]_{i\ell} = \int_{-1}^{+1}\int_{-1}^{+1} \frac{\partial \bar{N}_i(\xi,\eta)}{\partial x}\, M_\ell(\xi,\eta)$$

$$\det \underline{\underline{J}}(\xi,\eta)\, d\xi d\eta\,, \qquad (2.67)$$

and

$$[C_y]_{i\ell} = \int_{-1}^{+1}\int_{-1}^{+1} \frac{\partial \bar{N}_i(\xi,\eta)}{\partial y}\, M_\ell(\xi,\eta)$$

$$\det \underline{\underline{J}}(\xi,\eta)\, d\xi d\eta\,, \qquad (2.68)$$

where i, j and k = 1, 2, ..., 9 and ℓ = 1, 2, 3 for the combination of basis functions used in the present work, and as before, repeated indices imply summation.

Note that the right hand sides of equation (2.62) through (2.68) consist entirely of definite integrals of the form

$$\int_{-1}^{+1}\int_{-1}^{+1} f(\xi,\eta)\ \det \underline{\underline{J}}(\xi,\eta)\ d\xi d\eta\ . \qquad (2.69)$$

For quadrilateral elements with opposite sides parallel and equal, the term $\det \underline{\underline{J}}(\xi,\eta)$ is a constant related to the area of the element. As such it can be factored out from under the integral sign, leaving an integrand that can be integrated analytically using tables like those, for example, in Huebner and Thornton (37). For the more general isoparametric quadrilateral elements considered here, however, $\det J(\xi,\eta)$ is not a constant, but rather a rational function, which in general cannot be integrated analytically. It is for this reason that the integrals in equations (2.62) through (2.68) are evaluated numerically.

The most widely utilized quadrature rule for evaluating the components of the element coefficient matrices when isoparametric elements derived from quadrilaterals are employed appears to be the Gauss-Legendre numerical integration procedure (36,38). This is because in general this method requires fewer function evaluations to achieve a given accuracy than is required

by other comparable methods commonly used in numerical analysis, e.g. the Newton-Cotes formulas (18,36). The procedure is to simply replace the definite integral in a normalized coordinate system by a linear combination of weights, W_i, and function evaluations at n specified sampling (or "Gauss") points, $\bar{\xi}_i$:

$$\int_{-1}^{+1} g(\xi)d\xi \approx \sum_{i=1}^{n} g(\bar{\xi}_i)W_i \ . \qquad (2.70)$$

The positions of the sampling points and the corresponding weights for n = 1, 2, ..., 4 are summarized in Table 2.3.

Gauss-Legendre quadrature is extended to multi-dimensional integrations of the type encountered in the present analysis by following the same procedure that one would normally use to evaluate multi-dimensional integrals, namely successively evaluate the integrals from the innermost one out, holding the variables associated with the other integrals constant. Thus, for the two-dimensional case we have

$$\int_{-1}^{+1}\int_{-1}^{+1} g(\xi,\eta)\, d\xi d\eta = \int_{-1}^{+1}\left(\int_{-1}^{+1} g(\xi,\eta)d\xi\right) d\eta \qquad (2.71)$$

Table 2.3. Sampling points and weights in the Gauss-Legendre numerical integration formulas

n	ξ_i	W_i
1	0.000000	2.000000
2	± 0.577530	1.000000
3	0.000000	0.888889
	± 0.774597	0.555556
4	± 0.339981	0.652145
	± 0.861136	0.347855

$$\approx \int_{-1}^{+1} \left(\sum_{i=1}^{n} g(\bar{\xi}_i, n) W_i \right) d\eta$$

$$= \sum_{i=1}^{n} W_i \int_{-1}^{+1} g(\bar{\xi}_i, \eta)\, d\eta$$

$$\approx \sum_{i=1}^{n} W_i \left(\sum_{j=1}^{m} g(\bar{\xi}_i, \bar{\eta}_j)\, W_j \right)$$

or, since the summation is over a finite number of terms,

$$\int_{-1}^{+1} \int_{-1}^{+1} g(\xi, \eta)\, d\xi d\eta \approx \sum_{i=1}^{n} \sum_{j=1}^{m} g(\bar{\xi}_i, \bar{\eta}_j) W_i W_j \quad . \quad (2.72)$$

Finally, a note regarding the number of sample points. Zienkiewicz (18) has suggested that at least 2x2 sampling points be used for parabolic quadrilateral elements such as those incorporated in the present analysis. Indeed he has shown that for two-dimensional elasticity problems, the use of fewer than 2x2 sampling points with the aforementioned class of elements leads to a singular coefficient matrix. Taylor and Hughes (22)

reported that based upon their experience in obtaining solutions to the Navier-Stokes equations with a parabolic quadrilateral element, 3x3 sampling points were generally sufficiently accurate. In the present work, 4x4 sampling points were used for the sake of added conservatism.

2.8 Solution Method

As shown in section 2.4, the spatial discretization of the weak form of the governing equations results in a set of simultaneous, nonlinear, algebraic equations of the form

$$\underline{\underline{A}}(\underline{s})\ \underline{s} = \underline{b} \quad , \tag{2.73}$$

where

$\underline{\underline{A}}(\underline{s}) = [a_{ij}(\underline{s})]$ NEQxNEQ assembled coefficient matrix,

$\underline{s} = [s_i]$ NEQx1 column vector of unknowns,

$\underline{b} = [b_i]$ NEQx1 column vector of external forces,

and NEQ is the number of equations. The procedures used to resolve the nonlinearities and solve the resulting set

of linear, algebraic equations will now be presented.

2.8.1 Iterative Method

For nonlinear problems such as the present one, it is a linearization or iteration that produces the set of simultaneous, linear, algebraic equations that must eventually be solved. Given that most practical problems tend to involve literally thousands of equations, and that good a priori estimates of the velocity field are seldom available, the iterates must be generated by a method that: (1) exhibits a high rate of convergence; and (2) will converge with minimum sensitivity to initial estimates, i.e., one with a large radius of convergence.

The four most widely heralded procedures for generating such linearizations are: (1) successive substitution or Picard iteration; (2) the Newton-Raphson method; (3) the modified-Newton or chord method; and (4) the so-called quasi-Newton methods. Each of these methods will now be described.

The successive substitution method is a particularly simple fixed point iterating scheme described by

$$\underline{\underline{A}}(\underline{s}^{i})\ \underline{s}^{(i+1)} = \underline{b}\ ,\ i = 0,\ 1,\ 2,\ \ldots\ . \qquad (2.74)$$

That is, the updated estimates are obtained by solving a system of equations which is linearized by using the current estimates to evaluate the coefficient matrix. The advantages of this method are: (1) unlike the other procedures, the initial estimates do not have to satisfy the boundary conditions; and (2) of the methods considered here, it has by far the largest radius of convergence. Thus it is often possible to start this procedure with $\underline{s}^0 = \underline{0}$. The disadvantage of this scheme is that in many cases the rate of convergence is relatively slow when compared to that exhibited by the other methods.

In the Newton-Raphson method the updated estimates are generated by

$$\underline{s}^{i+1} = \underline{s}^i = [J(\underline{s}^i)]^{-1} \underline{r}(\underline{s}^i) \qquad (2.75)$$

where $\underline{r}(s^i)$ is the NEQx1 residual vector given by

$$\underline{r}(s^i) = \underline{\underline{A}}(s^i)\underline{s}^i - \underline{b} \ , \qquad (2.76)$$

and $\underline{\underline{J}}(s^i)$ is an NEQxNEQ Jacobian matrix defined by

$$[J(\underline{s}^i)] = \begin{bmatrix} \frac{\partial r_1(\underline{s}^i)}{\partial s_1^i} & \frac{\partial r_1(\underline{s}^i)}{\partial s_2^i} & \cdots & \frac{\partial r_1(\underline{s}^i)}{\partial s_{NEQ}^i} \\ \frac{\partial r_2(\underline{s}^i)}{\partial s_1^i} & \frac{\partial r_2(\underline{s}^i)}{\partial s_2^i} & \cdots & \frac{\partial r_2(\underline{s}^i)}{\partial s_{NEQ}^i} \\ \vdots & \vdots & & \vdots \\ \frac{\partial r_{NEQ}(\underline{s}^i)}{\partial s_1^i} & \frac{\partial r_{NEQ}(\underline{s}^i)}{\partial s_2^i} & \cdots & \frac{\partial r_{NEQ}(\underline{s}^i)}{\partial s_{NEQ}^i} \end{bmatrix} , \tag{2.77}$$

which in the present work becomes (13)

$$[J(\underline{s}^i)] = \left[\begin{array}{ccc|c} & \underline{\underline{K}} + \underline{\underline{N}}(\underline{s}^i) + \underline{\underline{J}}(\underline{s}^i) & & C \\ \hline & \underline{\underline{C}}^T & & 0 \end{array}\right] , \tag{2.78}$$

where

$$[J'(\underline{s}^i)] = \left[\begin{array}{c|c} \underline{\underline{J}}'_{ux}(\underline{s}^i) & \underline{\underline{J}}'_{uy}(\underline{s}^i) \\ \hline \underline{\underline{J}}'_{vx}(\underline{s}^i) & \underline{\underline{J}}'_{vy}(\underline{s}^i) \end{array}\right] , \tag{2.79}$$

$$[J'_{ux}(\underline{s}^i)]_{mn} = \int_\Omega \rho\, u_k^i \frac{\partial N_k}{\partial x} N_m N_n \, d\Omega , \tag{2.80}$$

$$[J'_{uy}(\underline{s}^i)]_{mn} = \int_\Omega \rho\, u_k^i \frac{\partial N_k}{\partial y} N_m N_n \, d\Omega \,, \qquad (2.81)$$

$$[J'_{vx}(s^i)]_{mn} = \int_\Omega \rho\, v_k^i \frac{\partial N_k}{\partial x} N_m N_n \, d\Omega \,, \qquad (2.82)$$

$$[J'_{vy}(\underline{s}^i)]_{mn} = \int_\Omega \rho\, v_k^i \frac{\partial N_k}{\partial y} N_m N_n \, d\Omega \,, \qquad (2.83)$$

the remaining variables are as previously defined and again, repeated indices imply summation. An alternative, more convenient formulation is obtained by defining

$$\delta\underline{s} = \underline{s}^{i+1} - \underline{s}^i \qquad (2.84)$$

so that equation (2.75) becomes

$$\delta\underline{s} = - [J(\underline{s}^i)]^{-1} \underline{r}(\underline{s}^i) \qquad (2.85)$$

or

$$\underline{\underline{J}}(\underline{s}^i)\ \delta\underline{s} = - \underline{r}(\underline{s}^i) \,. \qquad (2.86)$$

Note that while equations (2.74) and (2.86) have the same

form, the solution of equation (2.86) yields a column vector of adjustments to the results of the previous iteration, not a solution vector. The solution vector for each iteration is easily obtained however with the use of equations (2.84).

The advantage of the Newton-Raphson scheme is that it has a rate of convergence that is usually superior to that exhibited by the other lower order methods - its rate of convergence is quadratic so long as the initial solution vector is within its radius of convergence. The disadvantages of this method are (1) the initial solution vector, $\underline{s}^o$, must satisfy any constrained velocity degrees of freedom; and (2) the radius of convergence is relatively small.

The modified-Newton or chord method is obtained if the initial Jacobian matrix $\underline{\underline{J}}(\underline{s}^o)$ is used in place of $\underline{\underline{J}}(s^i)$ at each iteration. The obvious advantage of this method is that only a single NEQxNEQ coefficient matrix, $\underline{\underline{J}}(\underline{s}^o)$, must be constructed and inverted. Both the successive substitution and Newton-Raphson schemes require the formation and inversion of a coefficient matrix at each iteration. Unfortunately, while the cost per iteration for this method is significantly lower than that of the other methods mentioned above, its convergence rate

is very slow and a relatively good initial estimate that satisfies any specified velocity boundary conditions is required for this method to converge at all.

A compromise between the chord and Newton-Raphson methods can be found in the so-called "quasi-Newton" algorithms. As noted by Burden (39), in this class of methods the Jacobian matrix is replaced by an "approximation" matrix which is inverted only once; from then on it is adjusted in a relatively simple manner after each iternation. However, while the convergence rates associated with such methods are significantly better than that exhibited by the chord method, they generally do not achieve the quadratic convergence rates characteristic of the Newton-Raphson update procedure. In addition, like the chord and Newton-Raphson methods, the quasi-Newton methods also require a relatively good initial estimate of the velocity field that satisfies any specified velocity component boundary conditions.

It should be obvious from the above discussions that no single iterative scheme satisfies both criteria set forth in the beginning of this section. The method with the largest radius of convergence (successive substitution) has the lowest rate of convergence, and conversely that which converges the fastest (Newton-

Raphson) requires the best initial estimate. It is for this reason that two of the methods described above, successive substitution and Newton-Raphson, were combined to yield the update strategy used in the present work. Specifically, the successive substitution method is used first to bring the usually crude initial estimates (e.g. $\underline{s}^{o} = \underline{0}$) inside the radius of convergence of the Newton-Raphson method, which is then used to accelerate the convergence. As is demonstrated throughout Chapter 3, this strategy proved quite effective in resolving the nonlinearlities associated with the problem considered here.

2.8.2 Matrix Inversion Procedure

As shown in the previous section, at each iteration both the successive substitution and Newton-Raphson procedures generate a linearization of equation (2.34) that can be expressed in the same form as equation (2.73). The methods used to effect solutions to equations of this type can be divided into two categories: (1) direct methods, and (2) indirect methods.

Direct methods are characterized by the fact that the number of steps and operations required to solve equation (2.73) can be predetermined in an exact manner. The most

effective algorithms in this category are those based upon applications of the Gauss elimination process (18, 36). Of these, the L-U factorization method is the most popular.

In the L-U decomposition method, the coefficient matrix, $\underline{\underline{A}}$, is factored using Gauss elimination such that it can be written as the product of an NEQxNEQ lower triangular matrix with unit diagonals and an NEQxNEQ upper triangular matrix, i.e.,

$$\underline{\underline{A}} = \underline{\underline{L}}\ \underline{\underline{U}} \tag{2.87}$$

where

$$\underline{\underline{L}} = \begin{bmatrix} 1 & 0 & & \cdots & 0 \\ L_{21} & 1 & 0 & \cdots & 0 \\ \vdots & & \ddots & & \\ L_{NEQ,1} & 0 & & \cdots & 1 \end{bmatrix}_{NEQxNEQ} \tag{2.88}$$

and

$$\underline{\underline{U}} = \begin{bmatrix} U_{11} & U_{12} & \cdots & U_{1,NEQ} \\ 0 & U_{22} & \cdots & U_{2,NEQ} \\ 0 & 0 & \ddots & \vdots \\ \vdots & \vdots & & \vdots \\ 0 & 0 & \cdots & U_{NEQ,NEQ} \end{bmatrix}^{NEQxNEQ} \tag{2.89}$$

Thus, equation 2.73 becomes

$$\underline{\underline{L}}\ \underline{\underline{U}}\ \underline{s} = \underline{r} \tag{2.90}$$

or

$$\underline{\underline{L}}\ \underline{w} = \underline{r} \tag{2.91}$$

where $\underline{w}$ is introduced to facilitate the solution process and is obtained by solving the NEQxNEQ set of equations represented by

$$\underline{\underline{U}}\ \underline{s} = \underline{w}\ . \tag{2.92}$$

Given the nature of the matrices $\underline{\underline{L}}$ and $\underline{\underline{U}}$, it can be shown (e.g, Reference 18) that the solutions to equations (2.91) and (2.92), and hence (2.73), are given by

$$w_1 = r_1$$

$$w_i = r_i - \sum_{j=1}^{i-1} L_{ij}\, w_j \qquad (i = 2, 3, \ldots, NEQ) \qquad (2.93)$$

and

$$s_{NEQ} = w_{NEQ}/U_{NEQ,NEQ} \qquad (2.94)$$

$$s_i = (w_i - \sum_{j=i+1}^{NEQ} U_{ij}\, s_j)/U_{ii} \qquad (i = NEQ-1, NEQ-2, \ldots, 1) .$$

One reason this method is so popular is that the triangular decomposition of $\underline{\underline{A}}$ can be carried out on "blocks" or "zones" of $\underline{\underline{A}}$, using values of $\underline{\underline{A}}$ only in the block being reduced or values of $\underline{\underline{L}}$ and $\underline{\underline{U}}$ from previously reduced blocks. This property is essential if the system of equations is very large, as is often the case for many practical problems. An excellent example of how the triangularization is performed in this manner is presented in the form of Table 24.13 of Zienkiewicz (18).

As for the indirect or iterative methods, e.g., Gauss-Seidel or Jacobi iteration, they are seldom used in the finite-element analysis of the Navier-Stokes equations. The reason is that these methods converge very

slowly, if at all, when the coefficient matrix results from a mixed formulation such as that used in the present analysis. The rate of convergence can be improved significantly by the introduction of an over-relaxation factor. Unfortunately, the optimum value of this parameter cannot be determined a priori and it does in fact change, sometimes drastically, from one iteration to the next. As such it is difficult to automate the process of selecting the relaxation parameter, so that for this class of methods to be competitive it is often necessary that the computations be performed in an interactive mode. This is usually considered to be simply too high a price to pay for the only real advantage offered by indirect methods - much lower central memory requirements.

As alluded to above, a direct (L-U decomposition) method was used here to solve linearizations of equation (2.34). Specifically, the out-of-core, profile algorithm by Hasbani and Engleman (40) was used to perform both the L-U decomposition and forward and backward substitutions. The solution procedure is described in great detail in the aforementioned reference and is not repeated here. However the terms "profile" and "out-of-core" will now be defined for the sake of completeness.

The term "profile" refers to the manner in which the

components of the coefficient matrix, $\underline{\underline{A}}$, are stored. Profile storage is one of the two schemes most widely used to take advantage of the sparse and banded nature of $\underline{\underline{A}}$. The other scheme is the so-called "banded" method. As is evident from Fig. 2.3, both of these storage modes achieve their increased efficiency over the full storage mode by taking advantage of the banded nature of $\underline{\underline{A}}$, and are of use because zeros outside the first and last non-zero elements in a given row (or column) do not need to be stored to effect a solution of equation 2.73.

In the bandwidth storage mode, the destination vectors (relationships between the local and global degrees of freedom) are scanned prior to assembly to determine a priori the distance between the first and last possible non-zero entries in each row of $\underline{\underline{A}}$. The largest such distance encountered, say NB, establishes the number of columns in the compacted array and is usually referred to as the "bandwidth" of $\underline{\underline{A}}$. Refer to Figs. 2.3 and 2.4. The reduction in the required storage for the assembled coefficient matrix using this procedure, namely (NEQ-NB)x(NEQ), is usually quite dramatic, for as pointed out by Zeinkiewicz (18), in many practical applications it is possible to assign the global node numbers so that NB is only 10 to 20 percent of NEQ. Furthermore, if the

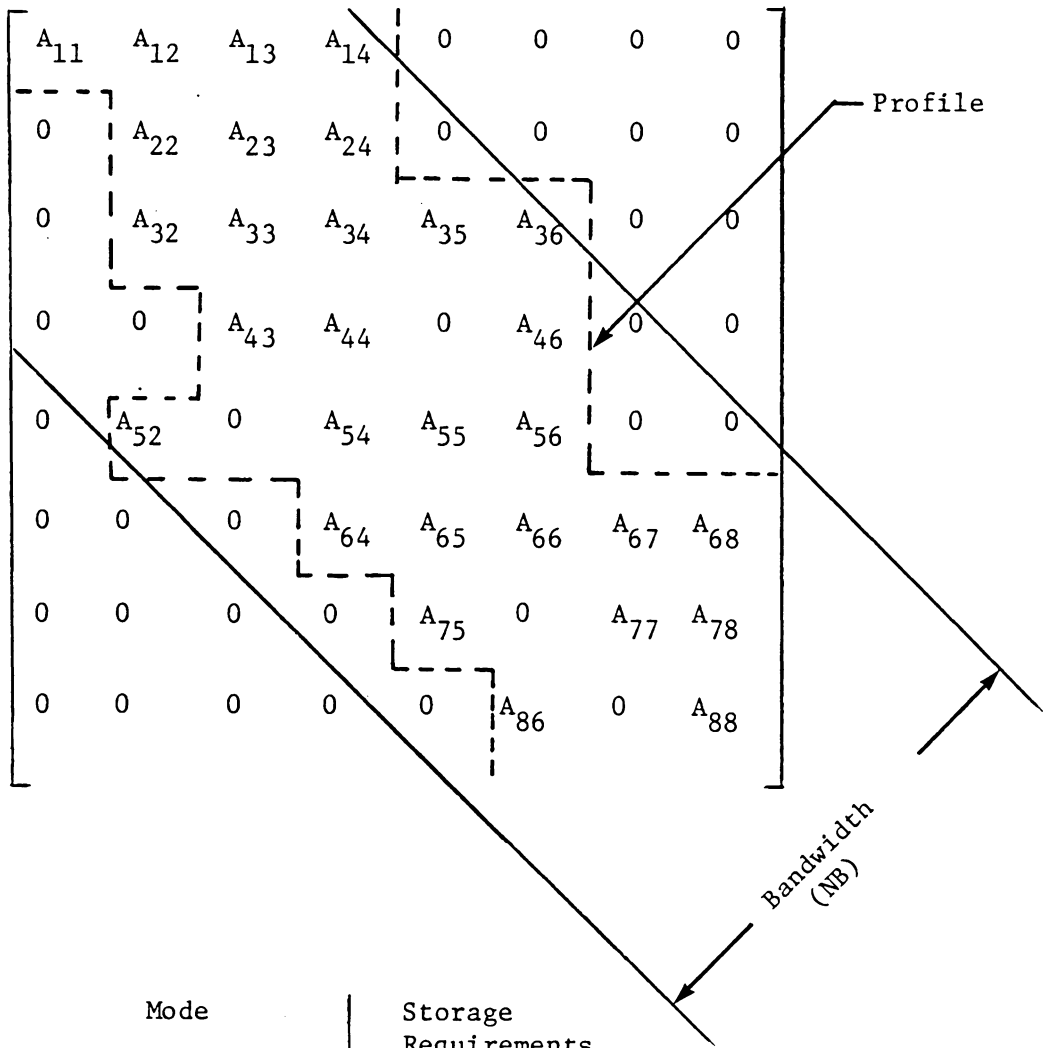

Mode	Storage Requirements
Full	64
Banded	56
Profile	41

Fig. 2.3. Typical structure of an assembled coefficient matrix.

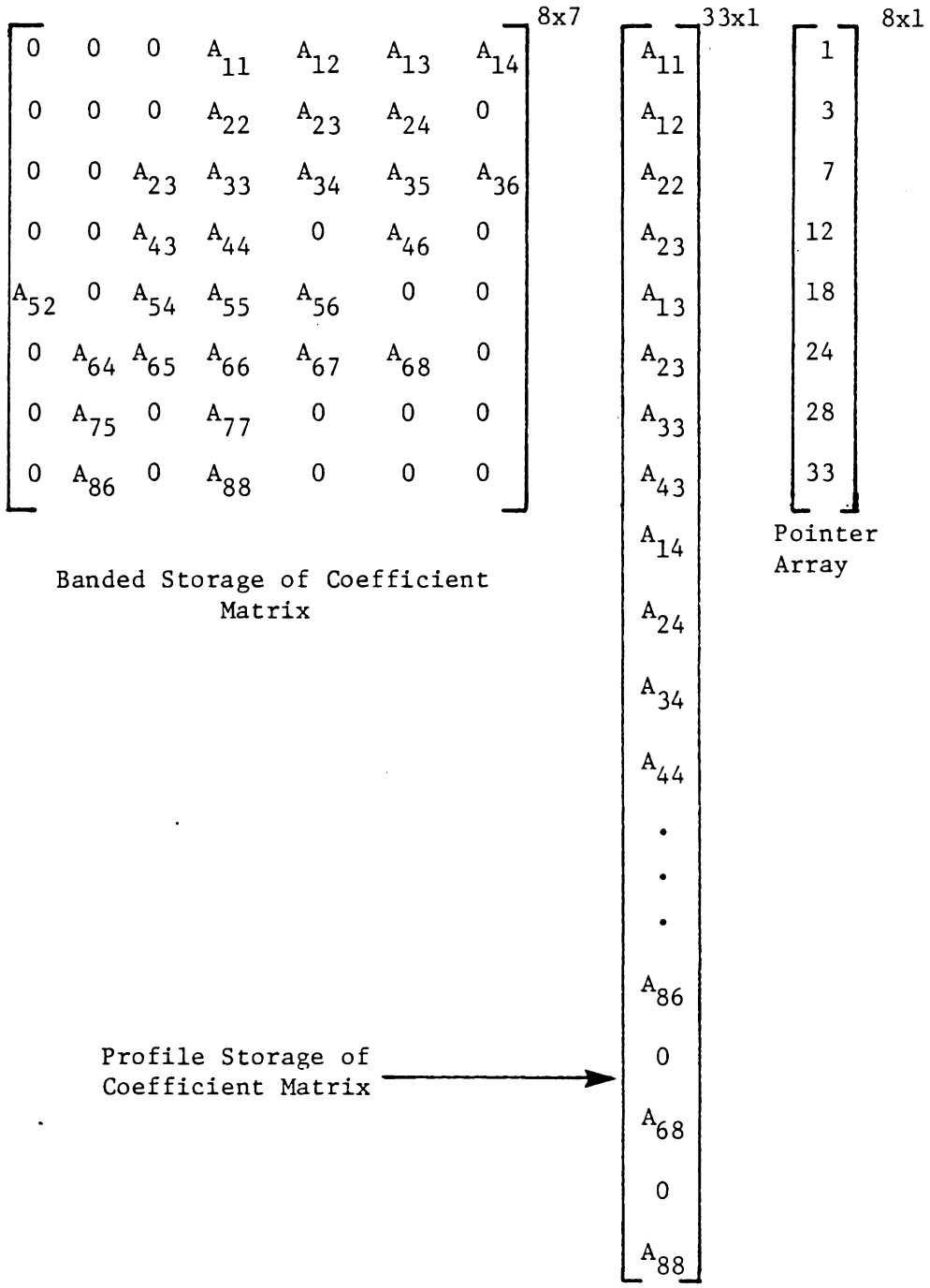

Fig. 2.4. Compact storage modes for the coefficient matrix in Fig. 2.3.

compacted global coefficient matrix is inverted using algorithms taylored to this storage mode, the number of operations and hence time required to obtain a solution to equation 2.73 can be reduced substantially. For more information on bandwith storage modes and solvers, refer to the extensive bibliography presented by Meyer in Reference 41.

As for the skyline or profile storage mode, it appears to be the most efficient compact storage scheme currently available. In this method the necessary portions of the upper triangular part of the assembled coefficient matrix are stored by columns and the lower triangular protion by rows in a one-dimensional array as shown in Fig. 2.4. A pointer array containing the whereabouts of the diagonal elements in the profile storage vector is also required. As is evident in Fig. 2.3 and noted by many authors, including Zeinkiewicz (18), this mode of storage has several advantages over bandwidth storage; (1) it always requires less storage (unless of course the matrix is diagonal in which case it requires the same amount); (2) the presence of a few very long non-zero rows or columns does not drastically alter the storage requirements, and (3) it enables both the triangular decomposition and substitution phases of the

solution procedure to be expressed in terms of vector dot products. This last fact is especially important if the computations are performed on vector oriented machines such as the CRAY or CDC-STAR.

"Out-of-core" profile solvers are algorithms in which the profile storage vector is stored in blocks on low speed auxiliary storage, usually disk files. The blocks are then brought into core, one at a time beginning with the first one, and reduced in sequence. This is possible, however, only if each block can be reduced using data contained either within that block or within previously reduced blocks. This in turn is made possible by the manner in which the elements of A are stored in the compacted storage array. The scheme depicted in Fig. 2.4 is an example of one such scheme that permits "blocking".

As mentioned above, the profile solver by Hasbani and Engleman (40) is used here. This solver was chosen over that provided by Bathe and Wilson (36) because it is an out-of-core solver that uses blocking to permit the solution of very large systems of equations, and over that given in Zeinkewicz (18) because it can be used to solve problems involving unsymmetric coefficient matrices. Again, refer to the aforementioned Reference 40 for the specific details of the algorithm used here.

3. RESULTS AND DISCUSSION

In the following sections, the results of calculations performed using the method described in the previous chapter are presented and discussed. For the sake of clarity and ease of interpretation, this material will be presented in two main segments. In the first, the results of an analysis of the flow over a backward facing step are presented and compared to both the results of other calculations and to experimental data. The second segment, on the other hand, is devoted entirely to the presentation of the results of a study to determine the cause and effects of the noticeable lack of development and skewness that characterized the experimental data both upstream of and at the step. Brief descriptions of all the cases studied are given in Table 3.1.

Before proceeding with the details of the various analyses, a few general comments are appropriate:

1. The Reynolds numbers quoted throughout this Section and presumed to characterize the various flows are based on the height of the step and the mean velocity just upstream of the step. This definition is consistent with that used by Ecer (4), Thomas (5), and Denham and Patrick (7) in reporting their results.
2. The nodal point coordinates and connectivity arrays for all the computational grids used in the

Table 3.1. Summary of the cases run.

Run No.	Mesh			Reynolds	Iterations		Run Time	Results	Description
	Elements	Nodes	Fig.	Number	S.S	N-R	CPU sec	Fig(s).	
101	50	231	3.2	73	2	5	63	3.6,3.9	Outflow boundary placement study.
102	64	291	3.3	73	2	5	81	3.7,3.10	
103	78	351	3.4	73	2	5	102	3.8,3.11	
201	312	1325	3.5	73	2	6	1062	3.12,3.13	Grid density study.
301	411	1749	3.14	125	5	5	1119	3.15,3.18	Analysis step flow at the higher
302	411	1749	3.14	191				3.16,3.19	Reynolds numbers.
303	411	1749	3.14	229	5	10	1724	3.17,3.20	
401	326	1401	3.23	73	2	6	641	3.25	
402	516	2199	3.24	125	5	5	1304	3.26	Analysis of the Denham and
403	516	2199	3.24	191	5	6	1439	3.27	Patrick (7) working section.
404	516	2199	3.24	229	5	8	1704	3.28	
501	551	2349	3.30	73	5	4	1254	3.31	
502	551	2349	3.30	125	5	5	1386	3.32	Analysis of an alternative
503	551	2349	3.30	191	5	7	1680	3.33	working section design.
504	551	2349	3.30	229	5	8	1823	3.34	
601	516	2199	3.24	229	5	7	1592	3.38	
602	516	2199	3.24	229	10	5	1927	3.39	Inflow boundary condition
603	516	2199	3.37	229	5	8	1733	3.40	sensitivity study.
701	516	2199	3.42	229	5	8	1712	3.44	Sensitivity to the geometry
702	516	2199	3.43	229	10	5	1925	3.45	of the fairing.

various analyses were generated by the semi-automatic mesh generator GEN2D by D. Pelletier (42).

3. The results of the various analyses are usually presented in the form of velocity-vector and u-velocity profile plots. The u-velocity profiles in these figures were constructed in segments by interpolating the appropriate nodal point data with the polynomials presented earlier in Table 2.1. This was done to be consistent with the assumed nature of the spatial variation of the velocity field. The v-velocity components were neither measured by Denham and Patrick nor reported by Ecer or Thomas. In the present work they are therefore relegated to the appendices.

4. The computational algorithm described in the previous chapter was programmed in FORTRAN H Extended and run on an IBM 3081 processor complex. For each run, the number of iterations and execution time required to ensure that the maximum relative difference between the computed velocities of two successive iterations was less than 0.01 percent are given in the aforementioned Table 3.1. In all the runs, the initial velocity estimates, $\underline{u}^{o}$, were set to zero.

3.1 Analysis of the Downstream Facing Step Flow

This section is devoted to presenting the results of an analysis of the laminar flow over the backward facing step depicted in Fig. 3.1. this particular geometry was chosen because it afforded direct comparisons with both the prior calculations by Ecer (4) and Thomas (5), and more importantly, with the experimental data by Denham and Patrick (7).

The experimental data of Denham and Patrick (7) consists of measurements of the u-velocity profiles at the step, 20 mm upstream of the step and 12, 30, 60, 90 and 120 mm downstream of the step. All the data reported was taken with a Laser-Doppler-Anemometer along the centerline of the tunnel, which had a step-height to width ratio of 1:20. The measurements were made at Reynolds numbers of 73, 125, 191 and 229.

In addition to displaying the geometric details of the step, Fig. 3.1 also shows the type and general location of the boundary conditions used throughout the analysis as:

$$\left.\begin{aligned} u &= 0 \\ v &= 0 \end{aligned}\right\} \quad \text{on the solid boundaries,}$$

$$\left.\begin{aligned} u &= u_i(y) \\ v &= 0 \end{aligned}\right\} \quad \text{on the inflow boundary,}$$

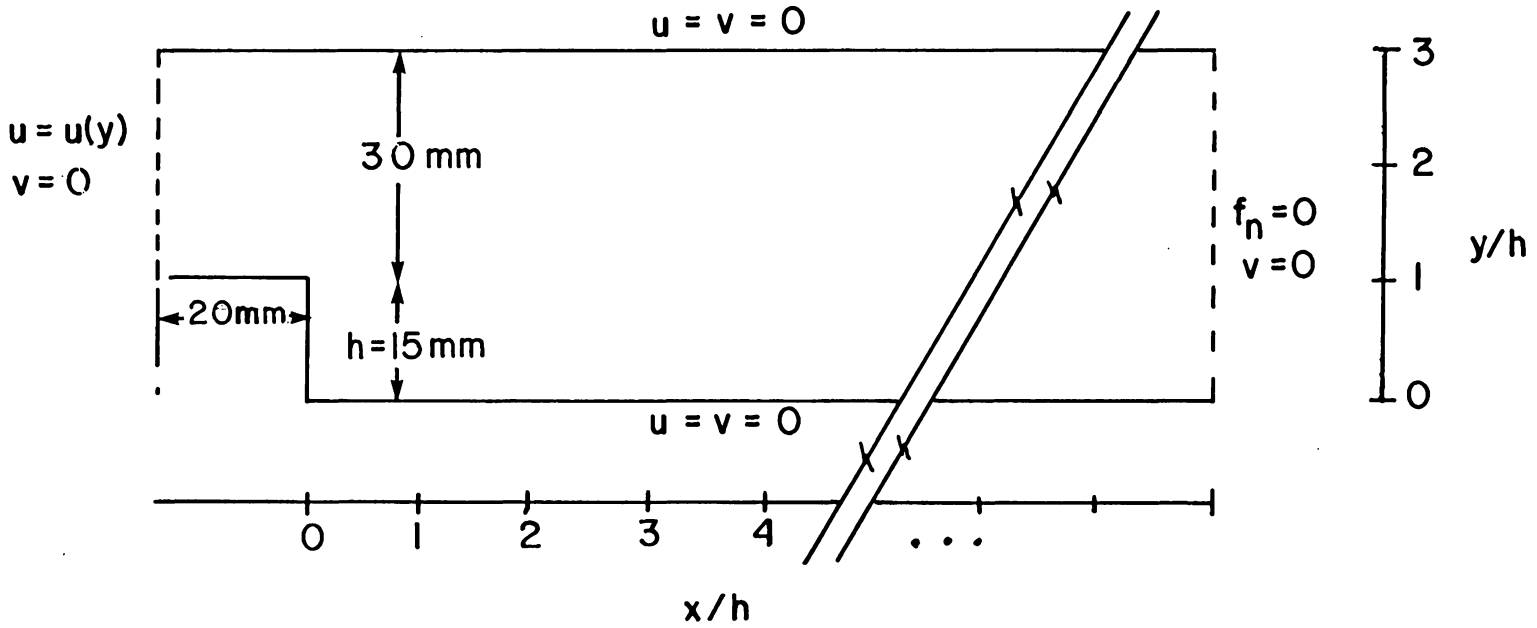

Fig. 3.1. Denham and Patrick (7) step.

and

$$\left.\begin{aligned} f_n &= 0 \\ v &= 0 \end{aligned}\right\} \quad \text{on the outflow boundary.}$$

where the $u_i(y)$ at the nodal points on the upstream boundary were obtained by linearly interpolating the experimental data measured at x/h = - 1.333, and the zero normal surface traction downstream boundary condition is as given earlier by equation (2.23), i.e.,

$$f_n = - P + 2\left(\frac{\mu}{Re}\right) \frac{\partial u}{\partial x} \quad .$$

In setting v = 0 on the outflow boundary, it was tacitly assumed that this boundary is located sufficiently far downstream of the step for this to indeed be the case. For two-dimensional internal flows like the one analyzed here, this is equivalent to stating that the downstream boundary must be located in a region where the flow field is fully developed. Unfortunately, the distance required for the flow to fully recover from the sudden expansion was unknown a priori. The approach taken here to resolve this paradox was to first choose a location for the outflow boundary and then examine the results of the ensuing calculation. If the results in the vicinity of the outflow boundary exhibited the characteristics normally associated with fully developed internal flows, e.g., parabolic u- and zero v-velocity profiles together

with zero spanwise and constant streamwise pressure gradients, the analysis was pronounced successful. If the results near the outflow boundary did not exhibit the proper trends, the computational domain was extended and another run was made. To illustrate this procedure, the intermediate as well as final results of the analysis of the step at Re = 73 will be presented. Only the final results will be given here for the three higher Reynolds number cases.

The computational grids used in the analysis of the flow over the step depicted in Fig. 3.1 at Re = 73 are presented in Figs. 3.2 through 3.5. As indicated by the streamwise location of the last column of nodal points in Fig. 3.2, the outflow boundary conditions were initially applied at x/h = 8.0. The results of run 101, which are presented and discussed below, indicated that the flow field was not fully developed in this exit plane. Thus it was necessary to repeat the calculations, this time using the finite element mesh depicted as Fig. 3.3, and subsequently that presented as Fig. 3.4. Note that in each of these cases, the computational domain was extended by adding new elements rather than expanding existing elements. This was done in an effort to permit the effects of boundary condition placement to be distinguished from those attributable to grid density. These latter effects were studied by comparing the results of run 103 with

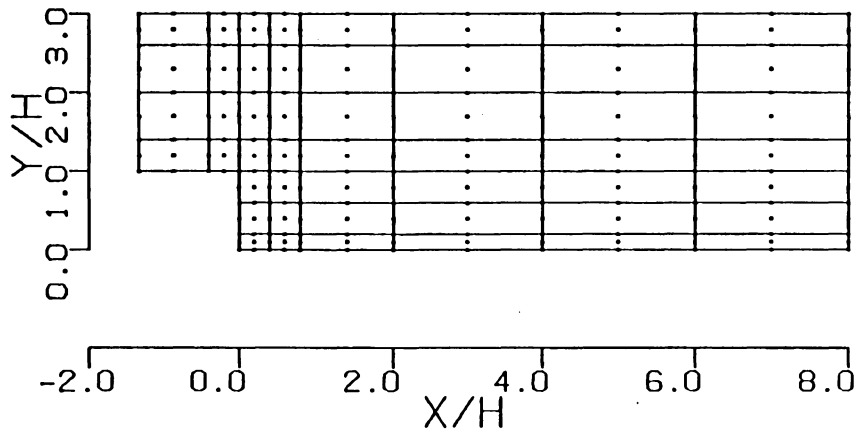

Fig. 3.2. Finite element mesh with 50 elements and 231 nodal points for run 101.

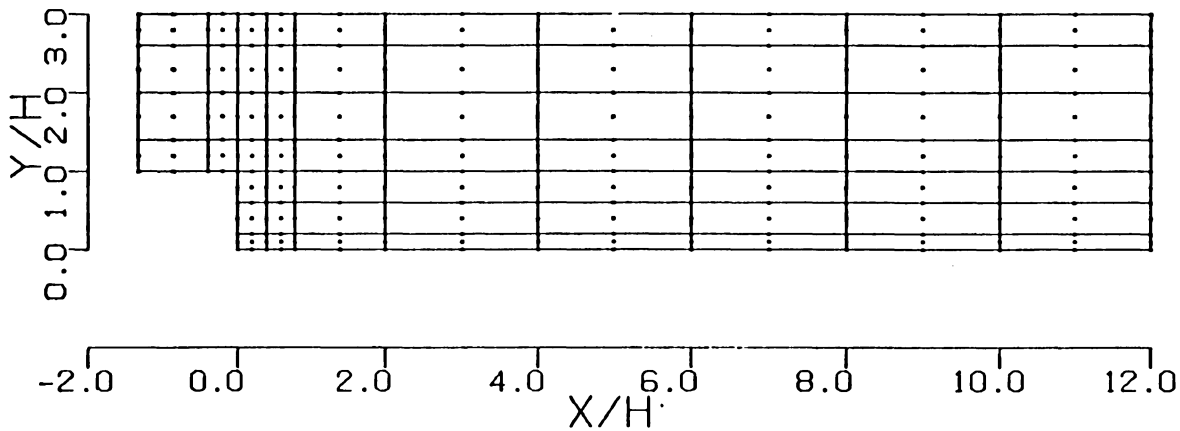

Fig. 3.3 Finite element mesh with 64 elements and 291 nodal points for run 102.

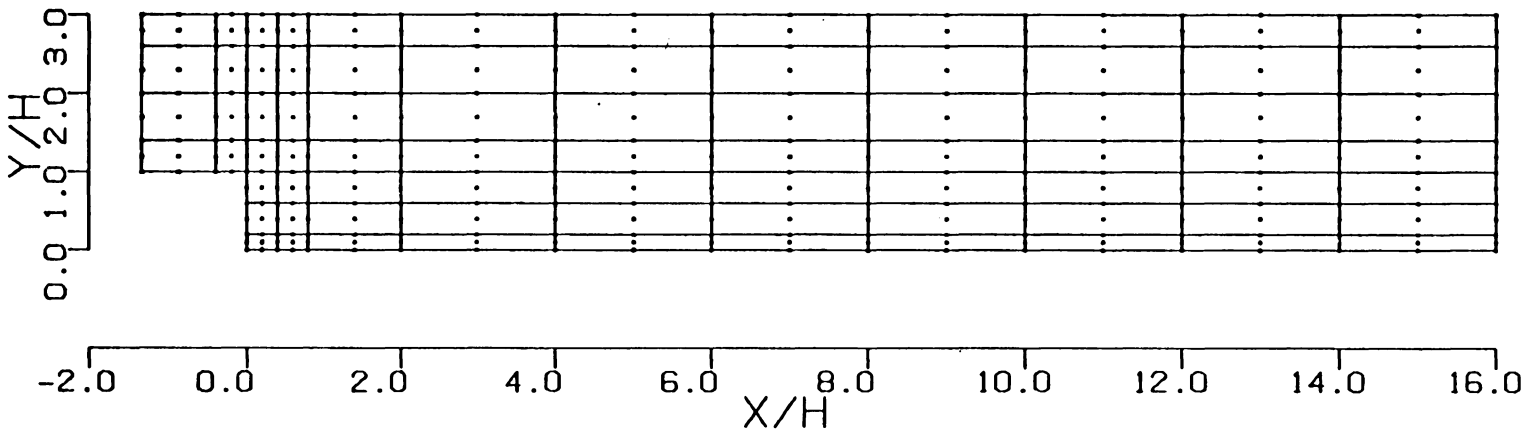

Fig. 3.4. Finite element mesh with 78 elements and 351 nodal points for run 103.

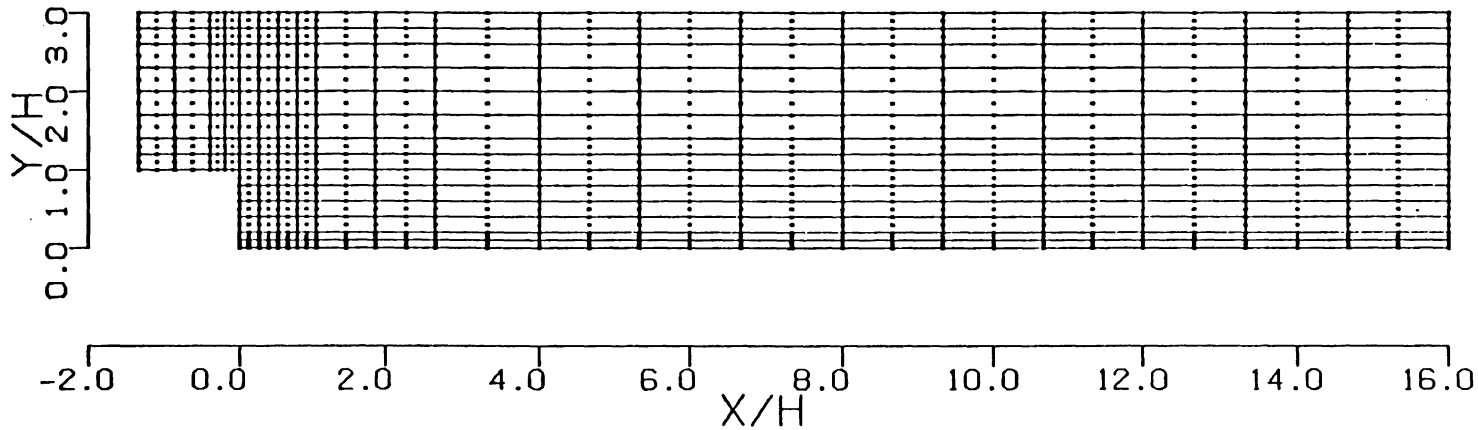

Fig. 3.5. Finite element mesh with 312 elements and 1325 nodal points for run 201.

those obtained using the mesh depicted in Fig. 3.5. This grid was obtained by dividing each of the elements of the mesh presented in Fig. 3.4 in half in each direction.

The results of the computations on the grids shown in Figs. 3.2 through 3.4 have been labeled the 100 series, and are presented in the form of Figs. 3.6 through 3.8, respectively. These figures illustrate not only the excellent overall agreement between the calculated and experimentally measured values, which are also shown in these figures, but also that despite the fact the velocity profiles continue to change until $x/h > 12$, as is evident in Fig. 3.8, the u-velocity profiles computed with the mixed downstream boundary conditions applied at $x/h = 8.0$ and 12.0 are virtually indistinguishable from those of run 103. That is, very good velocity estimates were obtained even when the mixed downstream boundary conditions were applied in a plane at which the outflow was clearly not fully developed. It is believed that this is so, because the v-velocity components even as far upstream as $x/h = 8.0$ are very small, as is evident in Table 3.2, so that little error is introduced into the calculations in the vicinity of the downstream boundary, and even less upstream.

The fact that the outflow is not fully developed until $x/h > 12$ is perhaps better illustrated by the contour plots of the dimensionless pressure coefficient shown

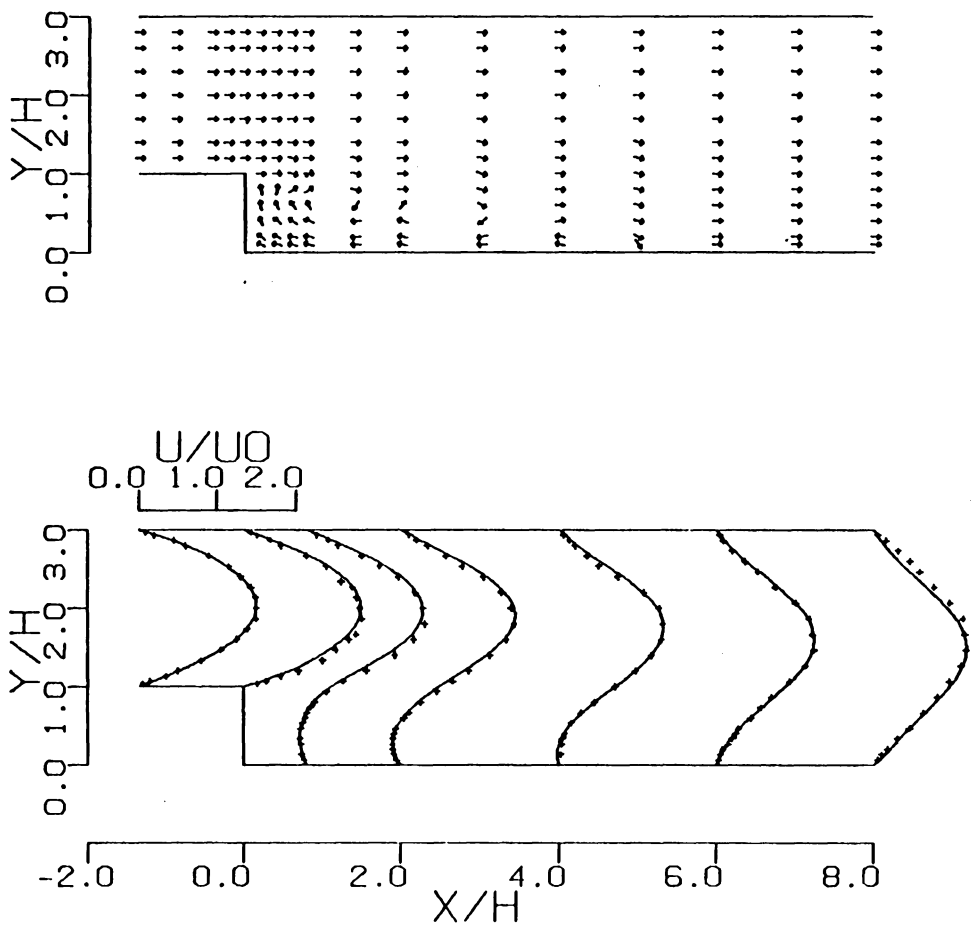

Fig. 3.6. Velocity-vectors and comparison of computed and experimental u-velocity profiles for the case with Re = 73 and the mixed downstream boundary conditions applied at x/h = 8.0. ___, run 101; +, Denham and Patrick (7).

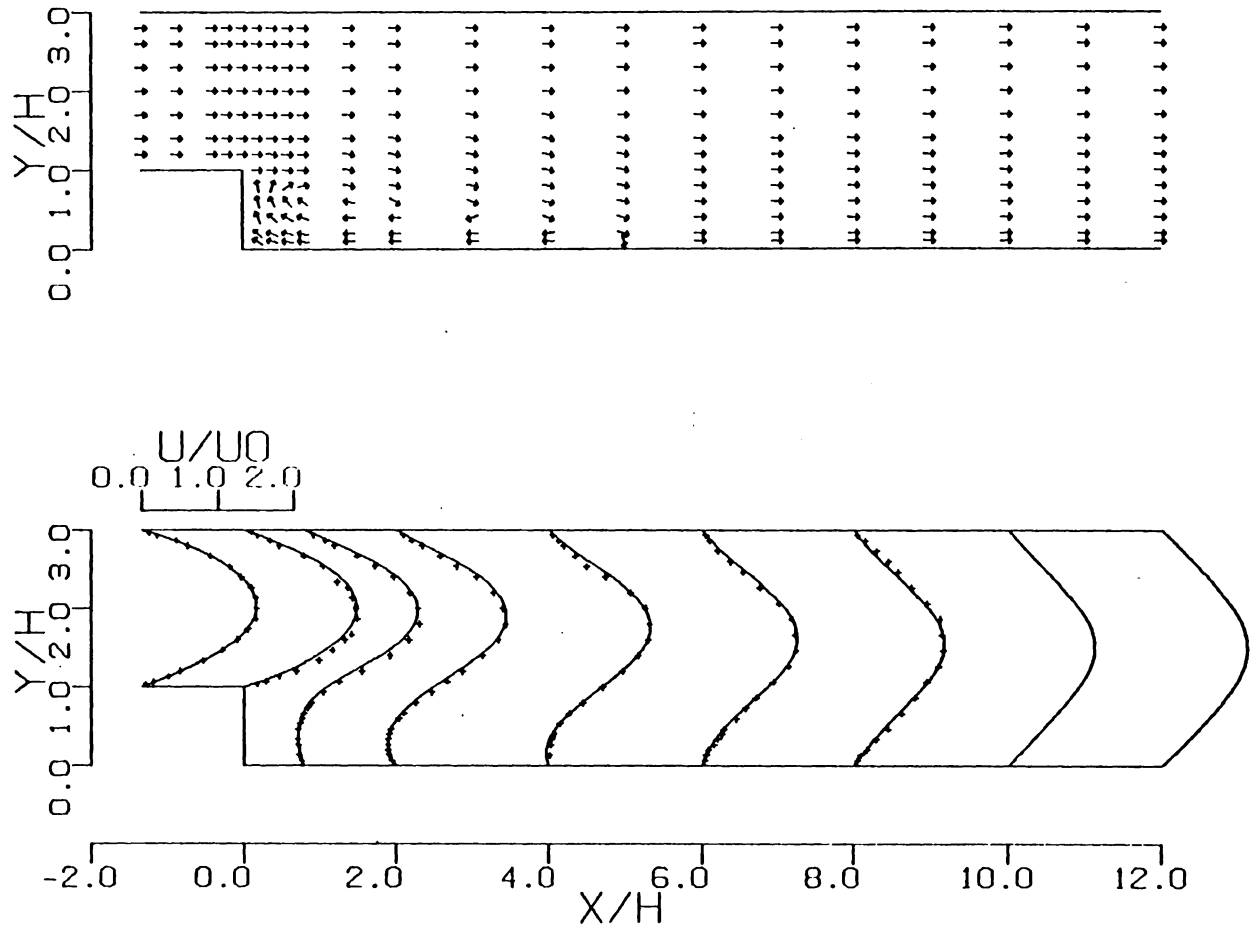

Fig. 3.7. Velocity-vectors and comparison of computed and experimental u-velocity profiles for the case with Re = 73 and the mixed downstream boundary conditions applied at x/h = 12.0. ___; + Denham and Patrick (7).

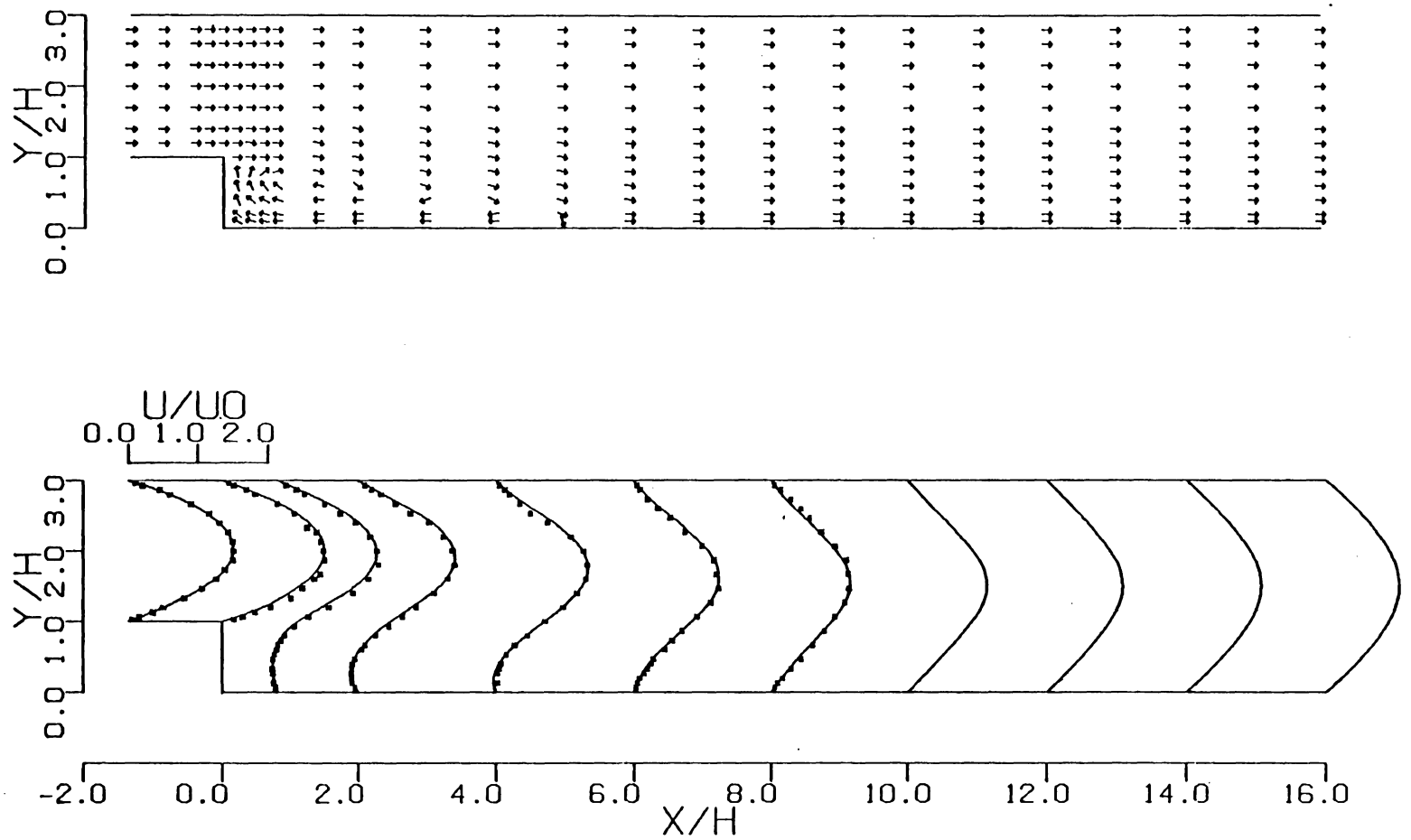

Fig. 3.8. Velocity-vectors and comparison of computed and experimental u-velocity profiles for the case with Re= 73 and the mixed downstream boundary conditions applied at x/h = 16.0. ___, run 103; +, Denham and Patrick (7).

Table 3.2. Computed (run 103) v-velocity components at x/h = 8.0.

y/h	v/U_o
0.0	0.0000
0.1	-0.0006
0.2	-0.0028
0.4	-0.0098
0.6	-0.0178
0.8	-0.0258
1.0	-0.0297
1.2	-0.0321
1.4	-0.0304
1.7	-0.0226
2.0	-0.0136
2.3	-0.0039
2.6	0.0001
2.8	0.0002
3.0	0.0000

in Figs. 3.9 through 3.11. These plots were generated by SURFACE II (43), and show that spanwise or y-direction pressure gradients exist until approximately 12.5 step-heights downstream of the step. They also show that while the general patterns exhibited by the contours remained relatively fixed from one run to the next, the values assigned to the contours shifted in the upstream direction as the computational domain was extended. This behavior was expected because specifying $v = 0$ on the downstream boundary implies that $\frac{\partial v}{\partial y} = 0$ also along this plane. This in turn implies $\frac{\partial u}{\partial x} = 0$ by virtue of the continuity equation, and reduces the traction free nornal boundary condition, Eq. (2.23), to $P = 0$ all along the downstream boundary. Since this is the only boundary on which the pressure is, in effect, specified, it acts as a reference value for the entire flow field. Thus, when the computational domain was extended, it shifted the position of the reference pressure and hence the entire pressure field.

As noted earlier, the effects of grid density were assessed by comparing the results of the runs using the grids depicted in Figs. 3.4 and 3.5. The results of run 103 were presented in the aforementioned Fig. 3.8, while those of the analysis on the grid in Fig. 3.5 are given in Fig. 3.12. Using the experimental data by Denham and Patrick (7) as a reference, it is evident from these figures that there is very little difference in the u-

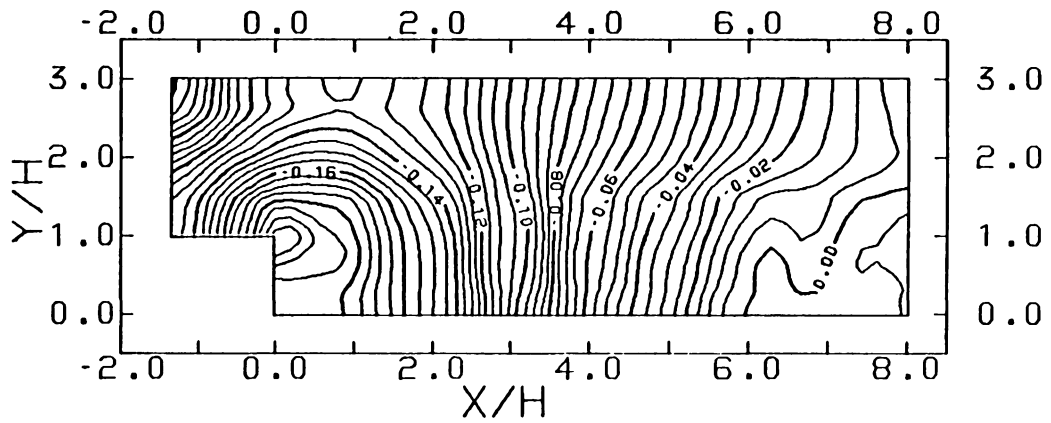

Fig. 3.9. Lines of constant pressure coefficient for run 101. Re = 73, with the mixed downstream boundary conditions applied at x/h = 8.0.

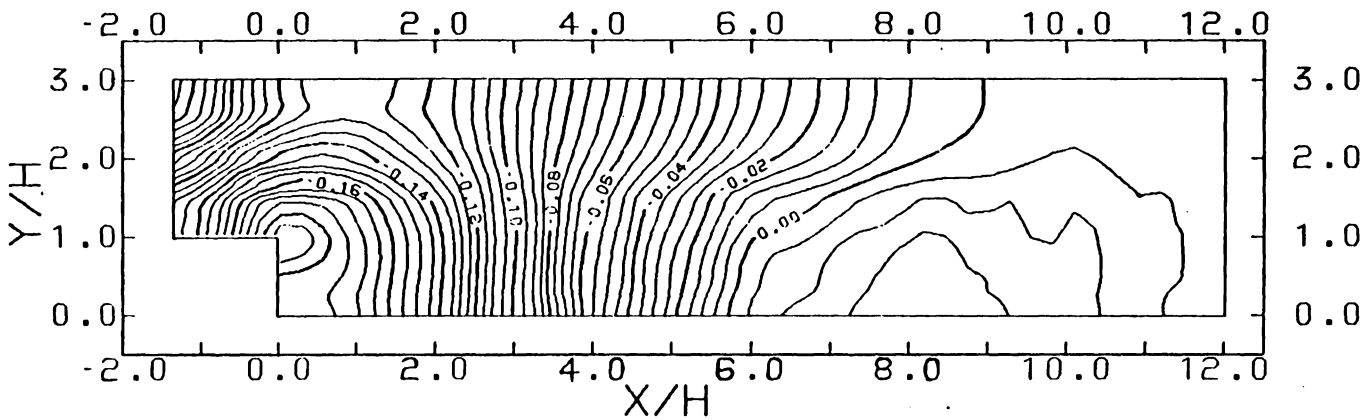

Fig. 3.10. Lines of constant pressure coefficient for run 102. Re = 73, with the mixed downstream boundary conditions applied at x/h = 12.0.

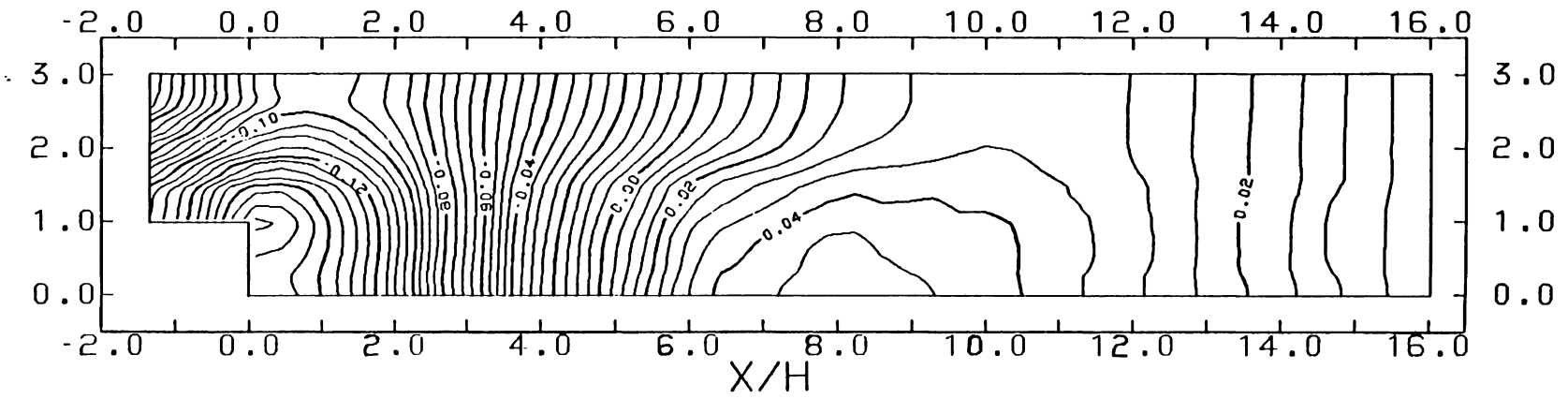

Fig. 3.11. Lines of constant pressure coefficient for run 103. Re = 73, with the mixed downstream boundary conditions applied at x/h = 16.0.

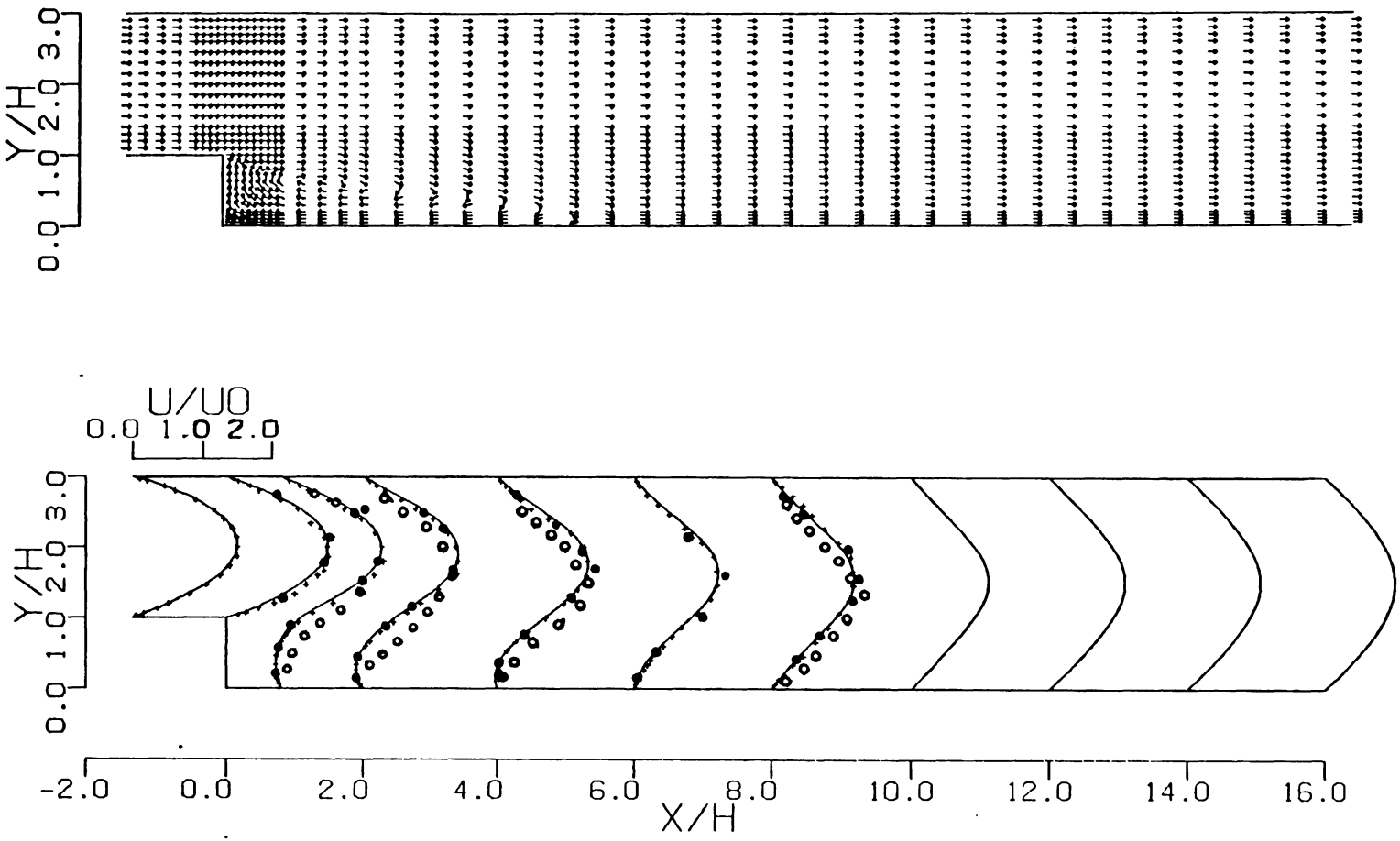

Fig. 3.12. Velocity-vectors and comparison of computed and experimental u-velocity profiles for the case with Re = 73 on the refined mesh (Fig. 3.5). ___, run 201; o, Ecer (4); •, Thomas (5); +, Denham and Patrick (7).

velocity components computed in runs 103 and 201, despite the fact that the number of grid points was increased from 351 to 1325. This can also be seen by comparing the entries in Table 3.3, which summarizes the results of runs 103 and 201 at corresponding nodal points in the plane x/h = 5.0. The relative differences in the values for u, given in this table are all less than 3 percent, while the v-velocity components are identical. This is viewed here as not only demonstrating the apparent convergence to the true solution, but also as showing that very good results for this problem can be obtained using the method described in Chapter 2 even on relatively crude grids such as those used in the 100 series runs. The results of run 201 are also presented in tabular form in Appendix A.1.

The only noticeable difference between the results of runs 103 and 201 appears in the contour plots of the dimensionless pressure coefficient, Figs. 3.11 and 3.13, respectively. As might be expected, increasing the number of grid points by nearly a factor of four resulted in much smoother contours, especially in the vicinity of the reattachment point.

All the runs at the higher Reynolds numbers were performed using the finite element mesh depicted in Fig. 3.14. The particular details of this mesh were arrived at using the iterative procedure described earlier in connection with the grids for the 100 series runs at Re=73, and

Table 3.3. Comparison of the results of runs 103 and 201 at x/h = 5.0

$\frac{y}{h}$	$\frac{U_{103}}{U_o}$	$\frac{U_{201}}{U_o}$	$\frac{\lvert U_{201}-U_{103}\rvert}{U_{201}} \times 100\%$	$\frac{V_{103}}{U_o}$	$\frac{V_{201}}{U_o}$	$\frac{V_{201}-V_{103}}{V_{201}} \times 100\%$
0.0	0.00	0.00	0	0.00	0.00	0
0.1	0.00	0.00	0	0.007	0.007	0
0.2	0.02	0.02	0	-0.01	-0.01	0
0.4	0.13	0.13	0	-0.02	-0.02	0
0.6	0.31	0.30	3	-0.04	-0.04	0
0.8	0.54	0.53	2	-0.06	-0.06	0
1.0	0.78	0.78	0	-0.07	-0.07	0
1.2	0.01	1.00	1	-0.09	-0.09	0
1.4	1.18	1.17	1	-0.09	-0.09	0
1.7	1.28	1.28	0	-0.08	-0.08	0
2.0	1.17	1.17	0	-0.07	-0.07	0
2.3	0.86	0.86	0	-0.04	-0.04	0
2.6	0.45	0.46	2	-0.01	-0.01	0
2.8	0.20	0.20	0	0.00	0.00	0
3.0	0.00	0.00	0	0.00	0.00	0

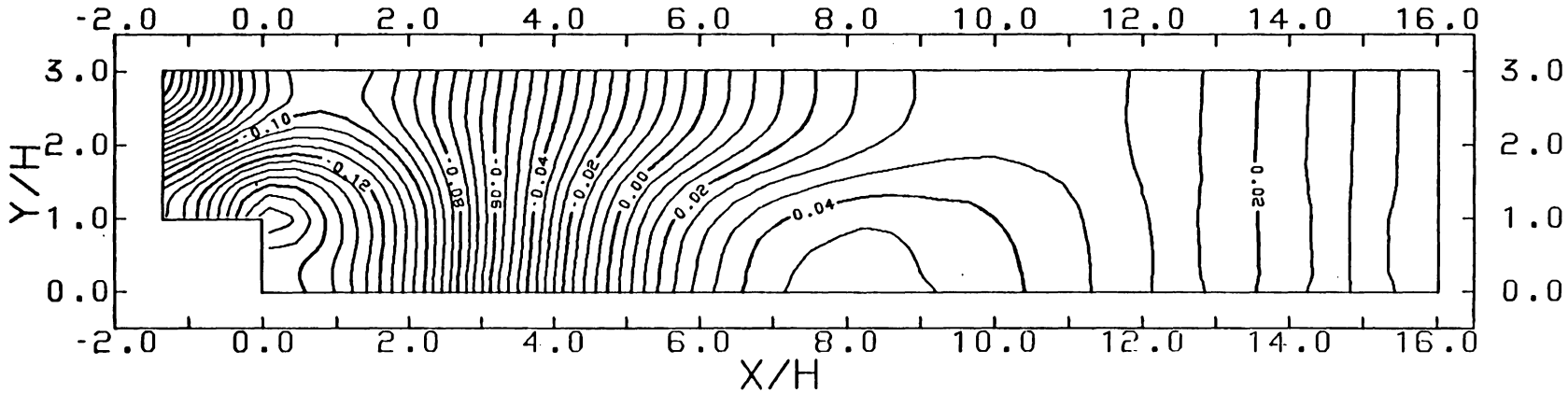

Fig. 3.13. Computed (run 201) lines of constant pressure coefficient for Re = 73 on the refined mesh (Fig. 3.5) with 312 elements and 1325 nodal points.

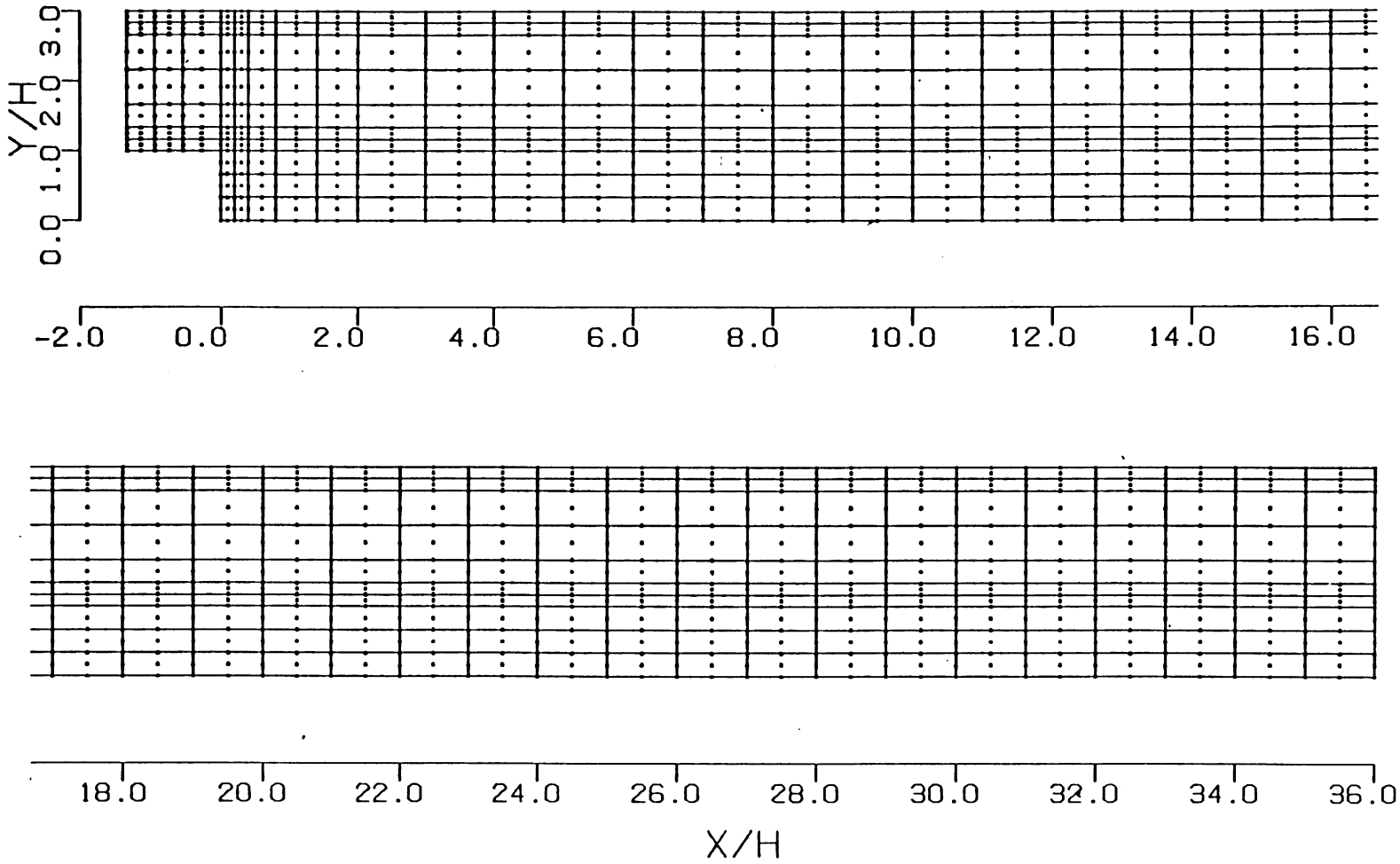

Fig. 3.14. Finite element mesh with 411 elements and 1749 nodal points for runs 301-303.

by extending the results of the grid density study.

The combination velocity-vector/u-profile plots for the runs at Reynolds numbers of 125, 191 and 229 are presented in Figs. 3.15 through 3.17, respectively. These figures also serve to illustrate the comparisons with not only the experimental data by Denham and Patrick (7), but also with the results of the earlier calculations by Ecer (4) and Thomas (5). Unfortunately, the results of the calculations by Ecer at Re=125 and 191, and by Thomas at Re=125 and 229 were not reported in the cited references, and as such do not appear in these figures. As was the case for the results of the analysis at Re=73, Figs. 3.15 through 3.17 clearly demonstrate that the method presented in Chapter 2 yields results that are in as good or better agreement with the available experimental data than those of the earlier calculations by either Ecer or Thomas. The computed nodal point velocity components and pressures for runs 301, 302 and 303 at selected streamwise locations are also presented in Appendices A.2, A.3 and A.4, respectively.

The plots of the dimensionless pressure coefficients for runs 301 through 303 are given in Figs. 3.18 through 3.20, respectively. As expected, the patterns formed by the contours in each of these plots are essentially the same as those that appeared in the pressure contour plots presented earlier, e.g., Fig. 3.13. This is especially

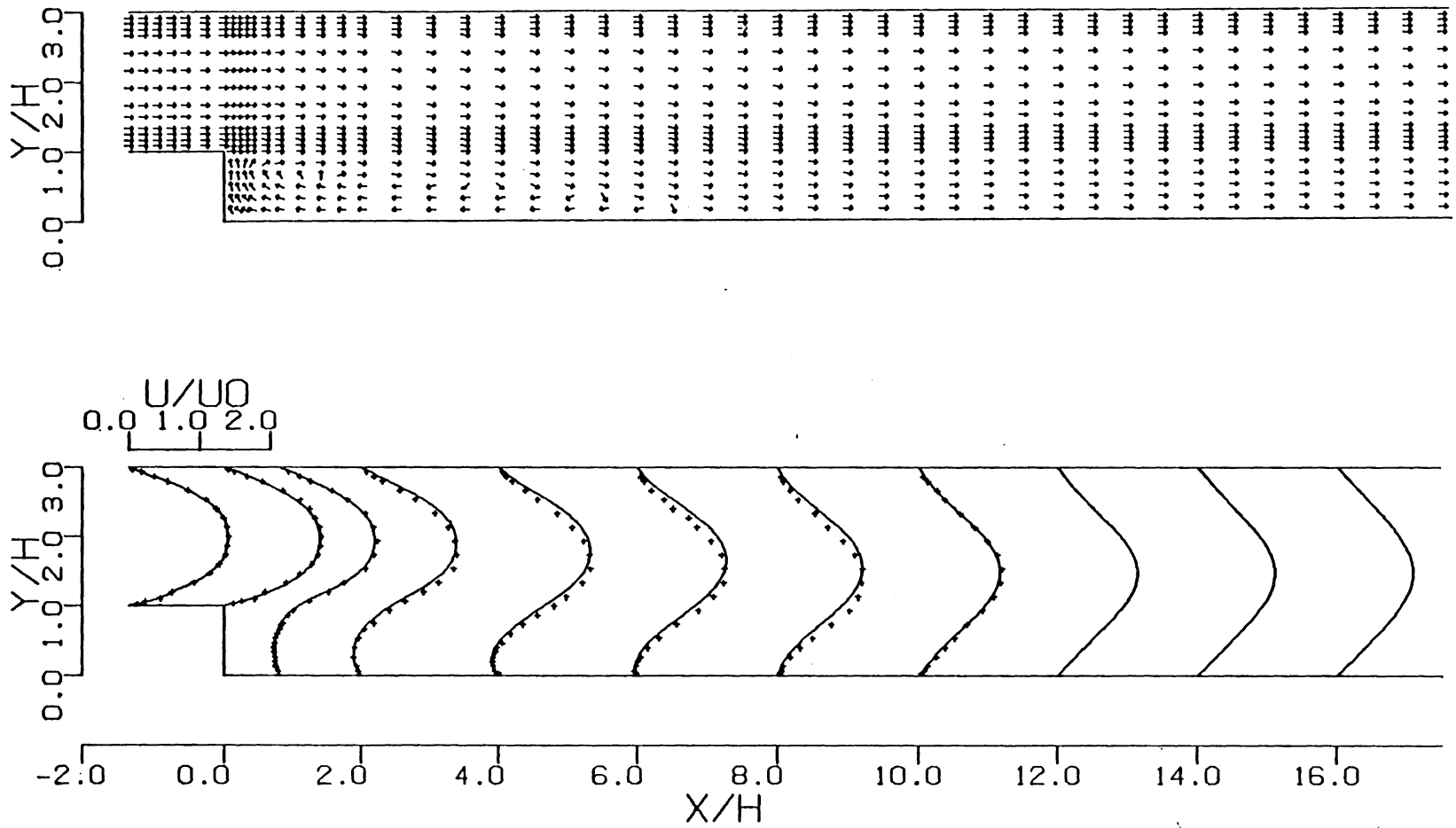

Fig. 3.15. Velocity-vectors and comparison of experimental and computed u-velocity profiles for the case with Re = 125 on the mesh depicted in Fig. 3.14. ___, run 301; +, Denham and Patrick (7). Continued on next page.

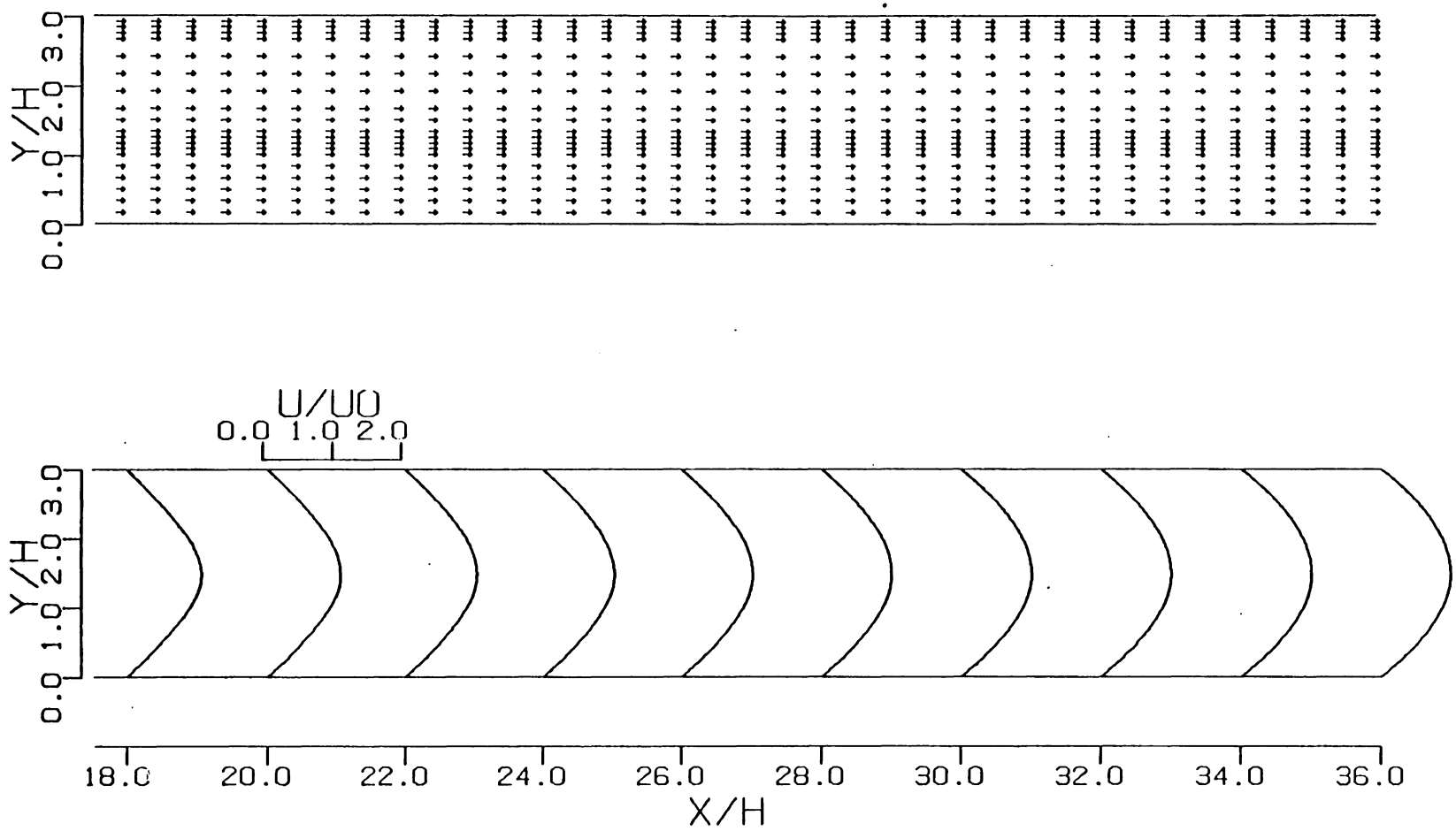

Fig. 3.15. (continued)

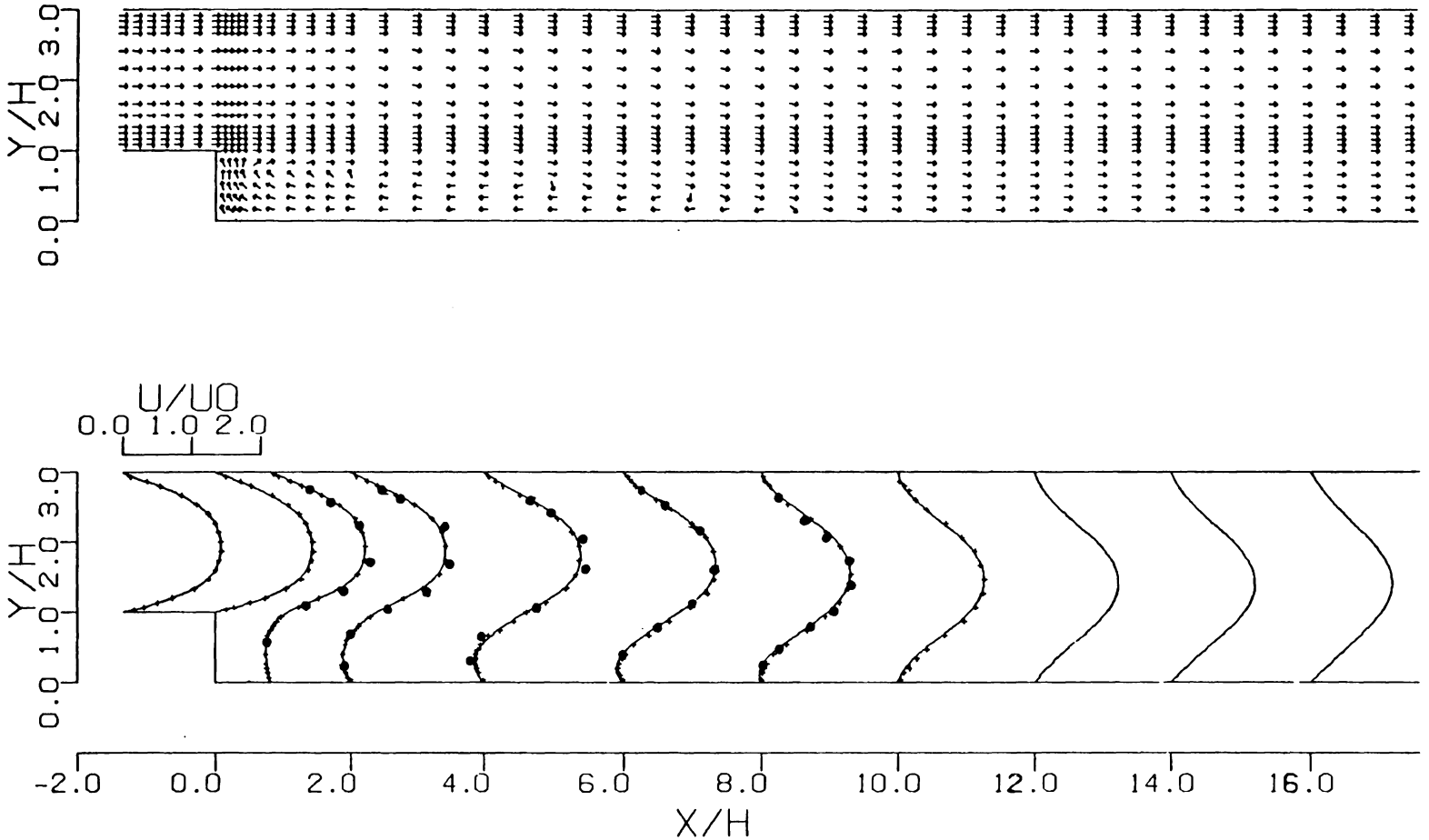

Fig. 3.16. Velocity-vectors and comparison of experimental and computed u-velocity profiles for the case with Re = 191 on the mesh depicted in Fig. 3.14. ____, run 302; •, Thomas (5); + Denham and Patrick (7). Continued on next page.

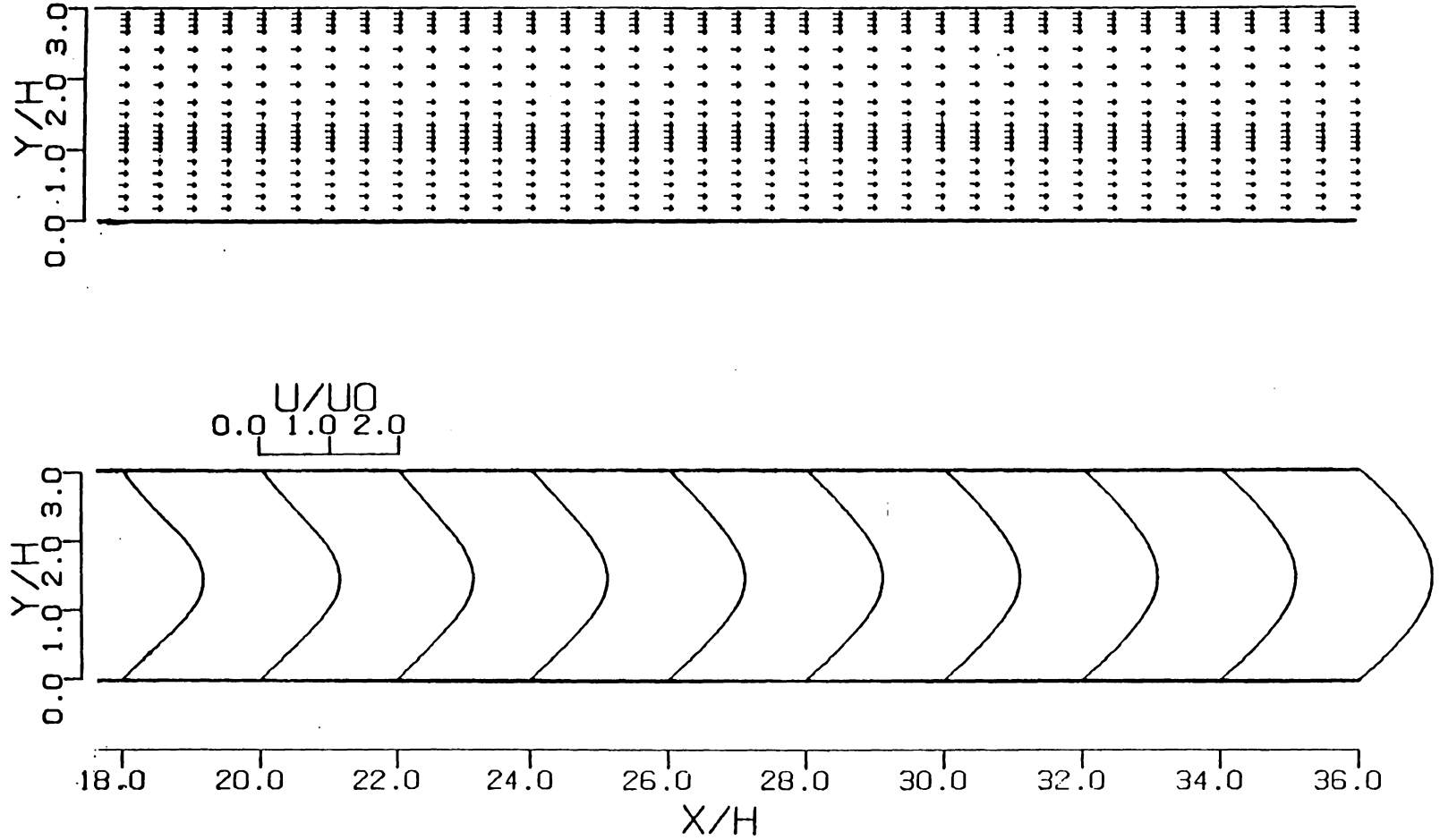

Fig. 3.16 (continued)

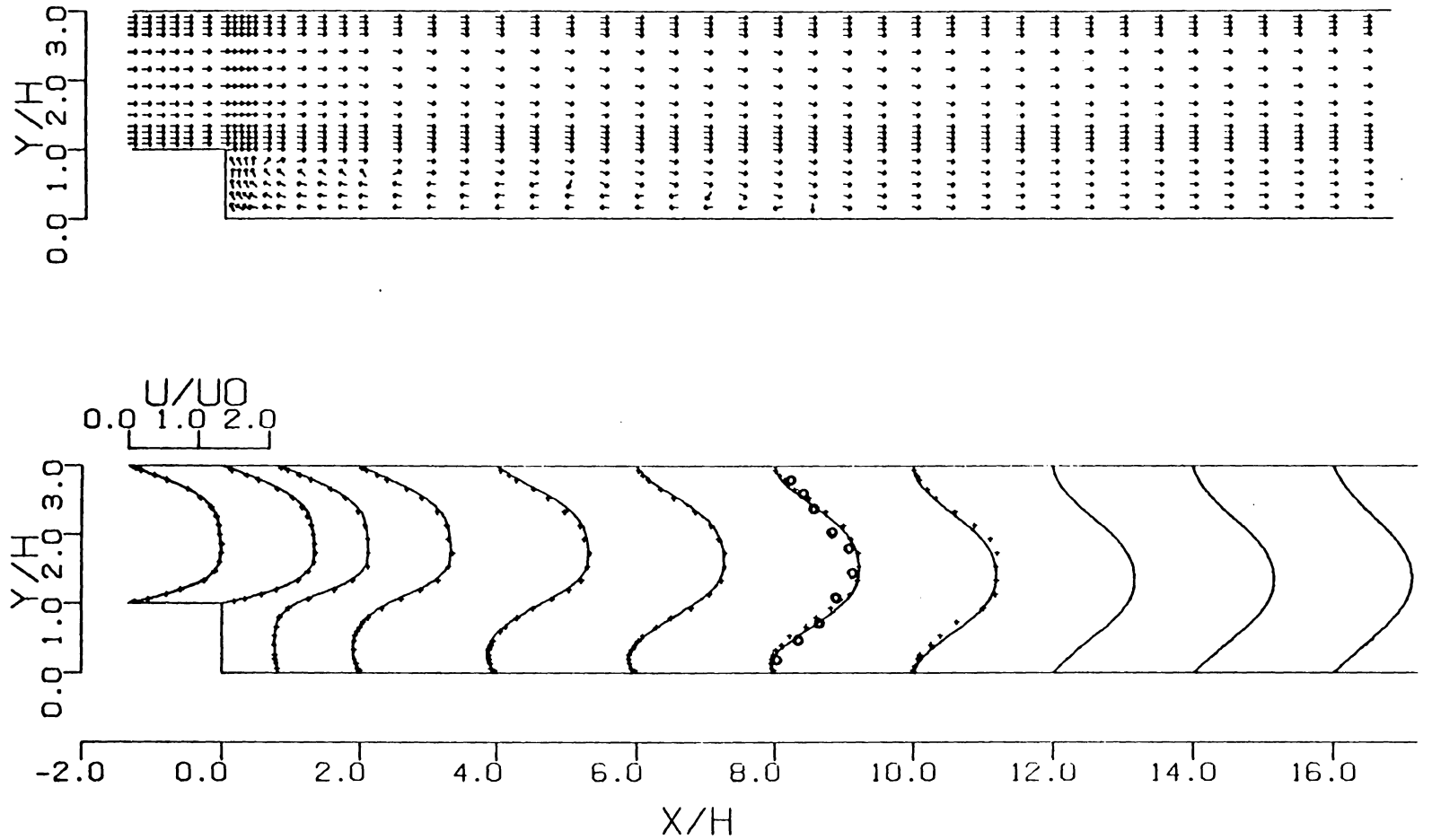

Fig. 3.17. Velocity-vectors and comparison of experimental and computed u-velocity profiles for the case with Re = 229 on the mesh depicted in Fig. 3.14. ___, run 303; o, Ecer (4); +, Denham and Patrick (7). Continued on next page.

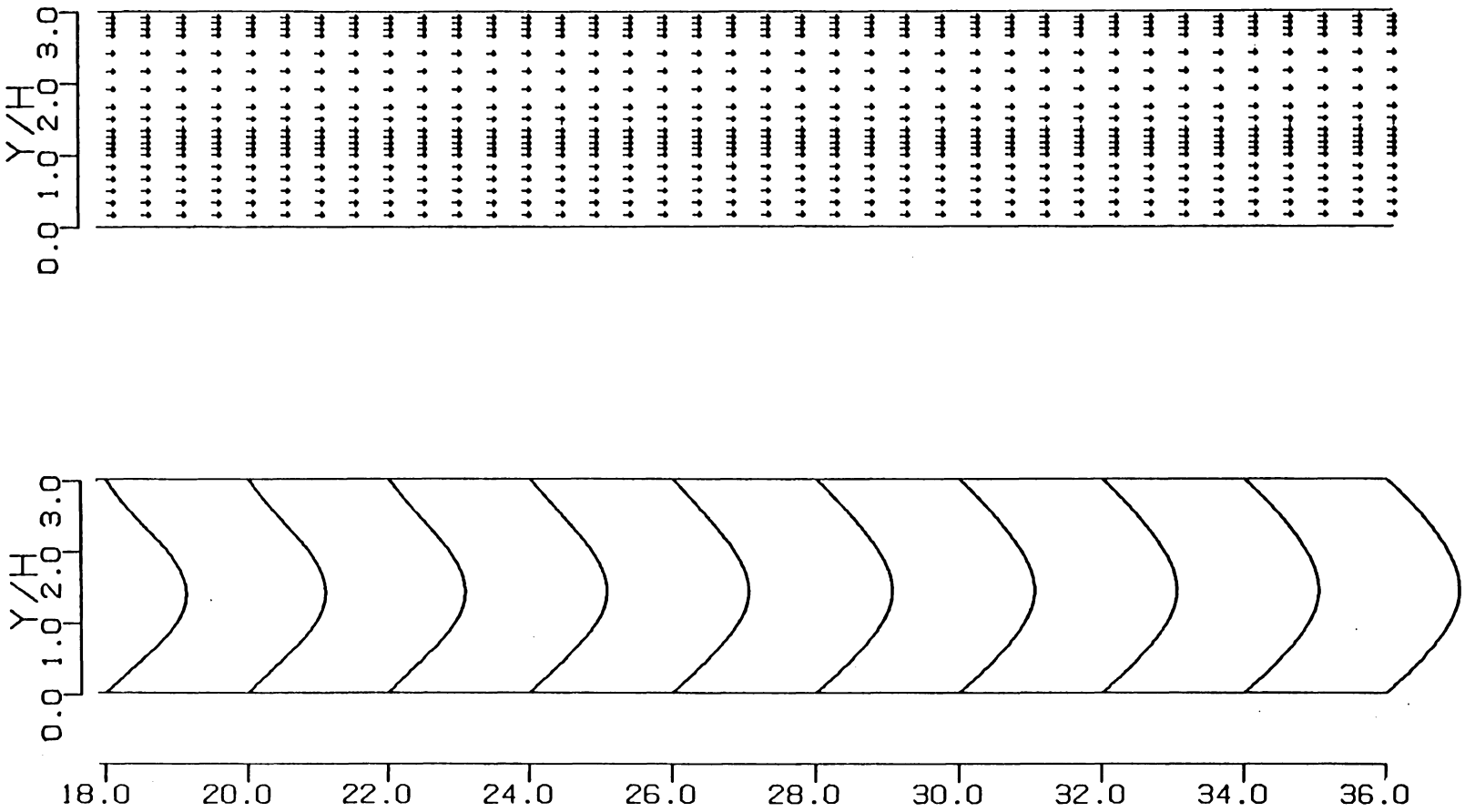

Fig. 3.17. (continued)

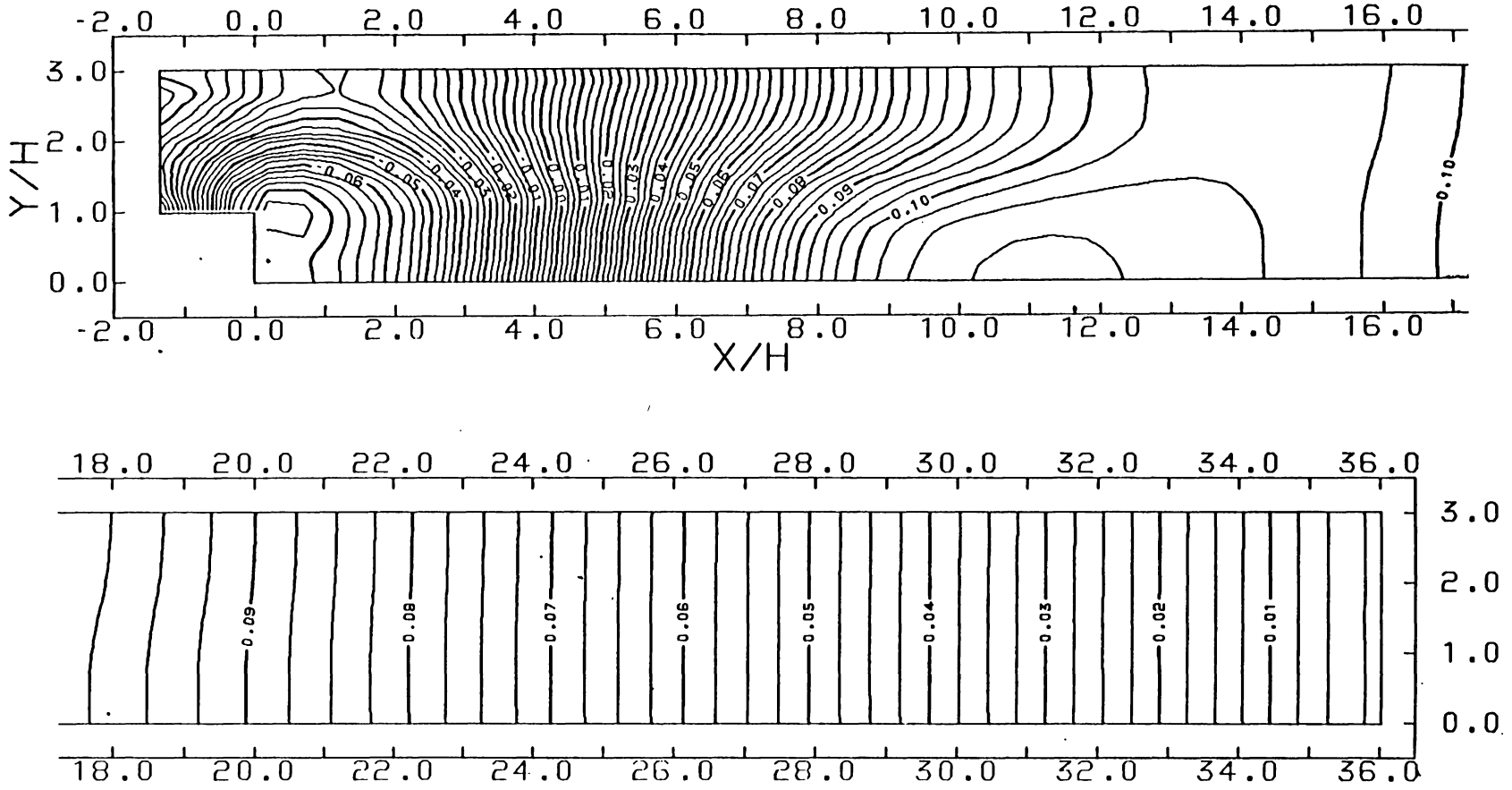

Fig. 3.18. Computed (run 301) lines of constant pressure coefficient for the Re = 125 case.

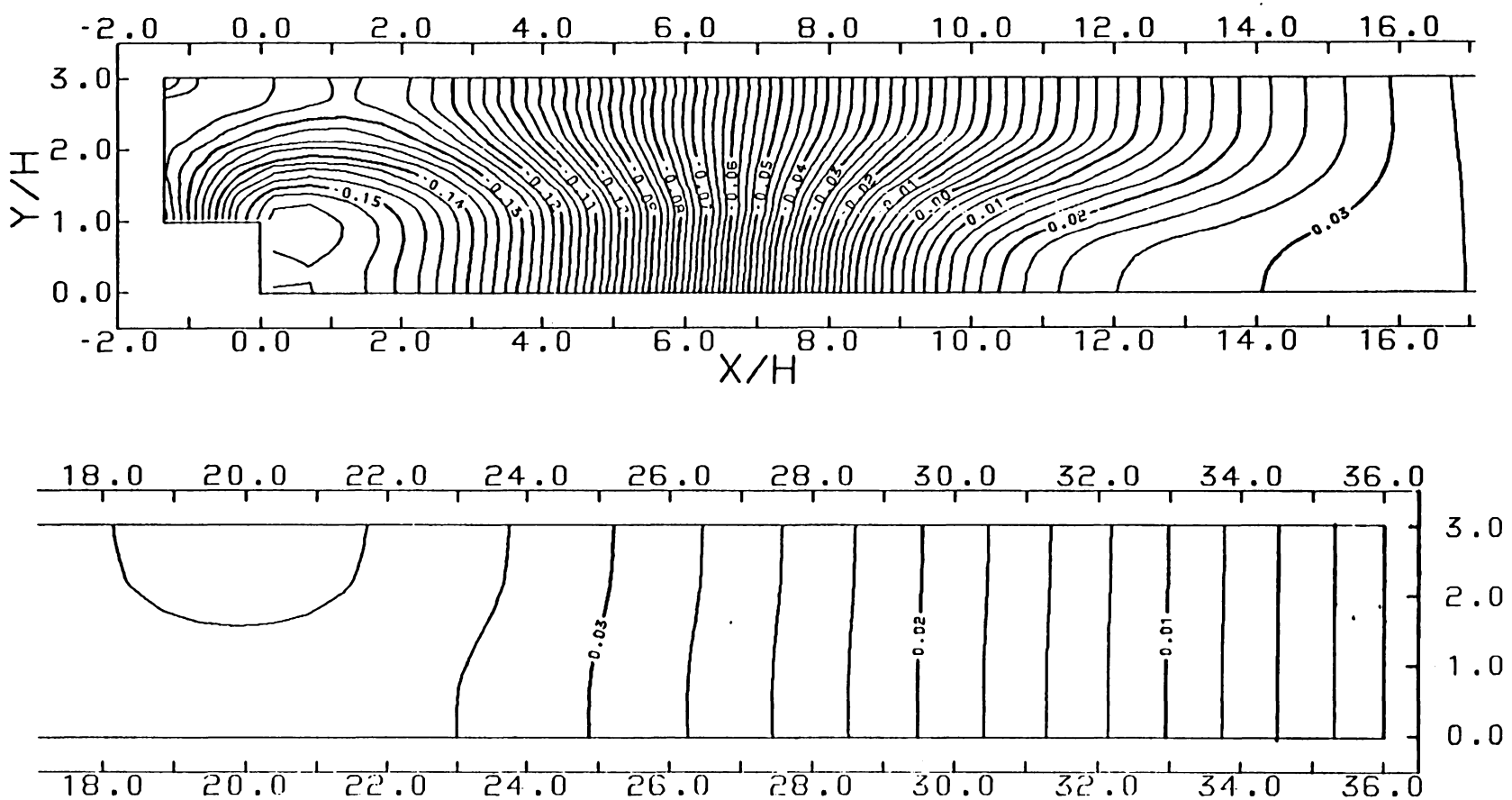

Fig. 3.19. Computed (run 302) lines of constant pressure coefficient for the Re = 191 case.

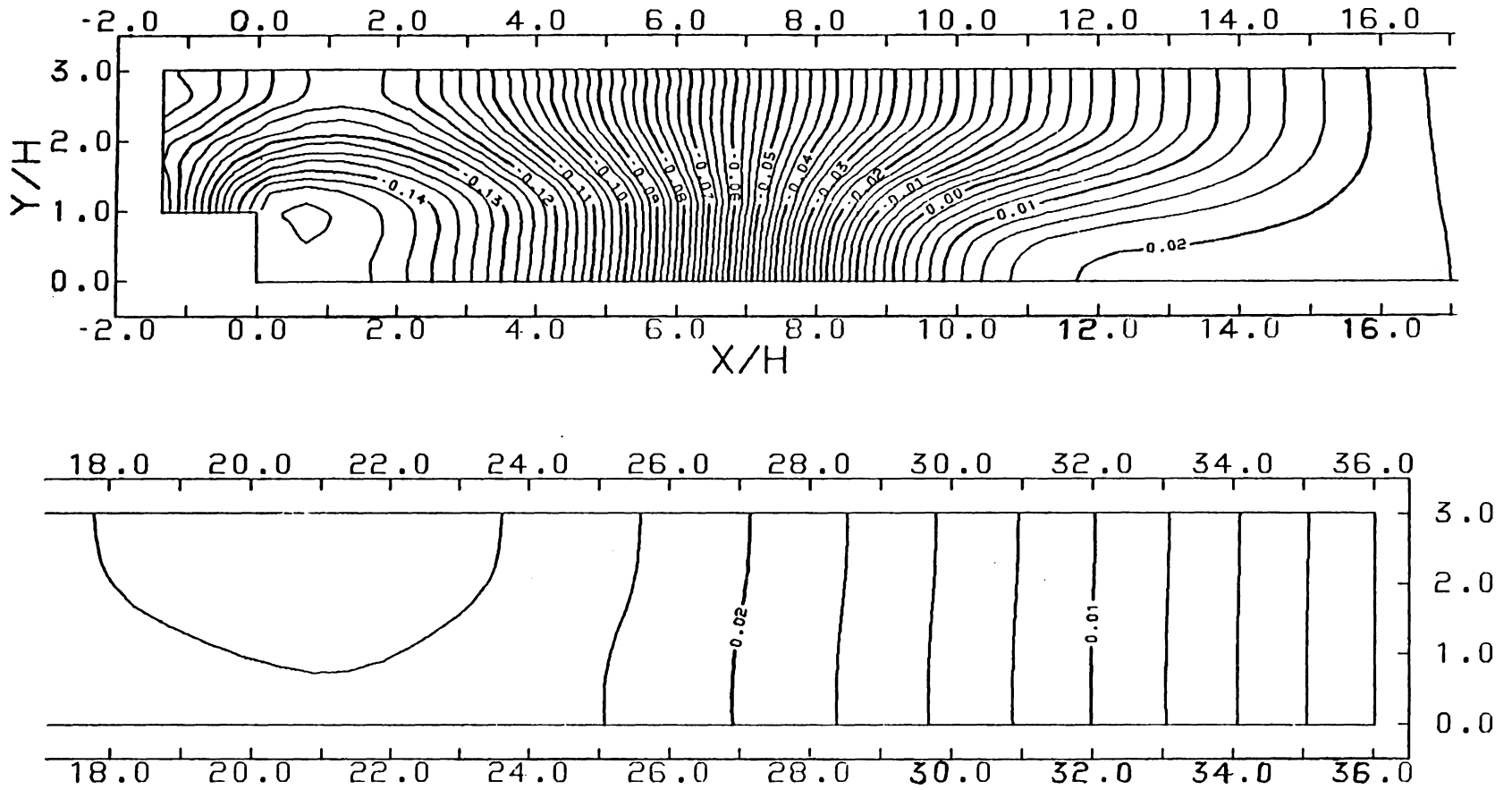

Fig. 3.20. Computed (run 303) lines of constant pressure coefficient for the Re = 229 case.

true in the vicinity of the outflow boundary, where the patterns clearly indicate that in each case the outflow boundary conditions were placed in a region where the flow field was fully developed.

3.2 Analysis of the Initial Plane of Experimental Data

As is evident in Figs. 3.15 through 3.17 and noted by Denham and Patrick (7), the experimental profiles that served here as inflow boundary conditions exhibit a noticeable lack of development and skewness that becomes more pronounced with increasing Reynolds number. Denham and Patrick suggested that the skewness was due to the asymmetry of the contraction leading up to the step rather than some upstream influence of the step itself. Refer to Fig. 3.21. To test this hypothesis and at the same time determine the sensitivity of the flow field downstream of the step to the degree of development of the inflow boundary data, the flows through two different flow sections, one as used by Denham and Patrick and the other with the step moved far downstream, were predicted and compared. The purpose, procedure and results of each of the analyses will now be presented and discussed.

3.2.1 Analysis of the Denham and Patrick Working Section

The Denham and Patrick (7) working secton is depicted in Fig. 3.21. This section was analyzed to both demon-

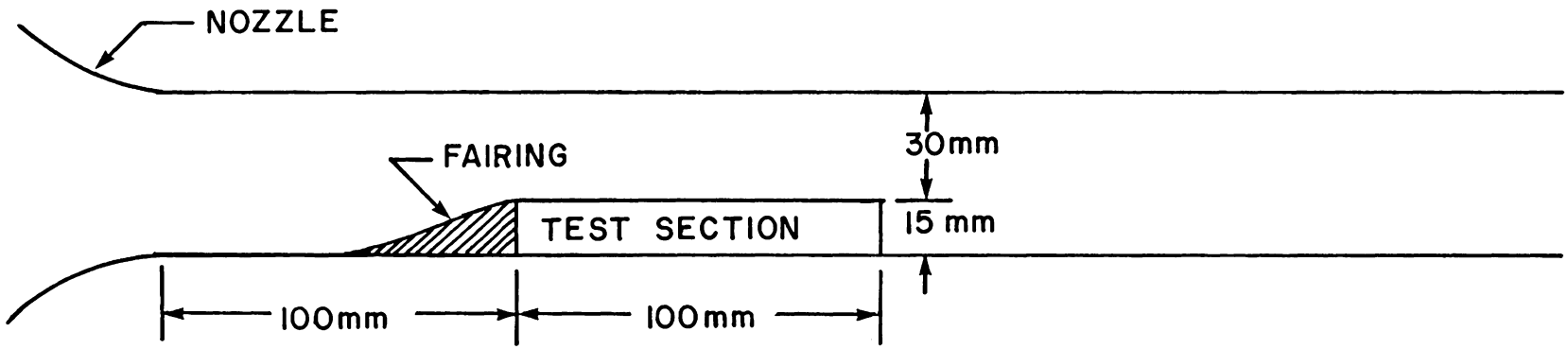

Fig. 3.21. The Denham and Patrick (7) working section.

strate the feasibility of modeling an entire working section using the method described in Chapter 2, and to establish a basis for later comparisons.

The four runs that comprised this analysis, runs 401 through 404, were made at Reynolds numbers of 73, 125, 191 and 229, respectively, using the inflow boundary conditions $v = 0$ and $u = g(y)$, where $g(y)$ is as depicted in Fig. 3.22. Admittedly, this profile is perhaps overly simplified. However it produces the same mass average velocities in the vicinity of the step as those reported by Denham and Patrick, and it does have at least some basis in theory-the central core of the flow field at the exit plane of a properly designed nozzle is characterized by constant u- and zero v-velocity components.

The finite element grid used in run 401 is depicted in Fig. 3.23, while the extended grid depicted in Fig. 3.24 was used in the three higher Reynolds number runs in this series. In this vein it should be noted that the details of the manner in which the step test section was faired into the floor of the tunnel were not available. However, as will be shown in secton 3.2.3, the flow field at and downstream of the step does not appear to be very sensitive to this parameter, provided of course the transition is not so abrupt that it induces separation.

The combination velocity-vector/u-velocity profile plots for runs 401 through 404 are presented in Figs. 3.25

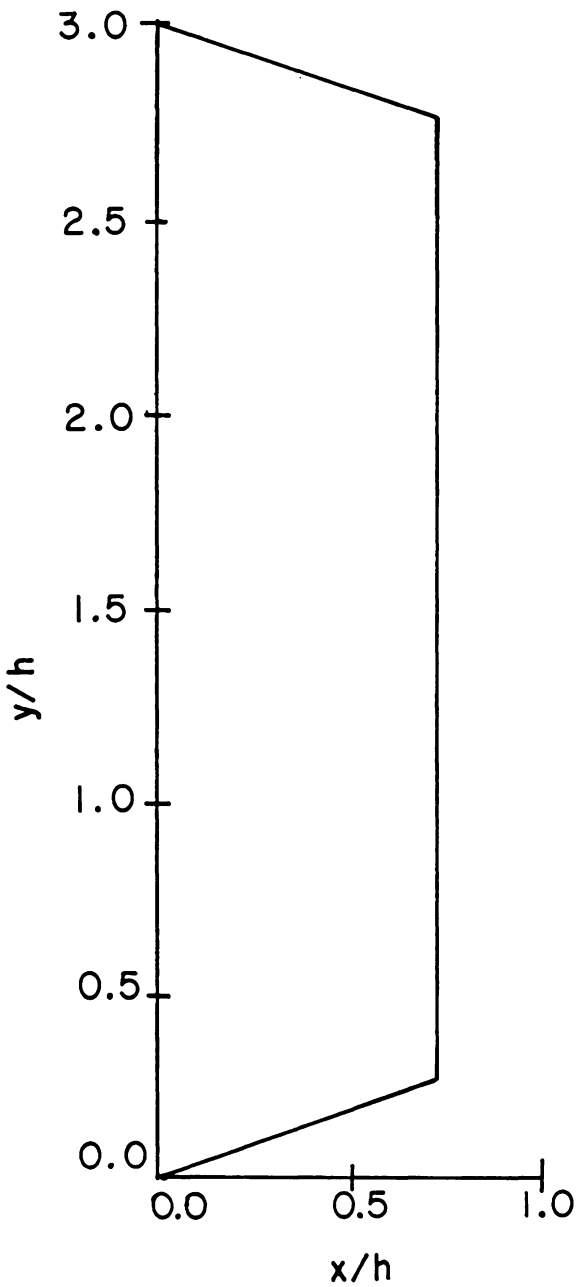

Fig. 3.22. Assumed inlet velocity profile for the analysis of the Denham and Patrick (7) working section (runs 401-404).

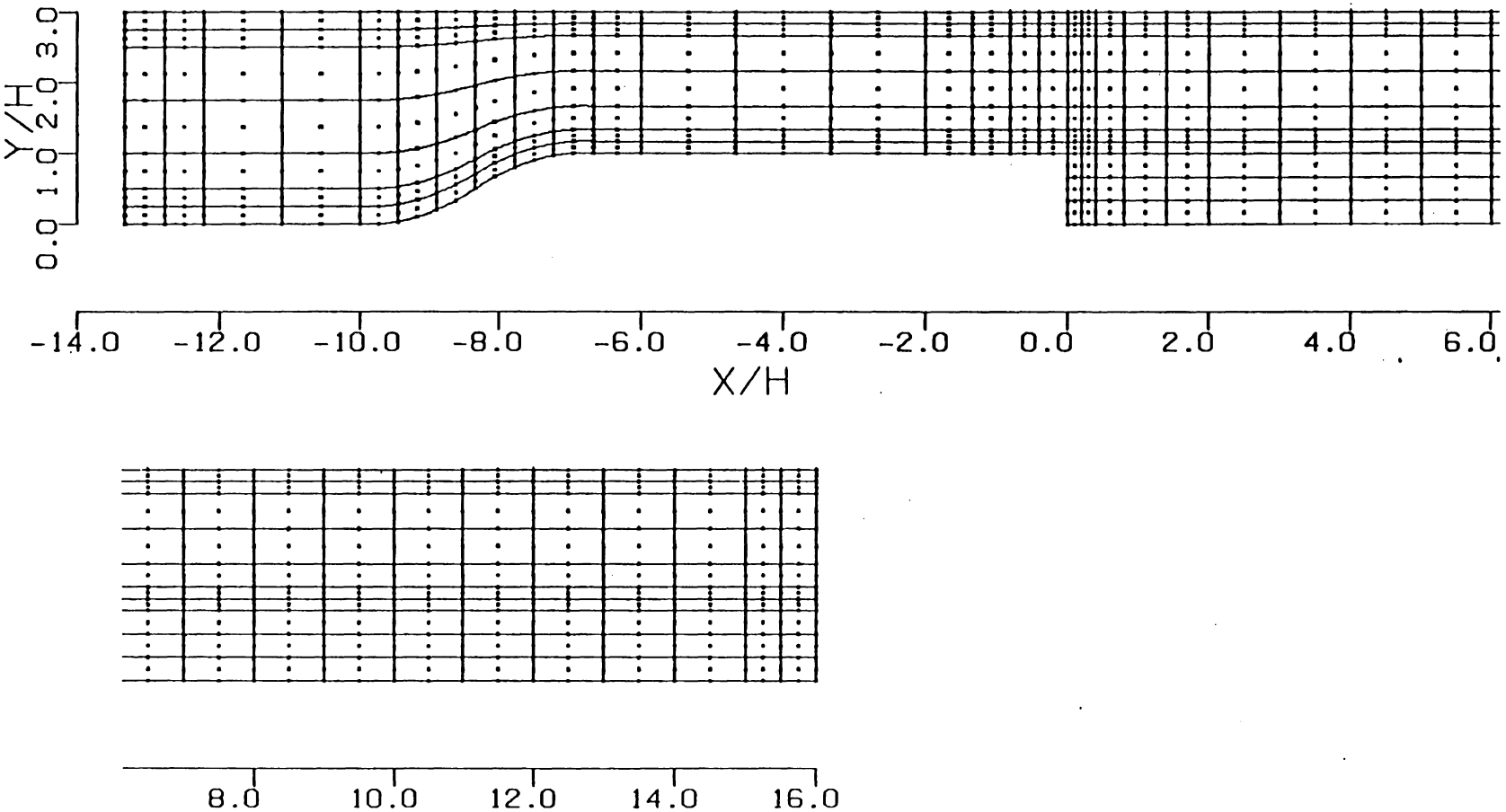

Fig. 2.23. Finite element mesh with 326 elements and 1401 nodal points for the analysis of the Denham and Patrick (7) working section at Re = 73 (run 401).

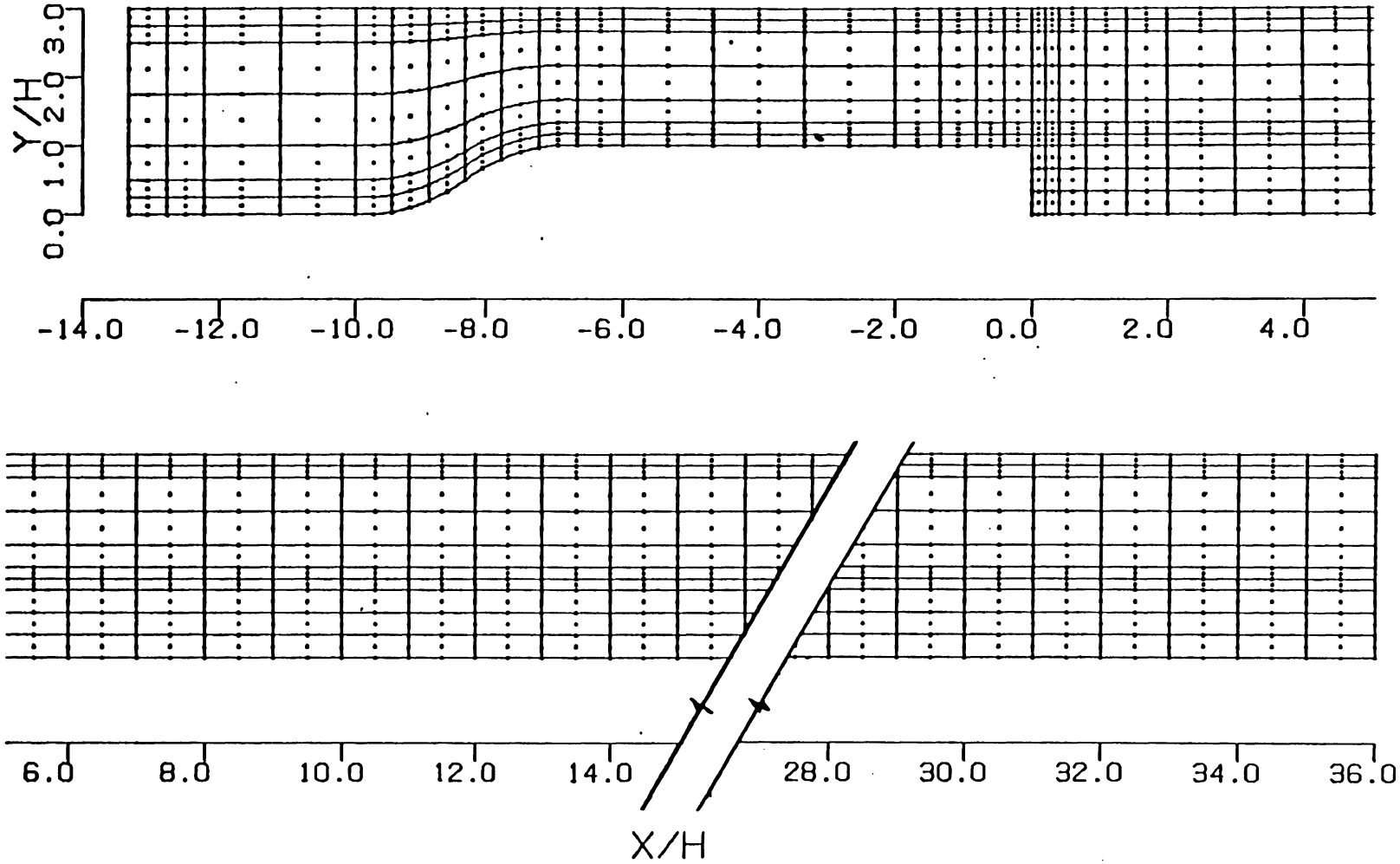

Fig. 3.24 Finite element mesh with 516 elements and 2199 nodal points for the analysis of the Denham and Patrick (7) working section at the higher Reynolds numbers (runs 402 - 404).

through 3.28, respectively. These figures clearly demonstrate the feasibility of using the computational method described in Chapter 2 to perform the two-dimensional calculations required here. The computed velocity profiles shown in these figures not only qualitatively exhibit the same lack of development and skewing that characterized the experimental data in the vicinity of the step, but also quantitatively are in very good overall agreement with the available experimental data.

Figures 3.25 through 3.28 also indicate at least the origin of the skewing in the velocity profiles at the step-the asymmetric contraction leading up to it. However, the degree to which this behavior might have been influenced by the presence of the step itself could not be ascertained from these results alone. To determine this it was necessary to compare the results presented in Figs. 3.25 through 3.28 with the corresponding results of an analysis of a working section that was modified to, in effect, remove any possible upstream influence of the step. Both the results of the analysis of the modified working section and the comparison with the results presented here will be given in the next section.

3.2.2 Analysis of an "Alternate" Working Section Design

In this section, the results of an analysis of a modified version of the Denham and Patrick (7) working

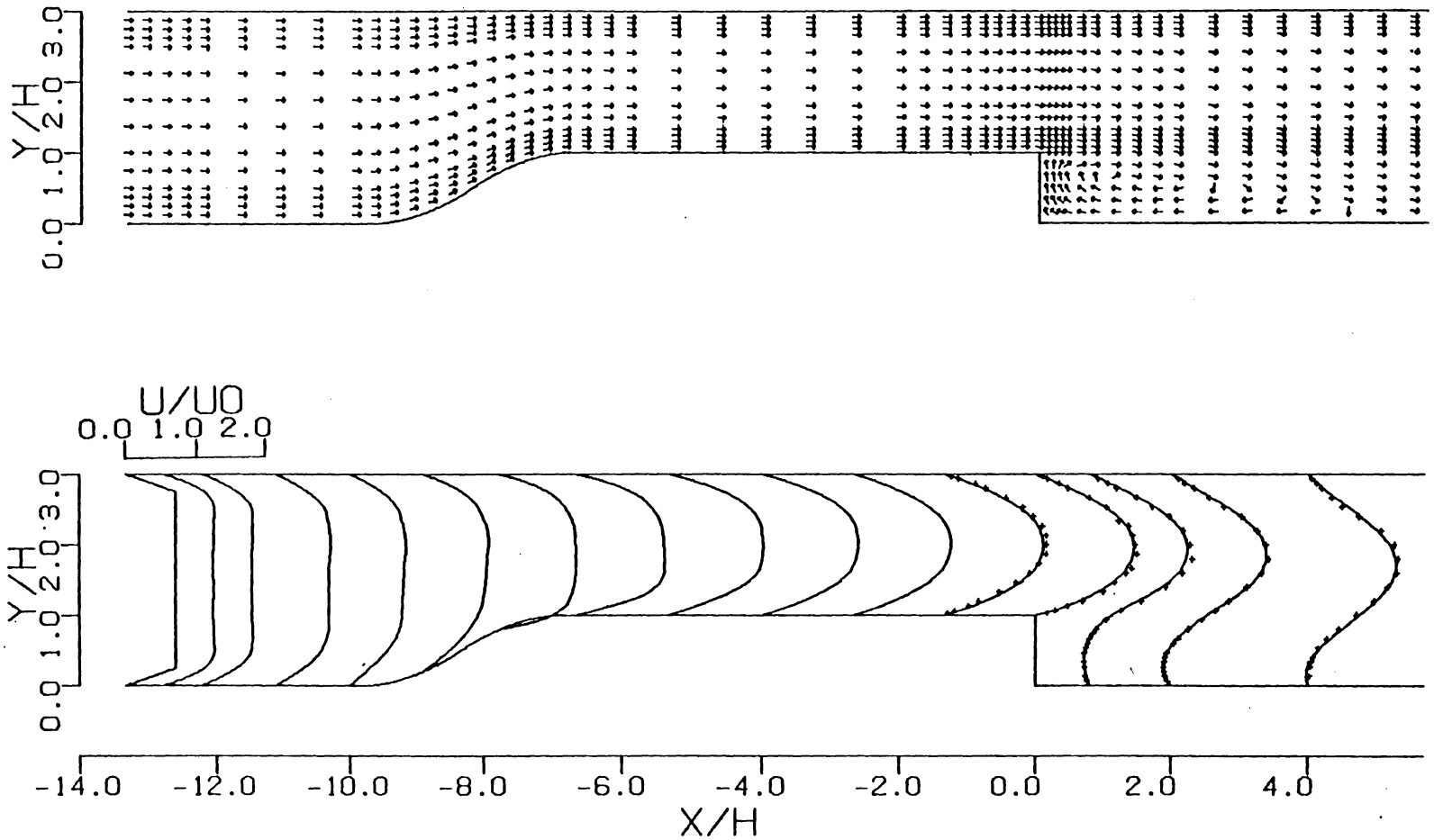

Fig. 3.25. Velocity-vectors and computed u-velocity profiles for the Denham and Patrick (7) working section at Re = 73. ___, run 401; +, Dehnam and Patrick. Continued on next page.

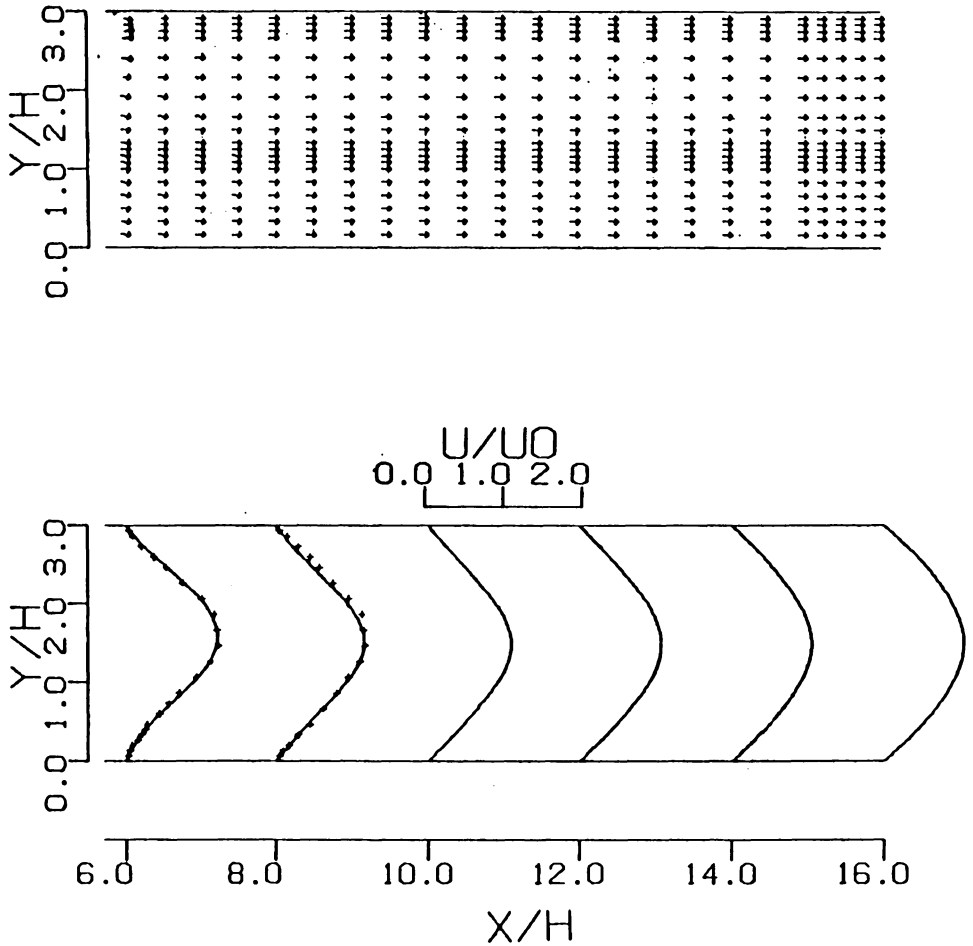

Fig. 3.25. (continued)

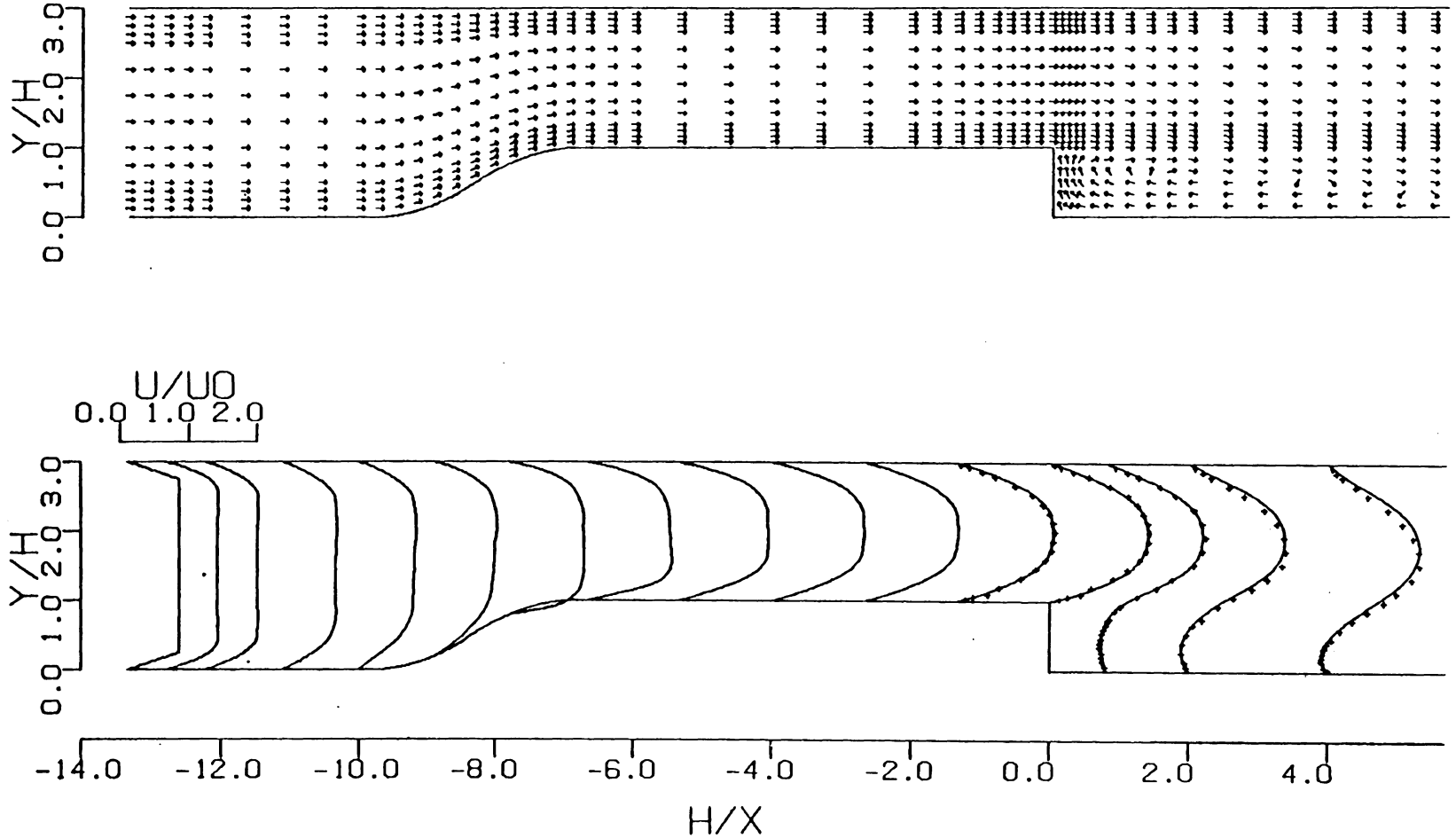

Fig. 3.26. Velocity vectors and computed u-velocity profiles for the Denham and Patrick (7) working section at Re = 125. ___, run 402; +, Denham and Patrick. Continued on the next page.

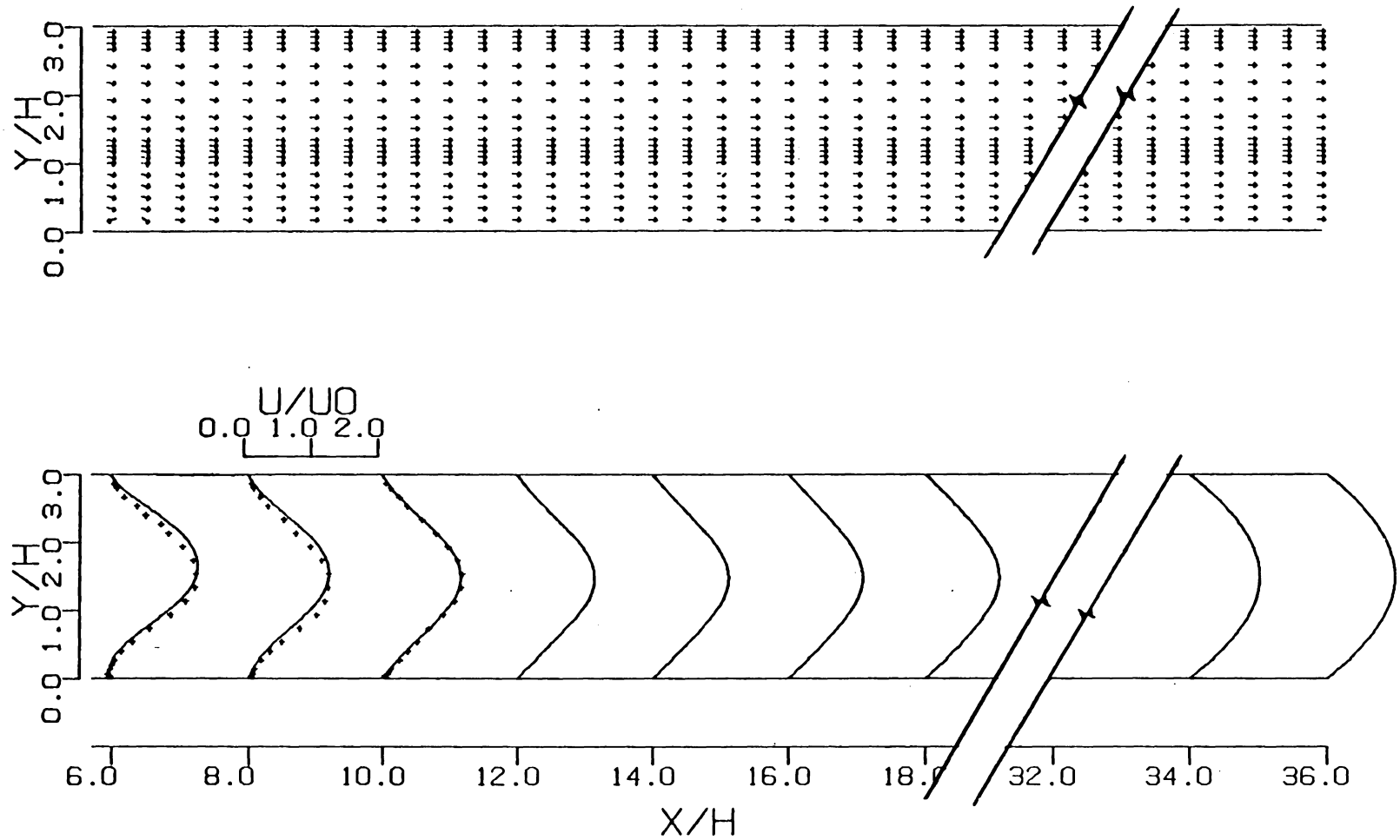

Fig. 3.26. (continued)

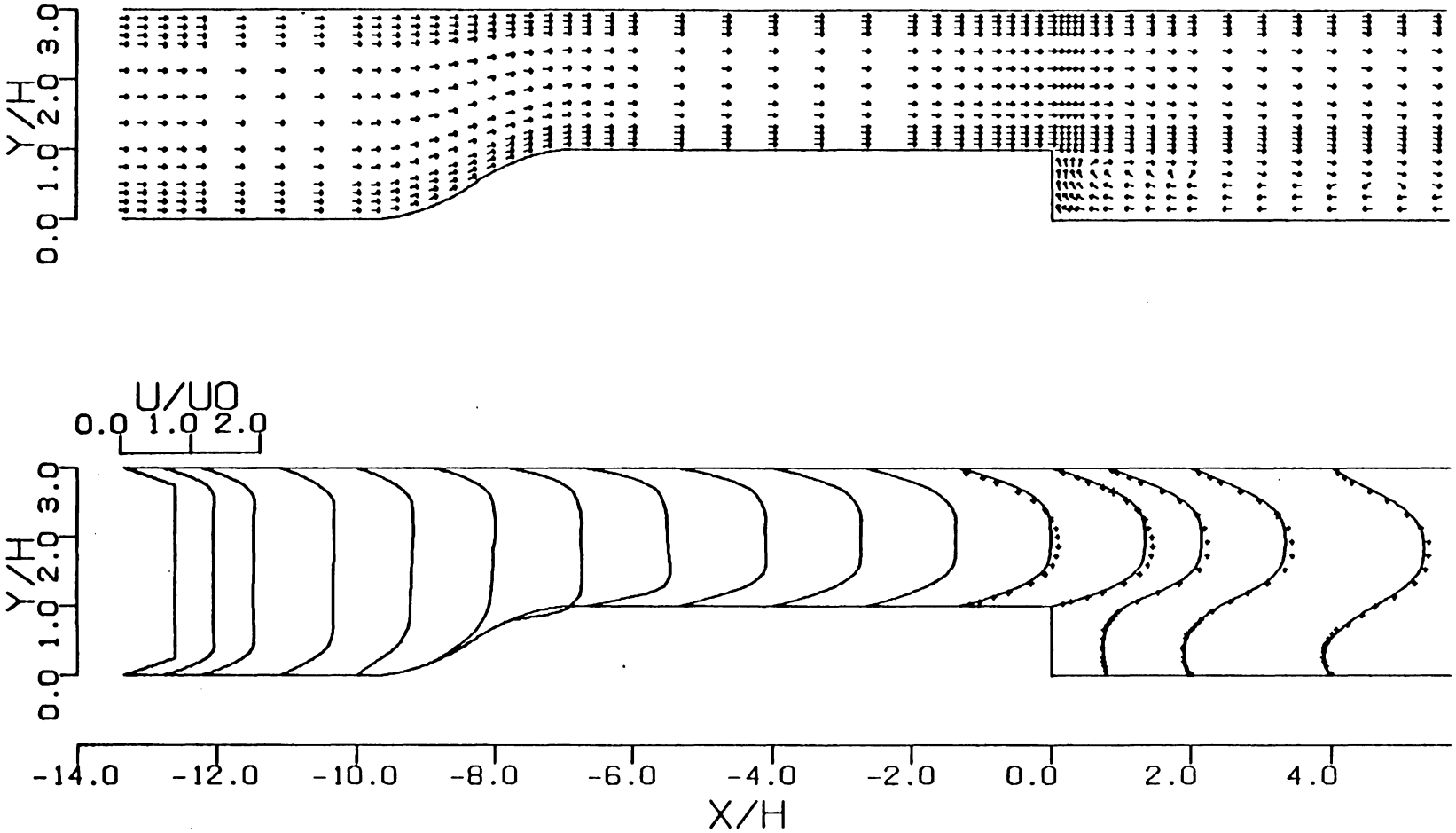

Fig. 3.27 Velocity-vectors and computed u-velocity profiles for the Denham and Patrick (7) working section at Re = 191. ___, run 403; +, Denham and Patrick. Continued on next page.

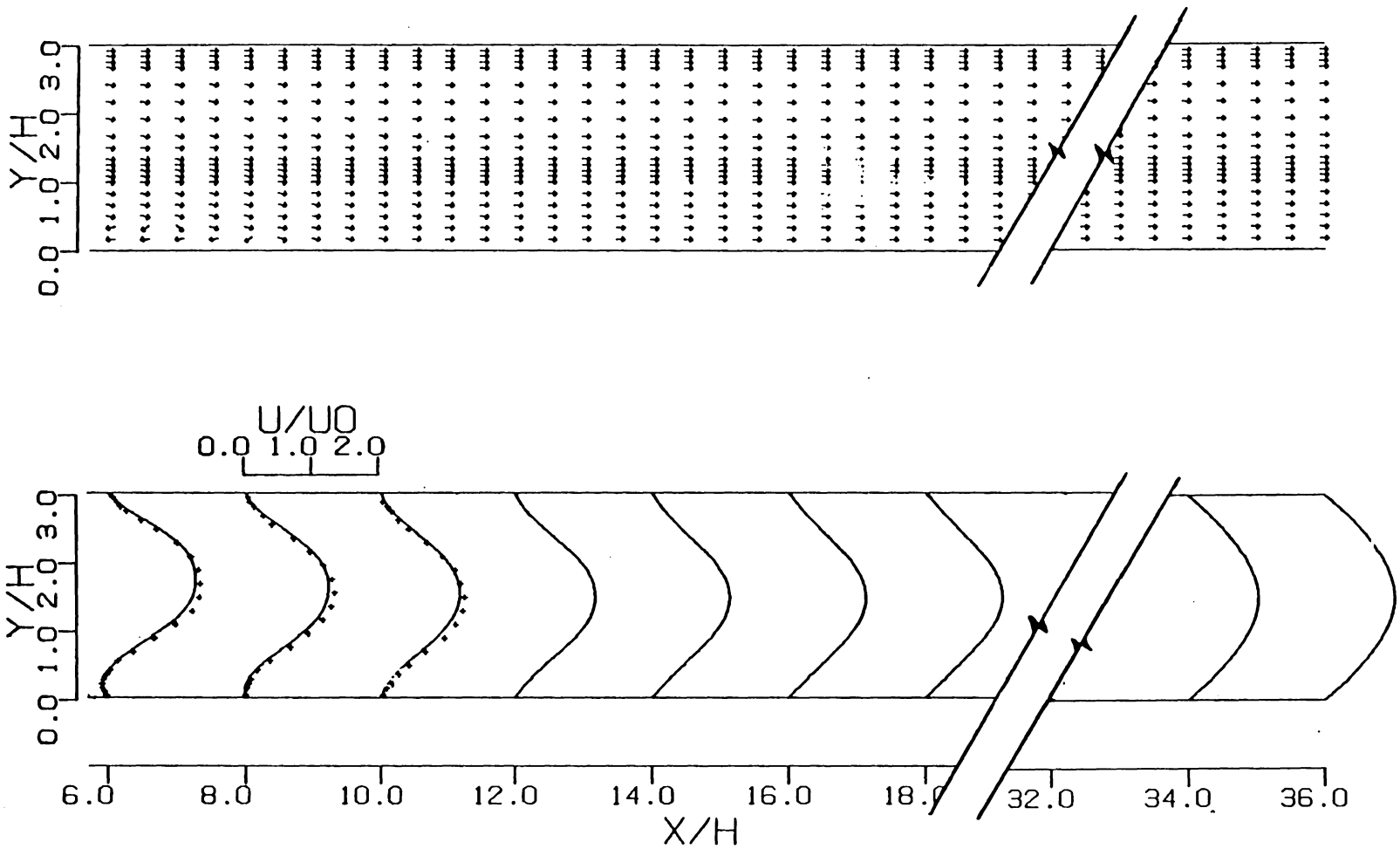

Fig. 3.27. (continued)

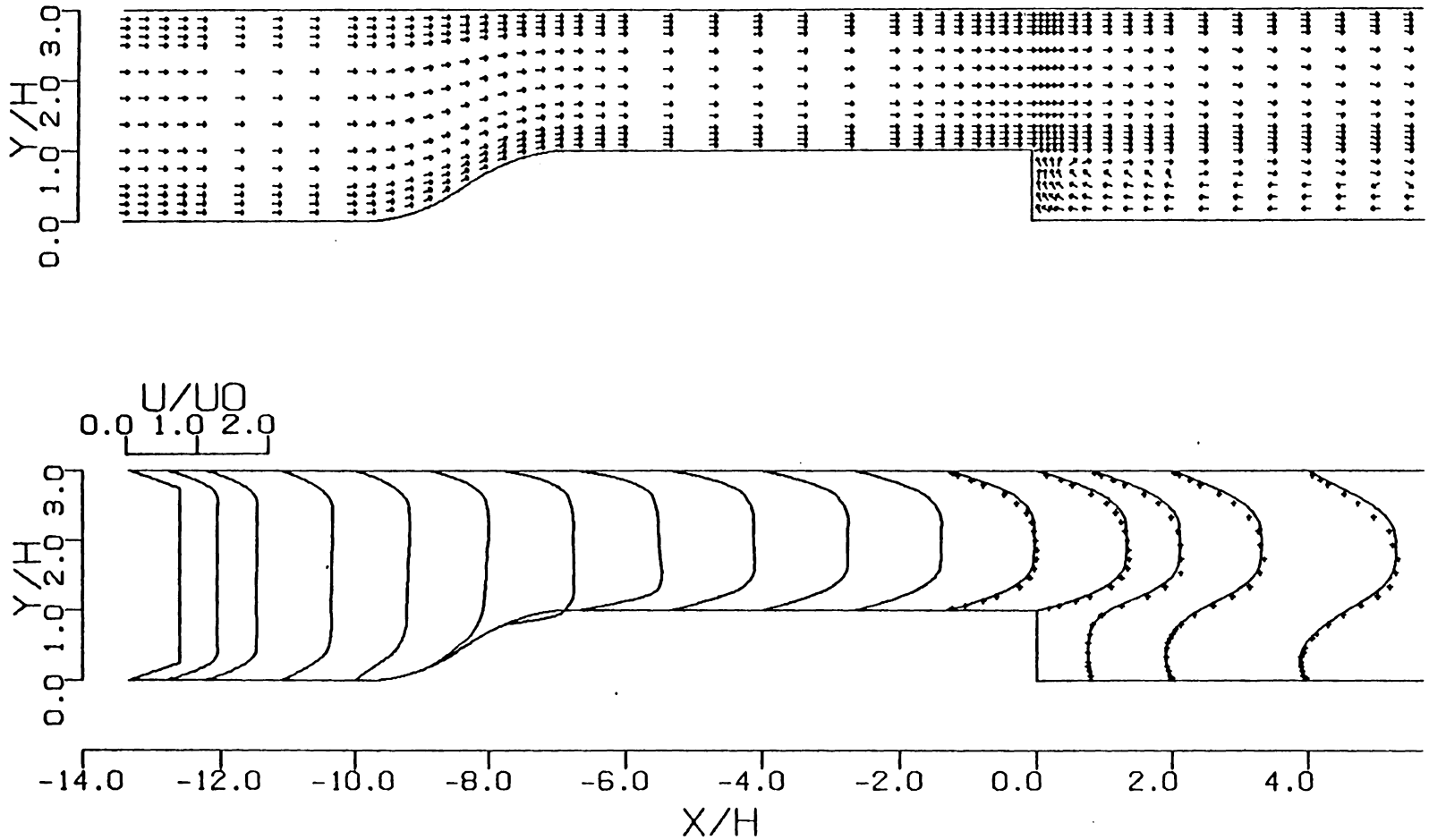

Fig. 3.28. Velocity-vectors and computed u-velocity profiles for the Denham and Patrick (7) working section at Re = 229. ___, run 404; +, Denham and Patrick. Continued on next page.

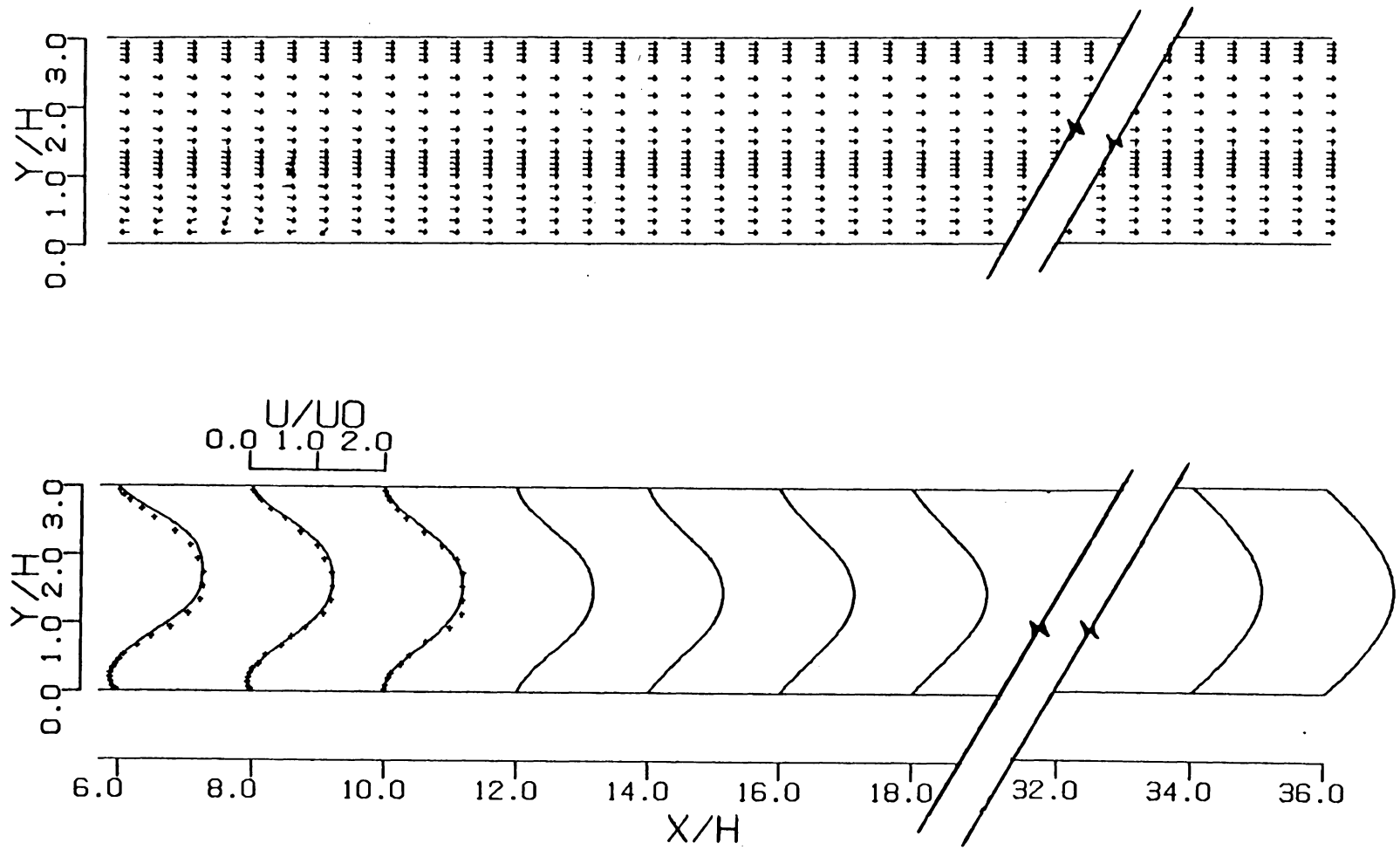

Fig. 3.28. (continued)

section are presented and compared to those presented in the previous section to determine: (1) the extent to which the initial plane of data was influenced by the step itself, and (2) the sensitivity of the flow field downstream of the step to the degree of development of the velocity field at the step.

The "alternate" working section considered here is depicted in Fig. 3.29. As indicated by the broken line segments, the modified configuration is identical to that analyzed in the previous section except for the length of the constant area section between the fairing and the step. This dimension was doubled in the modified design not only to shift any potential upstream influence of the step itself further downstream, but also to alter the degree of development of the velocity profiles in the plane of the step.

The calculations performed to predict the flow through the modified working section are labeled the 500 series. The boundary conditions and Reynolds numbers at which these calculations were performed are precisely the same as those employed earlier in the analysis of the as-built working section. The only difference between the 400 and 500 series runs is that the 500 series finite element mesh depicted in Fig. 3.30 required 35 more elements than the one used in runs 402 through 404 to account for the additional length of constant area duct installed

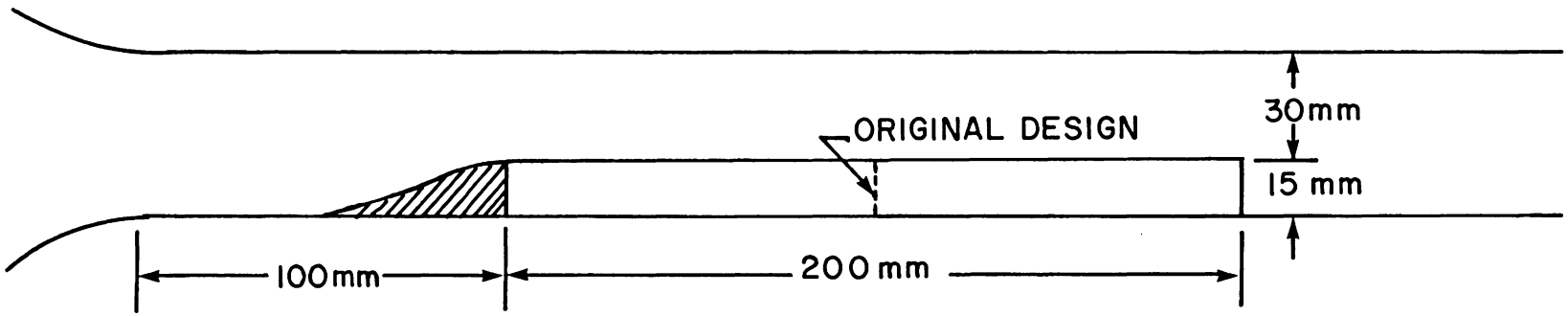

Fig. 3.29. Alternative working section design.

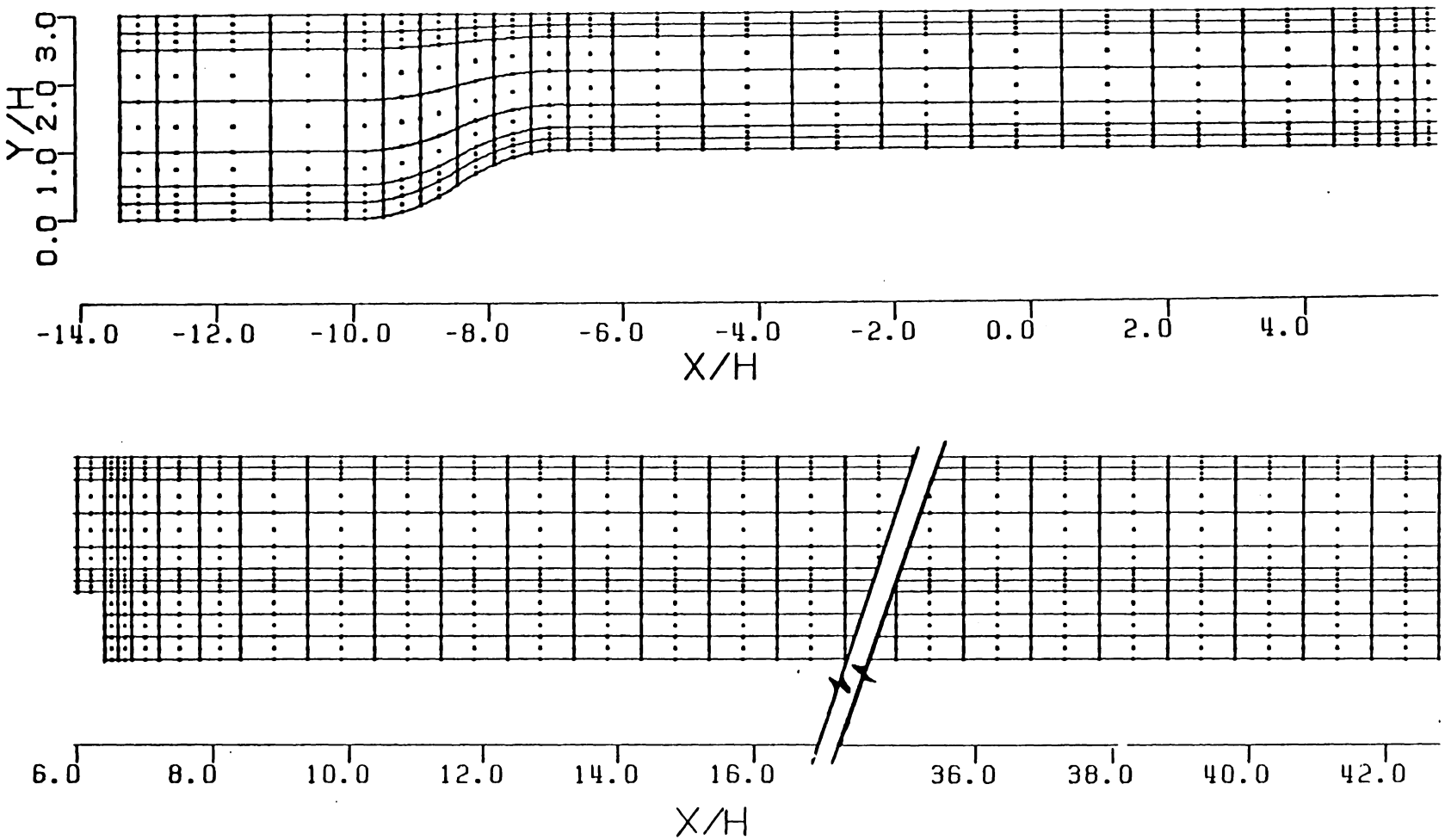

Fig. 3.30. Finite element mesh with 551 elements and 2349 nodes used in the analysis of the alternative working section design at all Reynolds numbers (runs 501-504).

upstream of the step.

The results of this series of runs are presented in the form of the combination velocity-vector/u-profile plots given in Figs. 3.31 through 3.34. Comparing the results of the 400 and 500 series runs, i.e., Figs. 3.25 through 3.28 and 3.31 through 3.34, respectively, indicates that:

(1) Both the magnitude of the skewness and the degree of development of the experimental profiles at x/h = - 1.333, the location of the initial plane of data, were unaffected by the presence of the step itself. This, in essence, confirms the hypothesis by Denham and Patrick (7) that the noticeable skewness in the experimental profiles at x/h = - 1.333 was caused by the asymmetry of the contraction leading up to the step rather than by some elliptic effect of the step itself.

(2) The lack of development of the velocity profiles at x/h = - 1.333 did indeed influence the velocity field well downstream of the step. The lengths of the recirculating region behind the step derived from the results of the 500 series analyses, for example, were up to 15 percent greater than either those reported by Denham and Patrick or exhibited by the 100 through 400

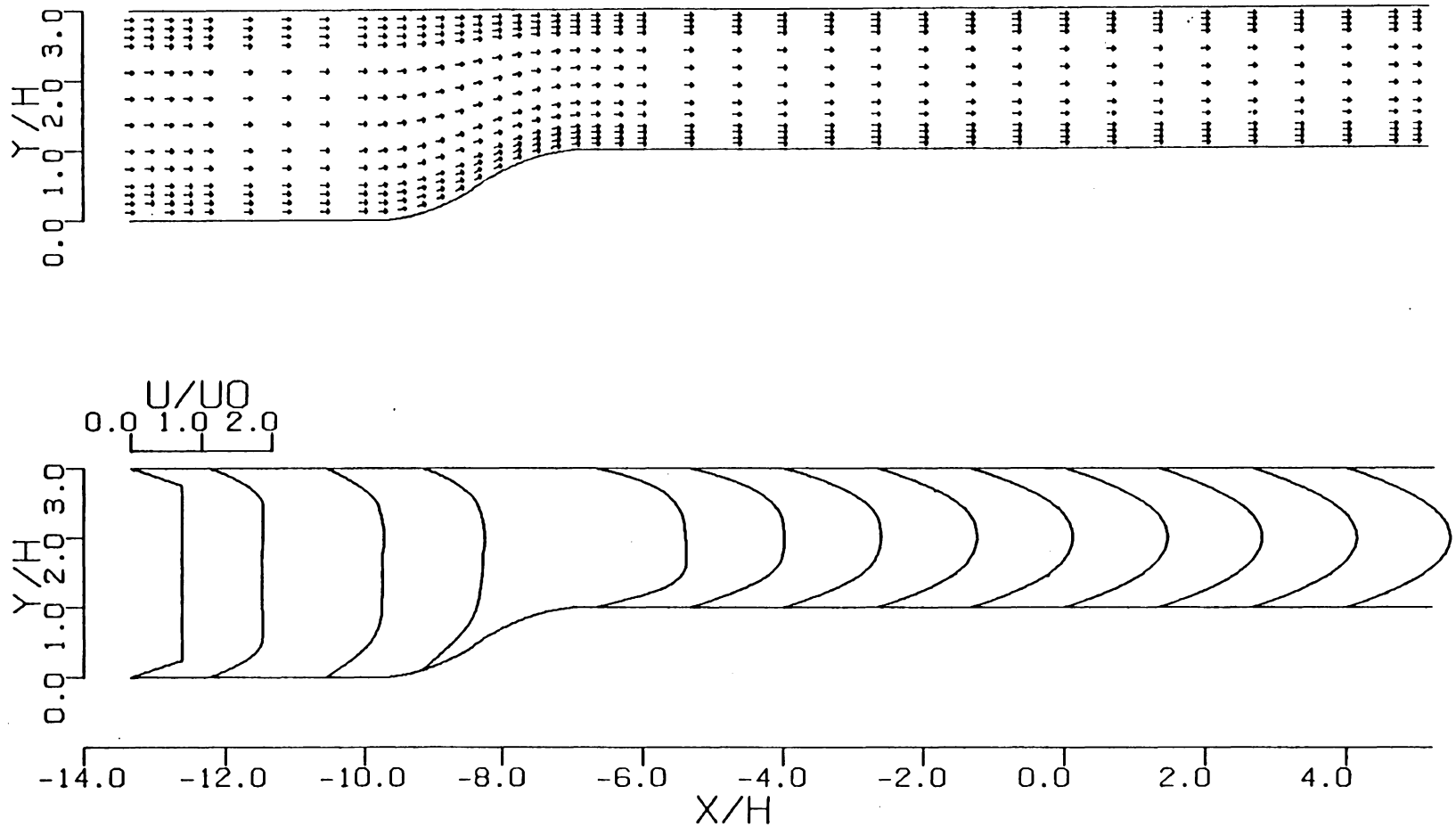

Fig. 3.31. Velocity-vectors and computed (run 501) u-velocity profiles for the alternative working section design at Re = 73. +, Denham and Patrick (7). Continued on the next two pages.

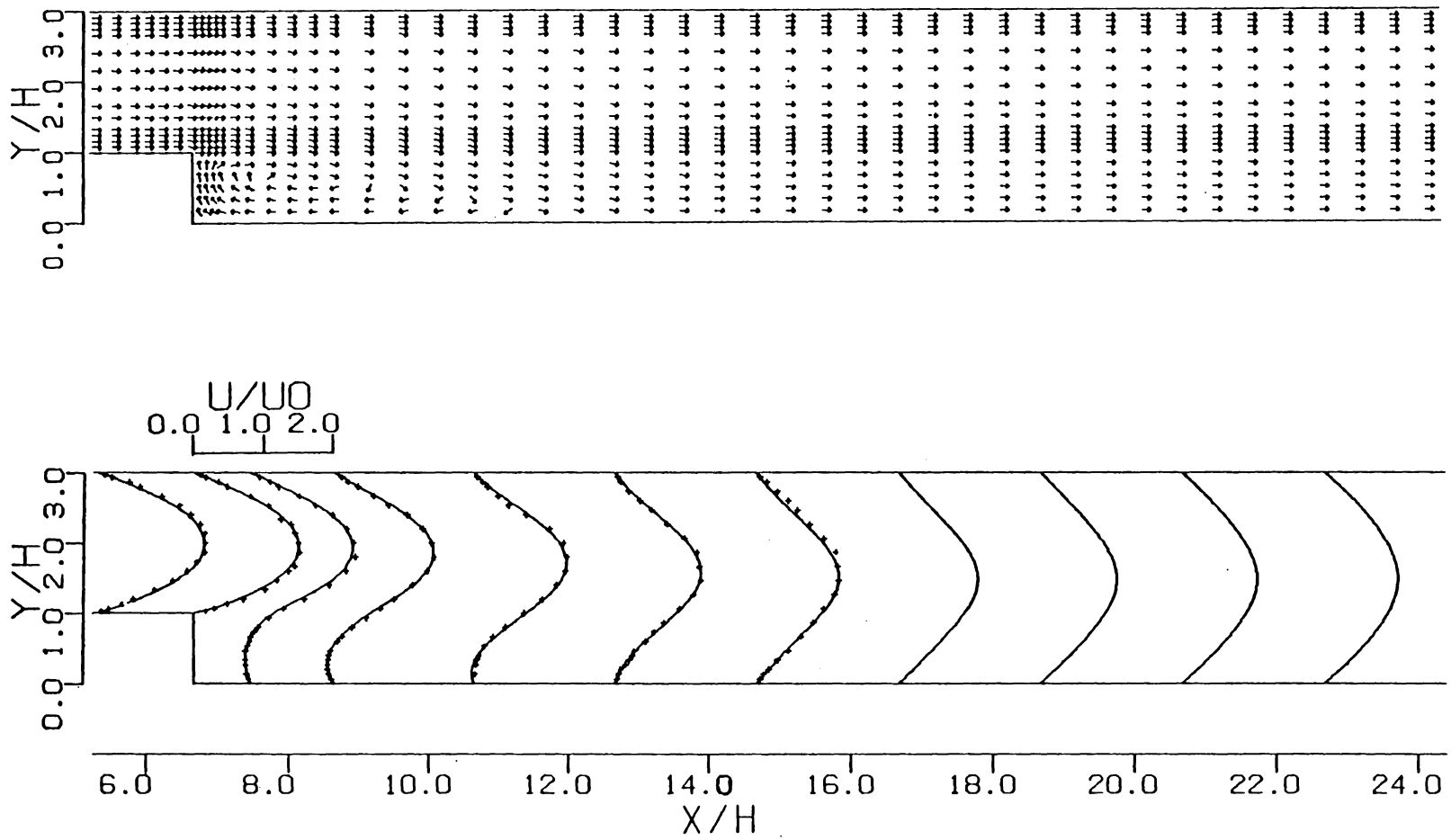

Fig. 3.31. (continued)

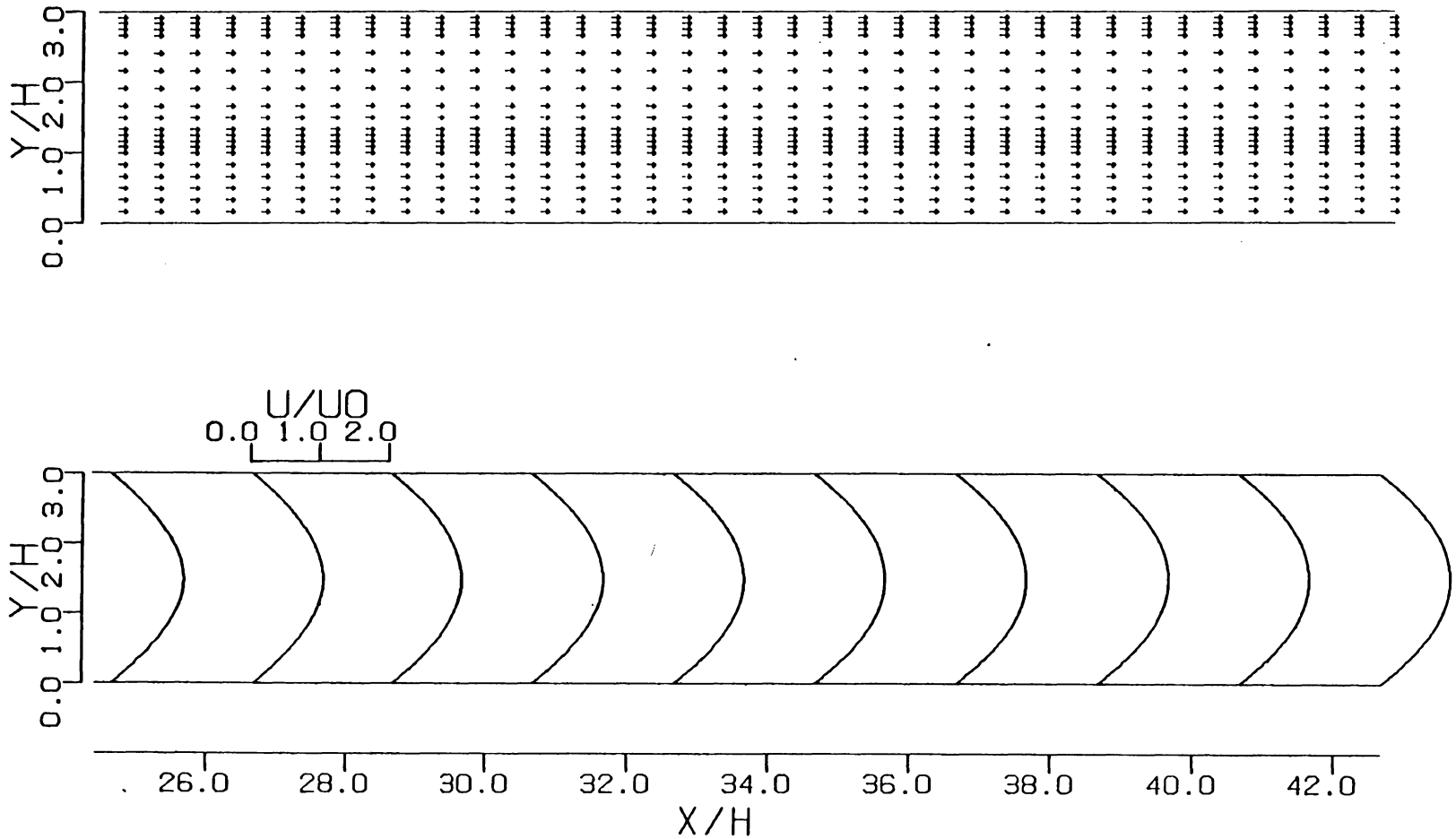

Fig. 3.31. (continued)

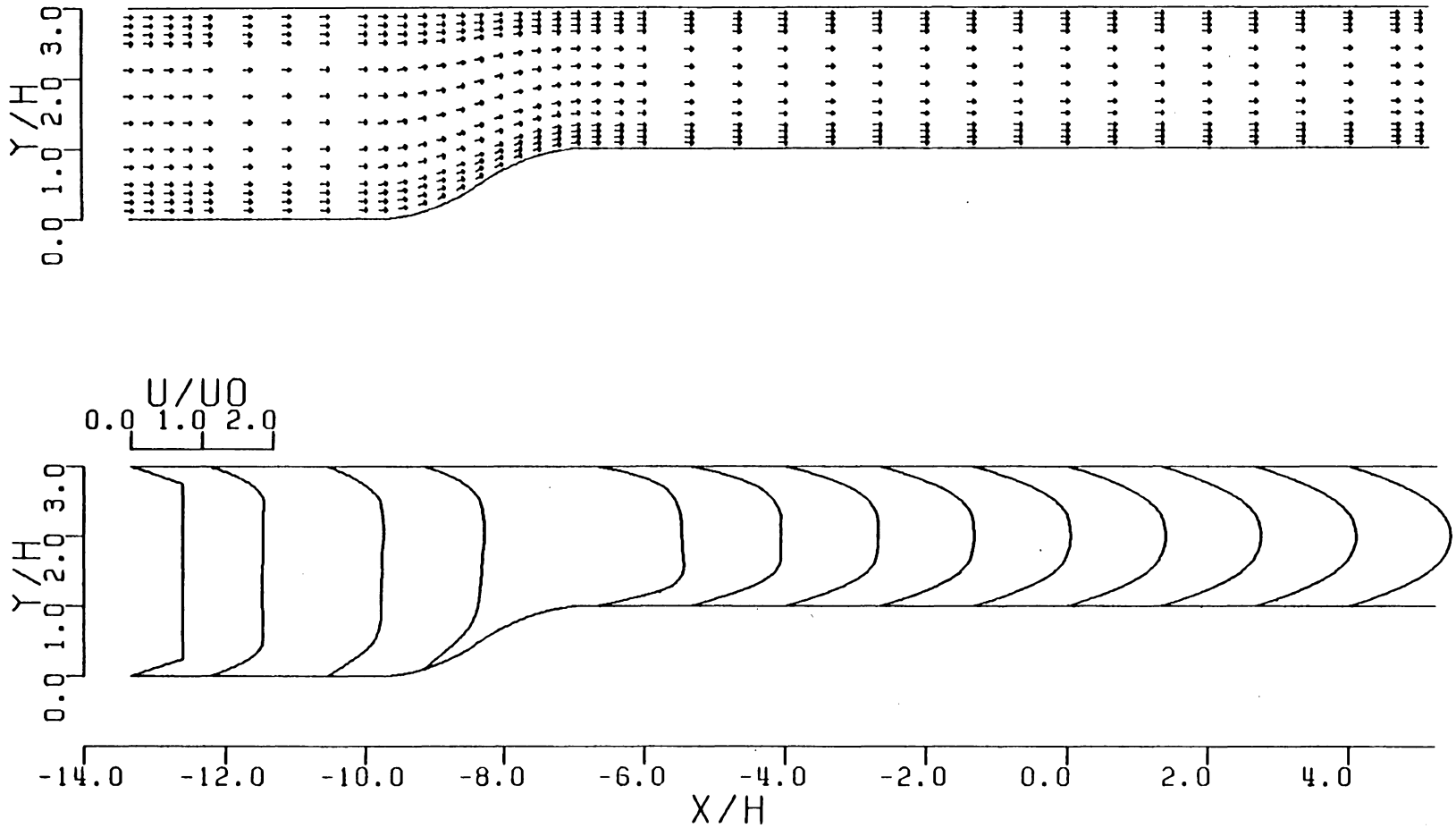

Fig. 3.32. Velocity-vectors and computed u-velocity profiles for the alternative working section design at Re = 125. ___, run 502; +, Denham and Patrick (7). Continued on the next two pages.

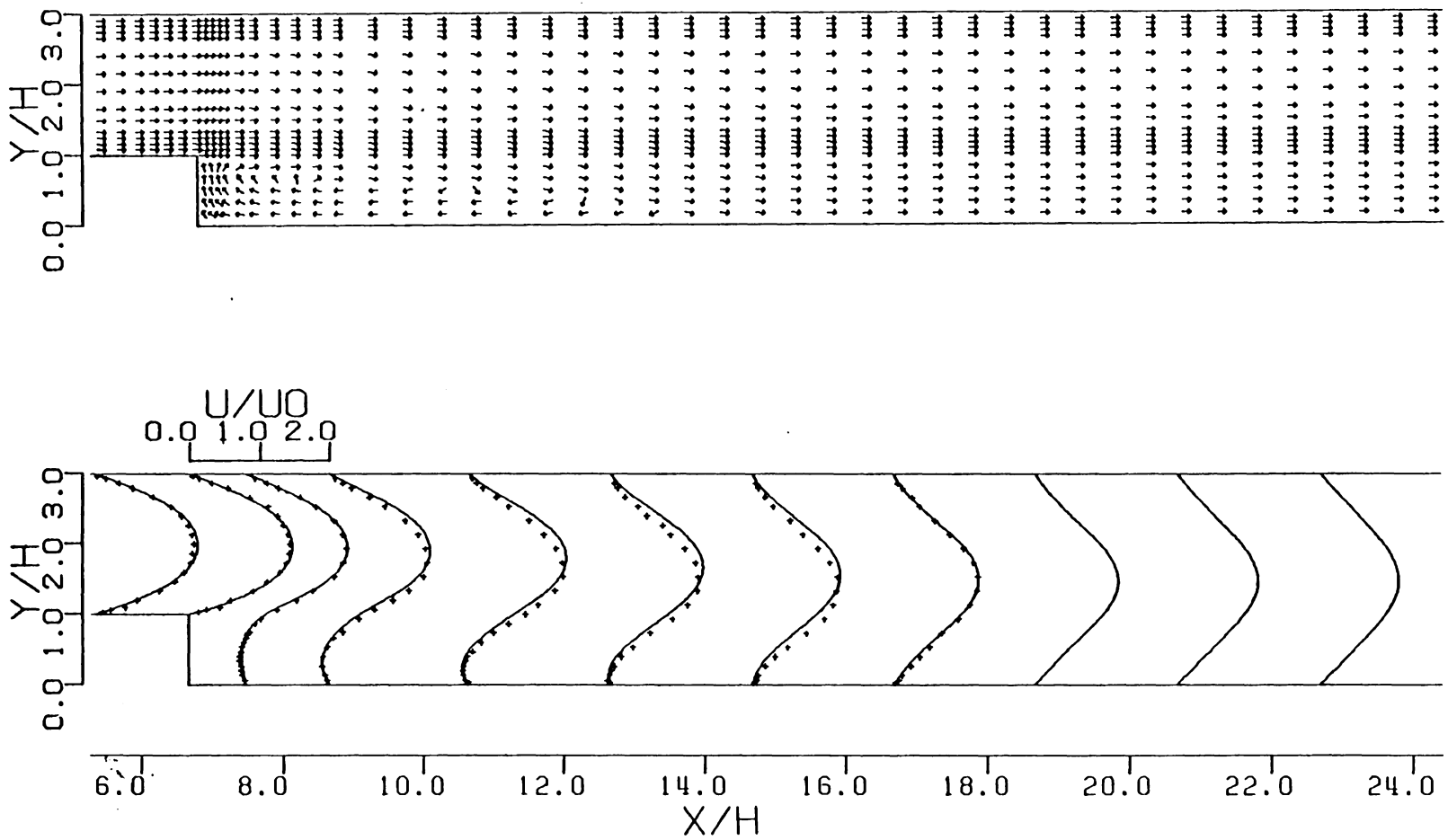

Fig. 3.32 (continued)

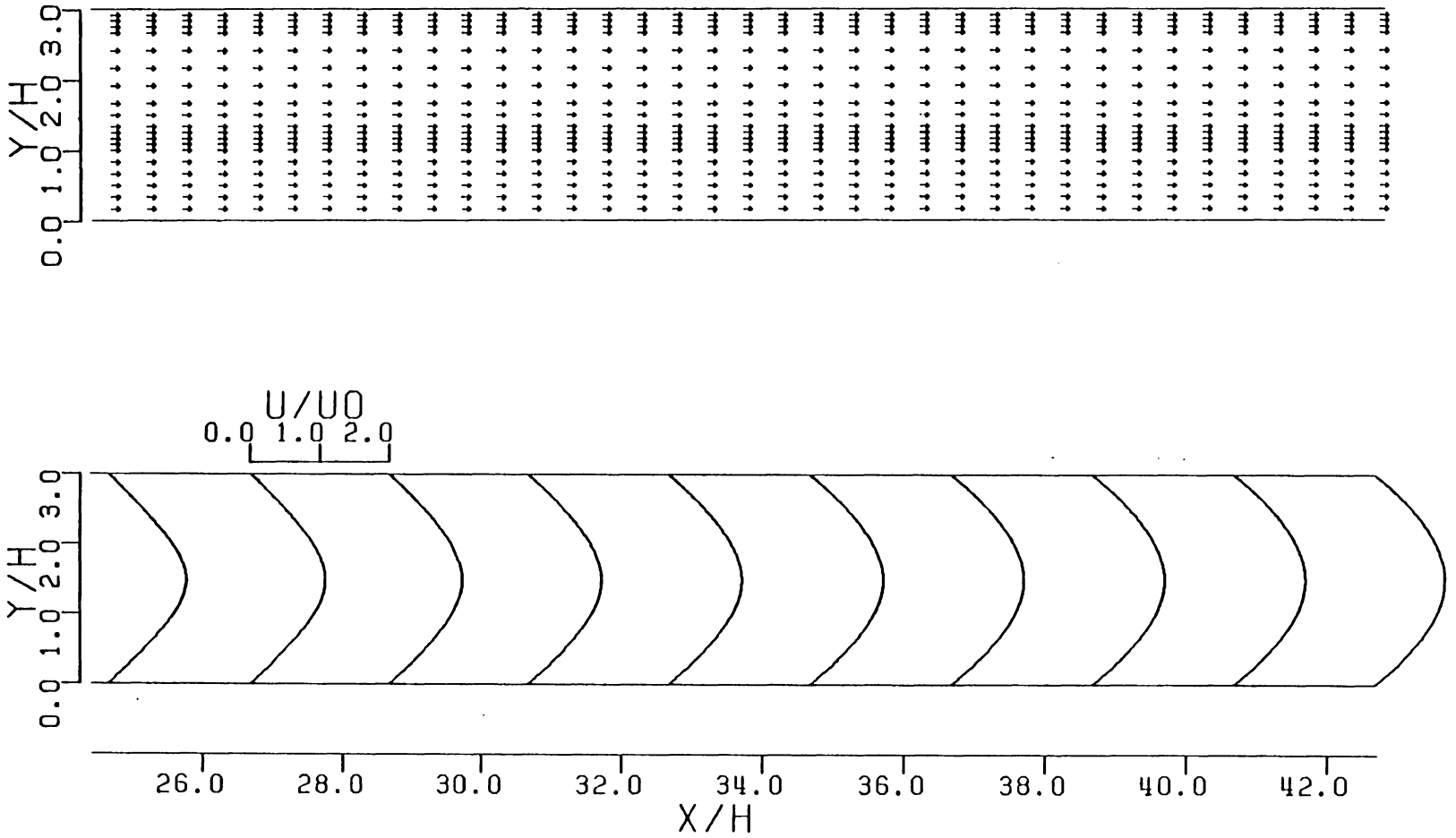

Fig. 3.32. (continued)

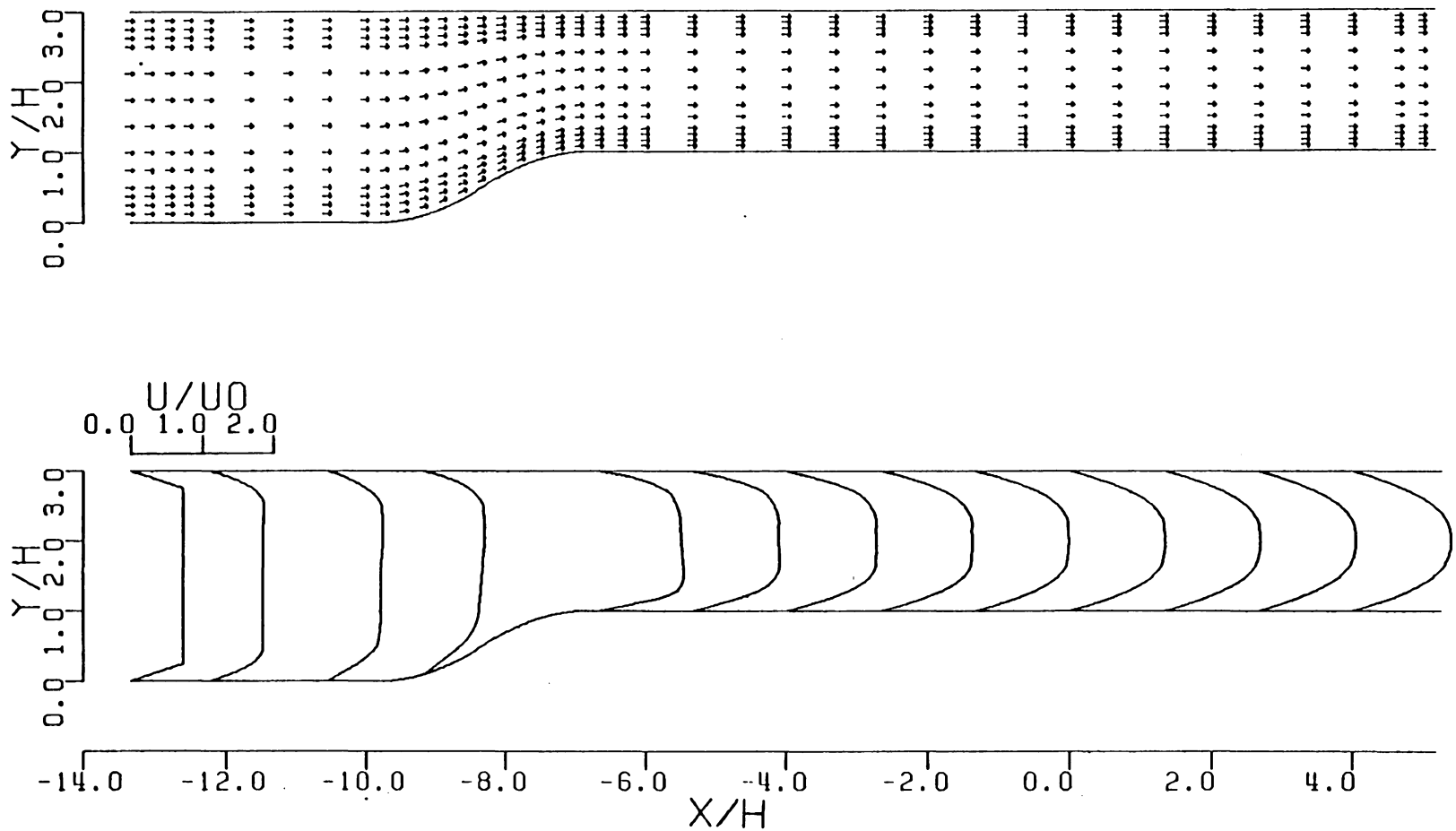

Fig. 3.33. Velocity-vectors and computed u-velocity profiles for the alternative working section design at Re = 191. ___, run 503; +, Denham and Patrick (7). Continued on the next two pages.

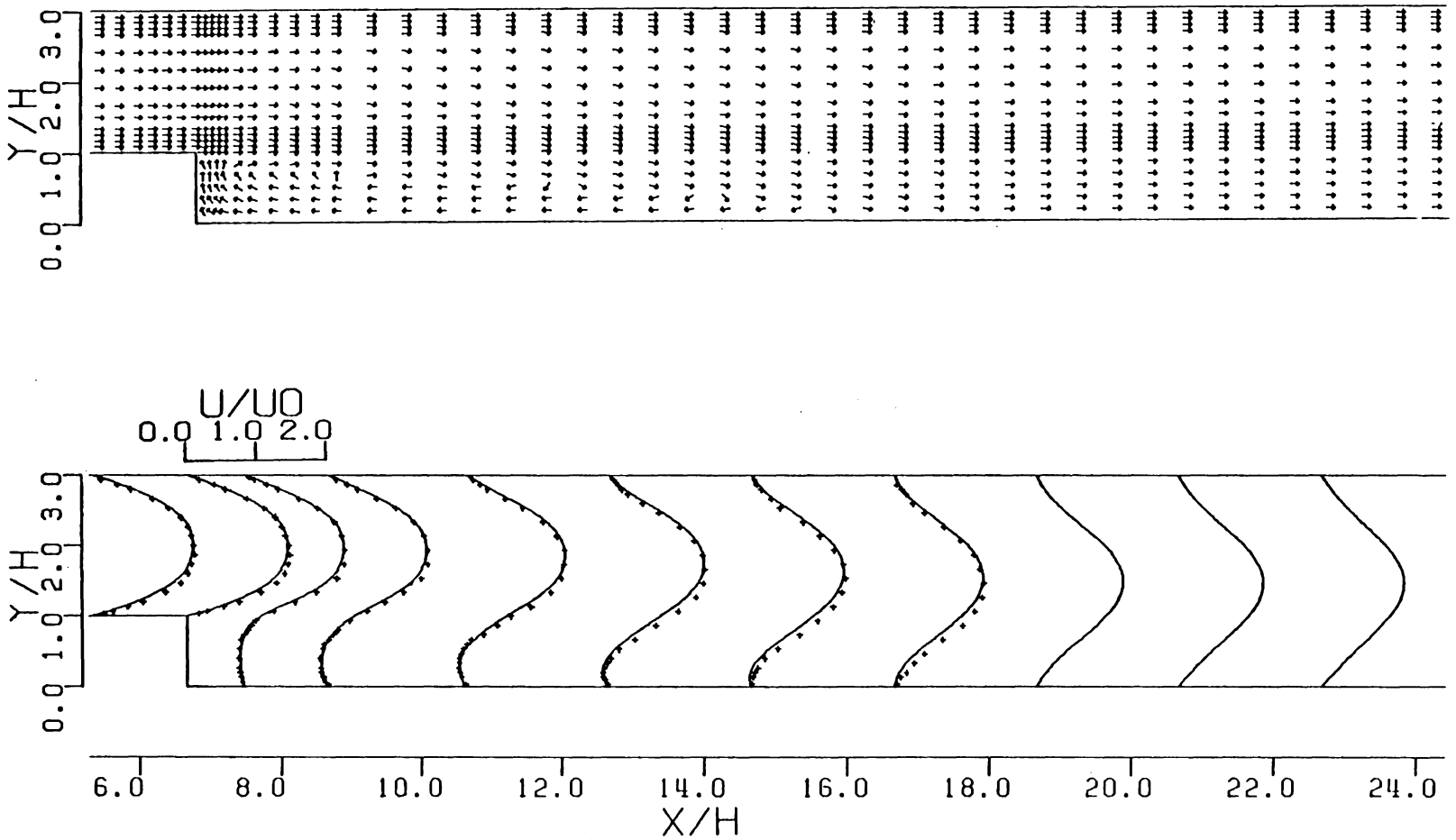

Fig. 3.33. (continued)

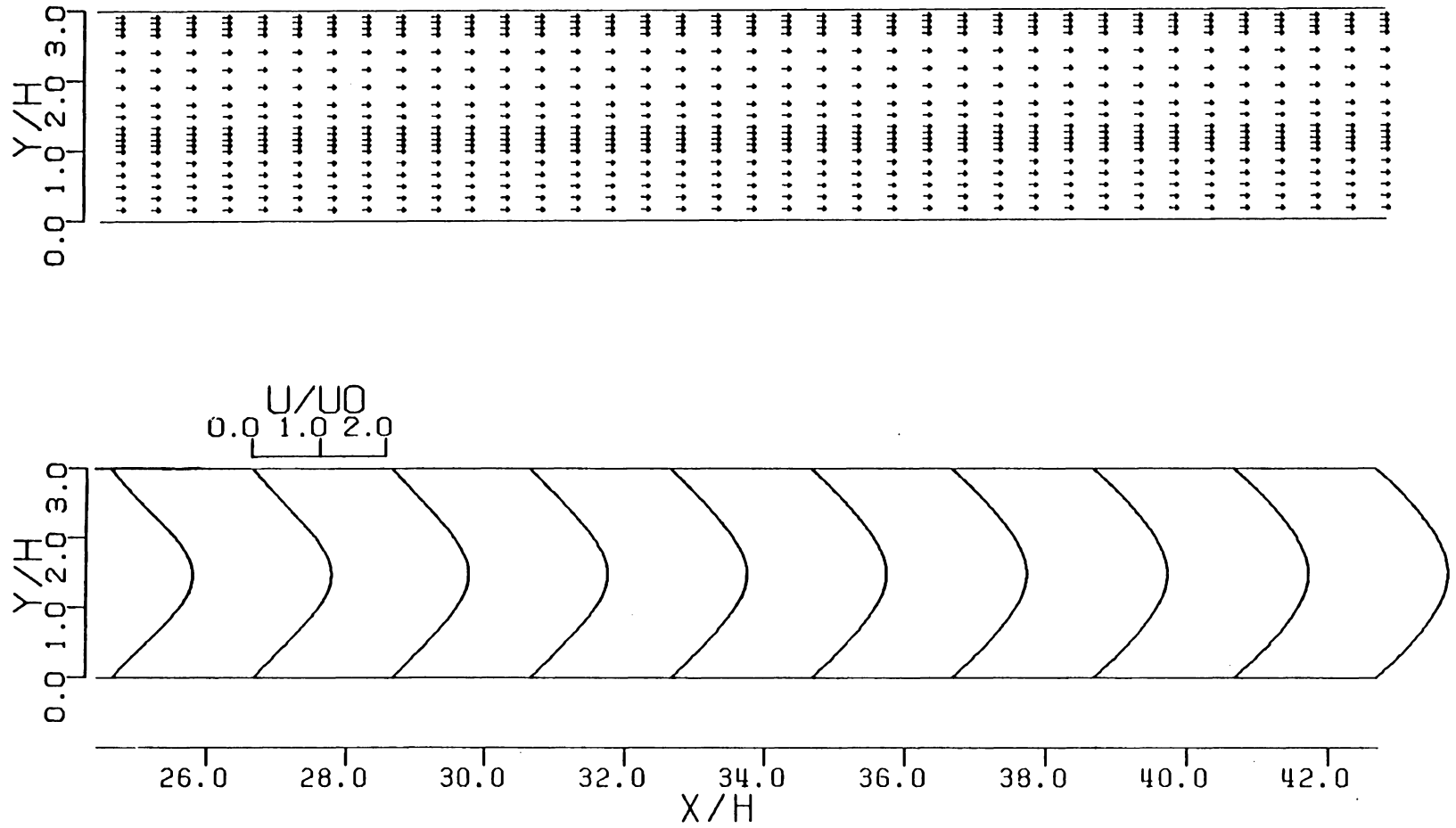

Fig. 3.33. (continued)

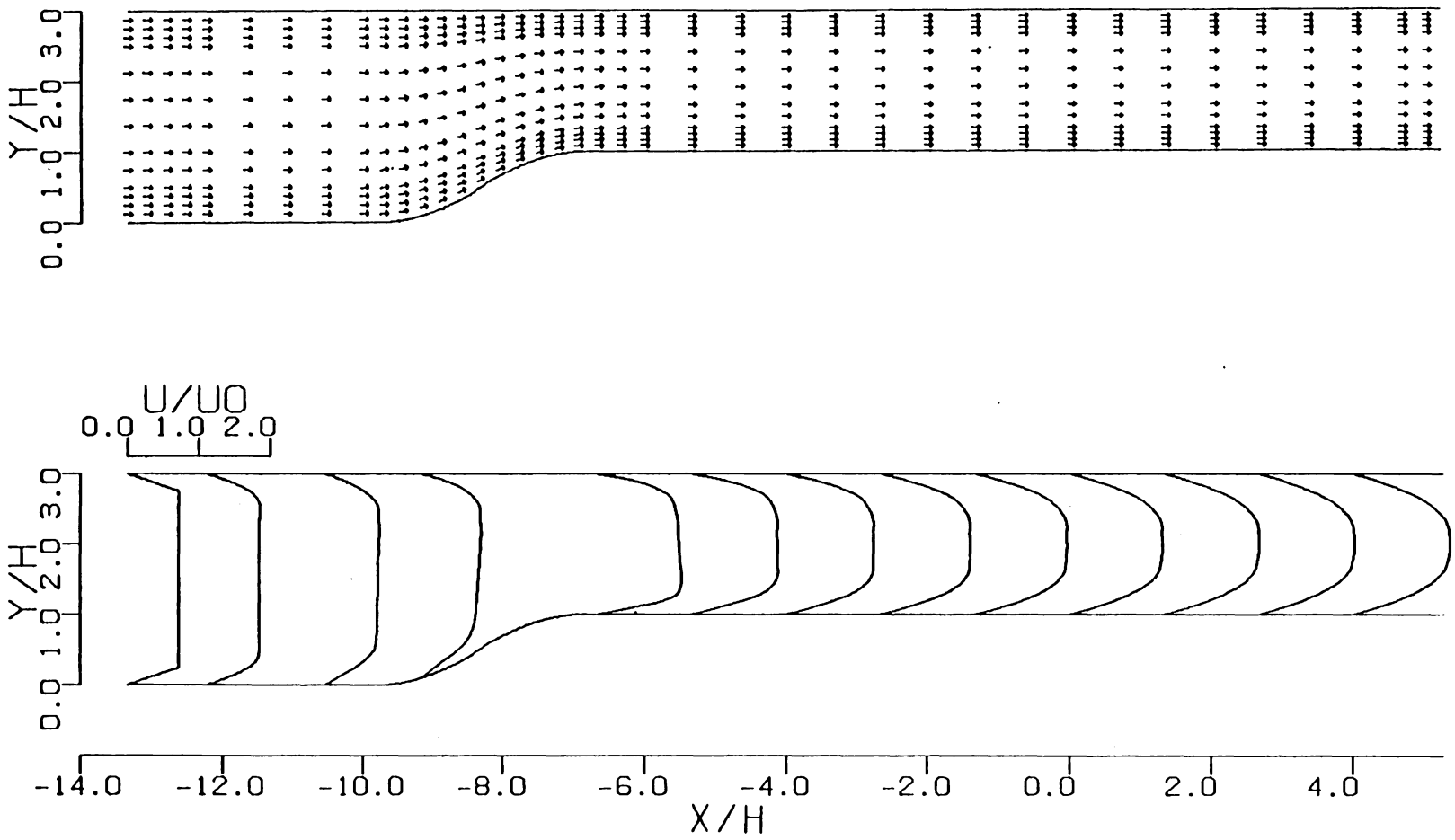

Fig. 3.34. Velocity-vectors and computed u-velocity profiles for the alternative working section design at Re = 229. ___; run 504; +, Denham and Patrick (7). Continued on the next two pages.

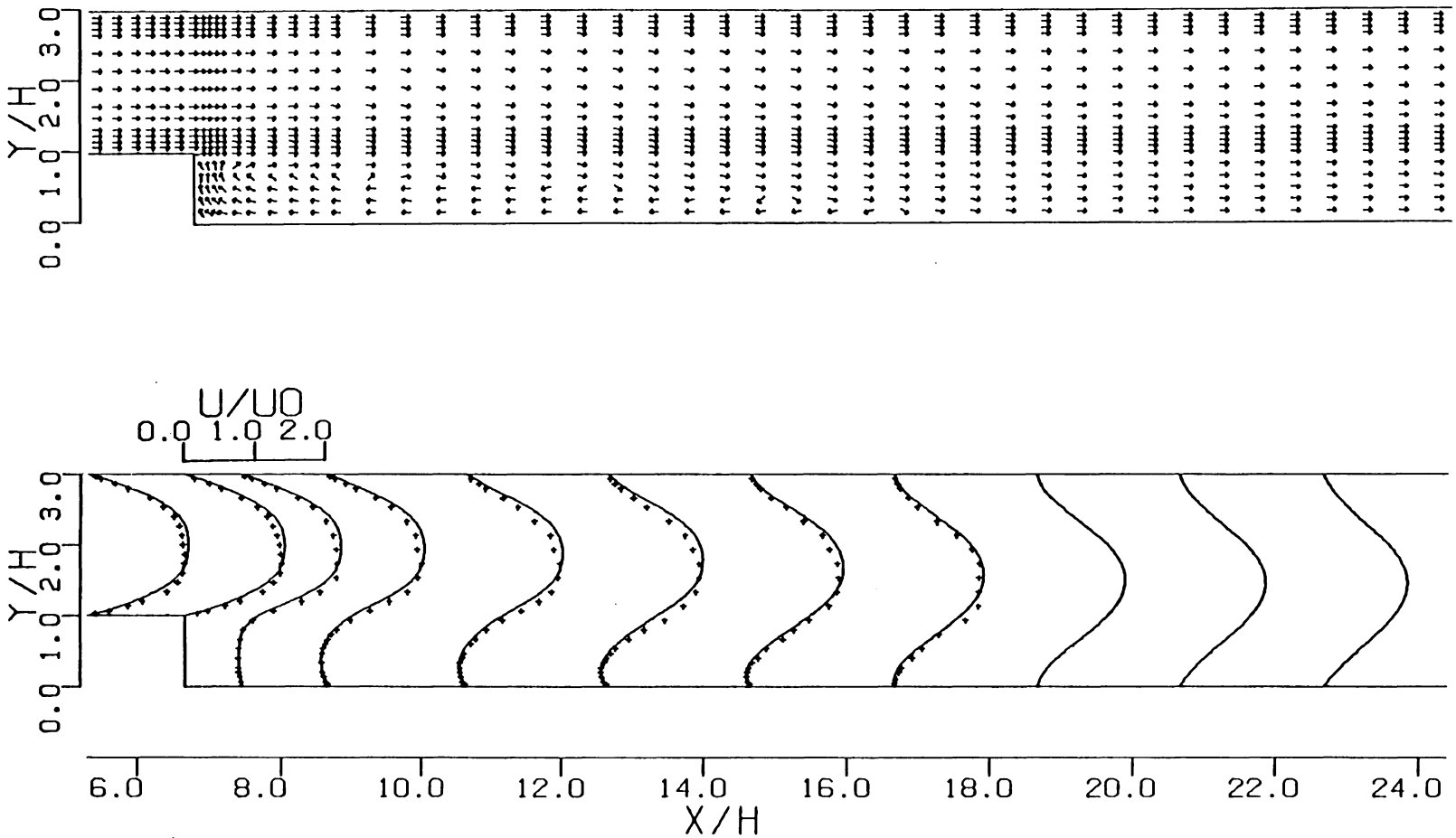

Fig. 3.34. (continued)

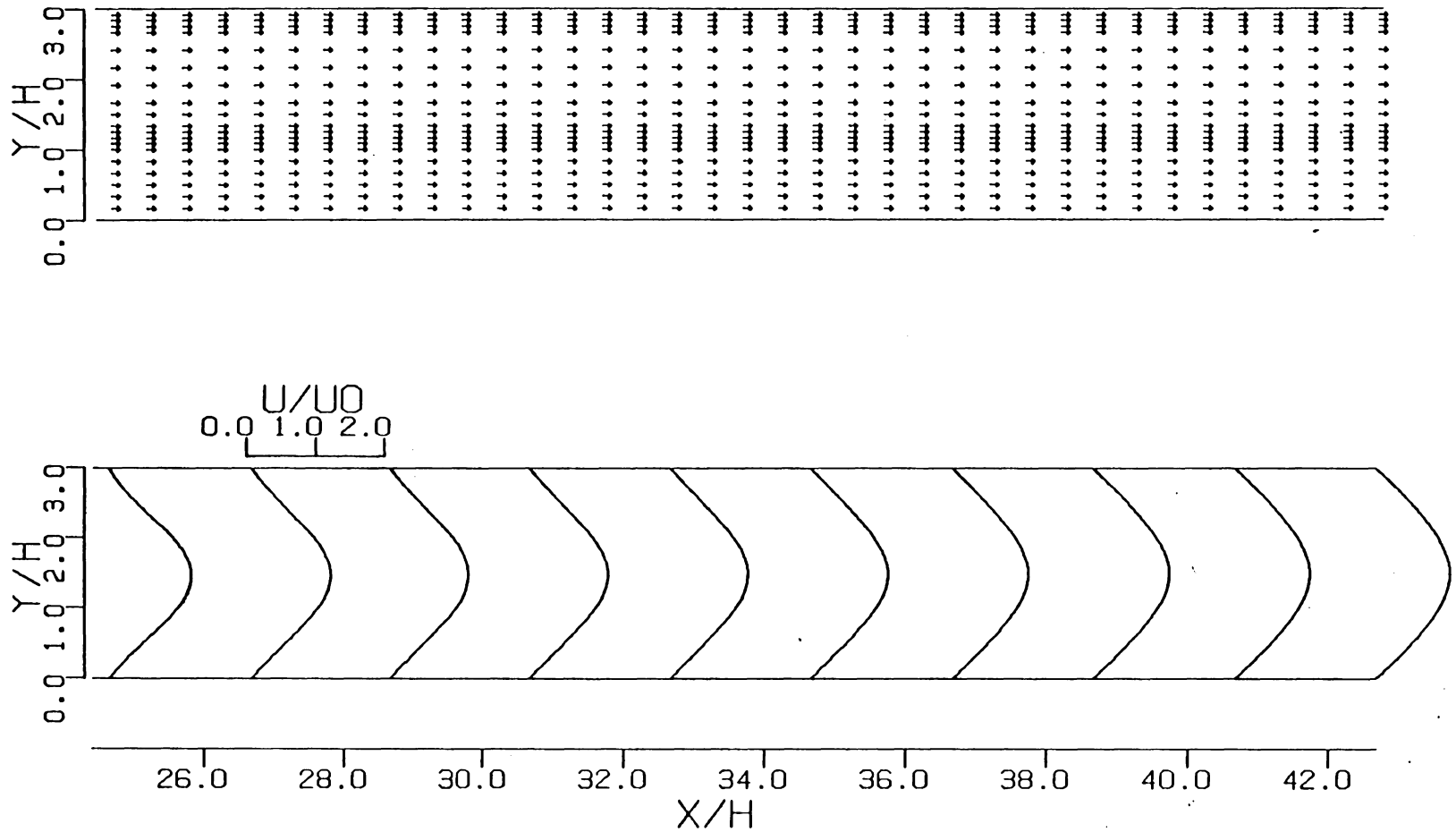

Fig. 3.34. (continued)

series results.

The specific details of the comparison that support these conclusions are:

(1) The corresponding 400 and 500 series velocity profiles at x/h = - 1.333, are for all practical purposes identical. This is perhaps better illustrated in Table 3.4, which summarizes the nodal point velocities from runs 404 and 504 in this plane. Note that all the corresponding entries in this table agree to within 2.4 percent.

(2) Using the experimental data as a reference, it can be seen that the corresponding velocity profiles displayed in Figs. 3.25 through 3.28 and 3.31 through 3.34 downstream of the step are noticeably different. Comparison of the entries in Table 3.5 confirms this observation. This table summarizes the computed nodal point velocities from runs 404 and 504 in the plane eight step-heights downstream of the sudden expansion. Note that the corresponding entries in this table differ by as much as 143 percent.

(3) As shown in Fig. 3.35, the length of the recirculating region behind the step are from 4 to 16 percent longer in those cases where the flow field upstream of the step was allowed to

Table 3.4 Comparison of the results of the original (run 404) and modified (run 504) working section analyses at x/h = - 1.333

$\frac{y}{h}$	$\frac{U_{404}}{U_o}$	$\frac{U_{504}}{U_o}$	$\frac{\lvert U_{404} - U_{504} \rvert}{U_{404}} \times 100\%$
1.000	0.0000	0.0000	0.0
1.083	0.3083	0.3012	2.3
1.167	0.5745	0.5642	1.8
1.250	0.7963	0.7857	1.3
1.333	0.9732	0.9630	1.0
1.500	1.191	1.186	0.0
1.667	1.276	1.273	0.0
1.917	1.293	1.293	0.0
2.167	1.285	1.287	0.0
2.417	1.241	1.244	0.0
2.667	0.9790	0.9891	1.0
2.750	0.8016	0.8120	0.0
2.833	0.5739	0.5842	1.8
2.917	0.3040	0.3112	2.4
3.000	0.0000	0.0000	0.0

Table 3.5 Comparison of the results of the original (run 404) and modified (run 505) working section analyses in the plane eight step heights downstream of the sudden expansion

$\frac{y}{h}$	$\frac{U_{404}}{U_o}$	$\frac{U_{505}}{U_o}$	$\frac{\lvert U_{404} - U_{505} \rvert}{U_{404}} \times 100\%$
0.0000	0.0000	0.0000	0
0.1667	-0.0510	-0.0684	34
0.333	0.0277	-0.0120	143
0.5000	0.1988	0.1831	8
0.6667	0.4229	0.3483	18
0.8333	0.6613	0.5865	11
1.000	0.8837	0.8264	6
1.083	0.9750	0.9338	4
1.167	1.052	1.030	2
1.250	1.113	1.112	0
1.333	1.157	1.176	3
1.500	1.210	1.263	4
1.667	1.223	1.292	6
1.917	1.180	1.241	5
2.167	1.023	1.057	3
2.417	0.7044	0.7228	3
2.667	0.3229	0.3336	3
2.750	0.2138	0.2219	4
2.833	0.1223	0.1277	4
2.917	0.0506	0.0532	5
3.000	0.0000	0.0000	

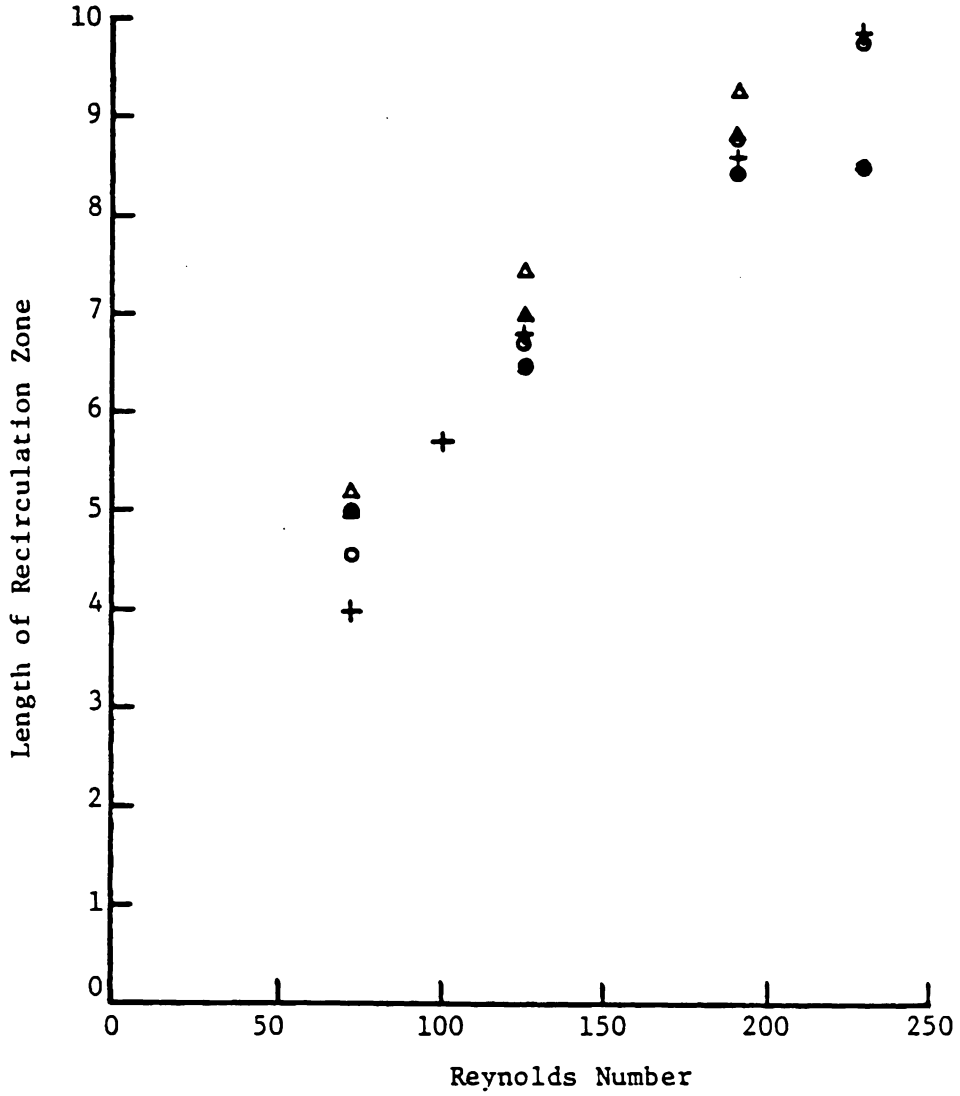

Fig. 3.35. Variation of separation length with Reynolds number. ▲ , experimental inlet profiles (5); △ ,fully developed inlet profiles (5); + , experimental data (7); ● , present calculations with experimental inlet profiles; o, present calculations of the flow through the modified working section design.

develop more fully. This trend was also reported by Thomas (5), whose numerical predictions are also presented in this figure.

3.2.3 Sensitivity Studies

As noted previously in section 3.2.1, to analyze the Denham and Patrick working section it was necessary to assume both the geometry of the fairing and the shape of the inlet velocity profile. To determine the extent to which the results of presented earlier in the vicinity of the step might have been affected by the particular values chosen for these parameters, two additional series of runs were made. The first, or 600 series, was used to determine the sensitivity of the flow near the step to changes in the velocity field in the plane of the nozzle exit, $x/h = -13.333$, while the second (700 series) examined the effects of altering the geometry of the fairing. The results of each of these studies will now be presented and discussed.

3.2.3.1 Inlet Velocity Profile

In choosing the inlet profile used in the earlier analyses, it was assumed that: (1) the flow at the entrance to the working section was free of the nonuniformities that are often present to at least some extent at the exit plane of real nozzles, and (2) the initial boundary

layer thickness on both the top and bottom walls of the tunnel was 8.33 percent of the tunnel height. To determine the extent to which these assumptions might have affected the results of the 400 and 500 series runs, three variations on the original inlet profile were constructed and tested. As shown in Fig. 3.36, the inlet profiles for runs 601 and 602 were constructed so as to shift the mass flow towards the bottom and top of the tunnel, respectively, without altering the degree of development of the original profile. The inlet profile for run 603, on the other hand, was more developed than that used in runs 401 through 504, but like the original profile is constant between the segments near the walls representing the boundary layers. The dimensionless mass averaged velocity for each of the inlet profiles in this series is equal to that of the original profile.

The finite element mesh used in runs 601 and 602 is depicted in the aforementioned Fig. 3.24. This is the same mesh used earlier in run 404. The computational grid for run 603 was the same as that used in runs 601 and 602 except that the nodal points were shifted towards the walls to facilitate the implementation of the inlet velocity profile. Refer to Fig. 3.37. All three runs in this series were made at Re = 229, the Reynolds number at which any deviations from the results reported earlier would have been expected to be the most pronounced.

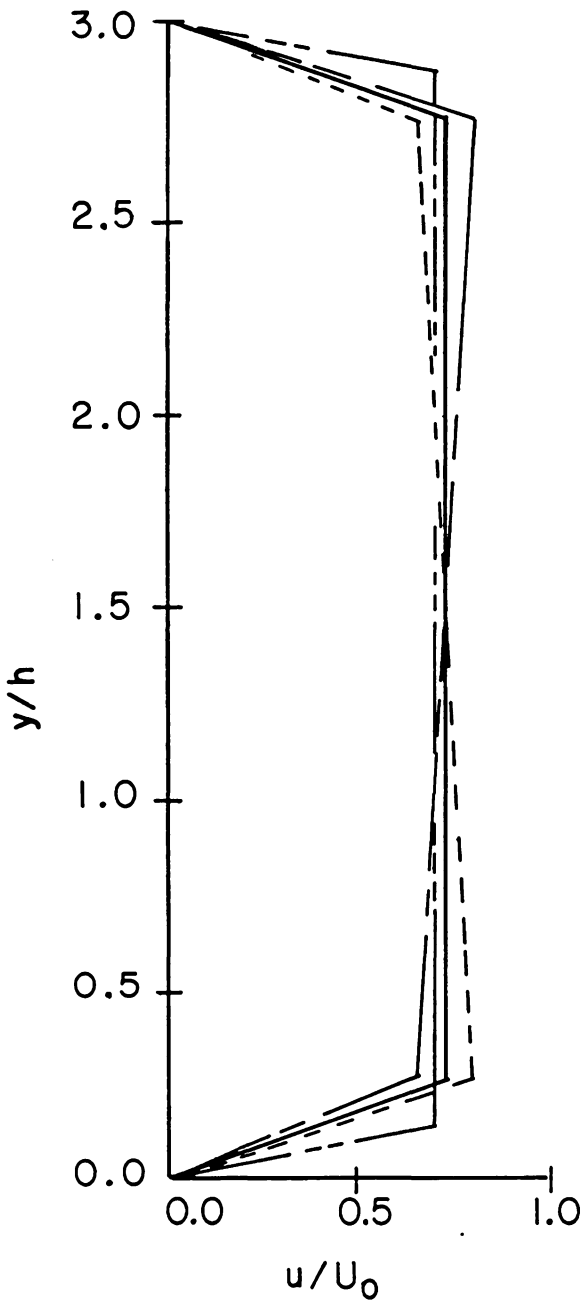

Fig. 3.36. Alternative inlet profiles. ——, run 404; ---, run 601; —·—, run 602; —·—·—, run 603.

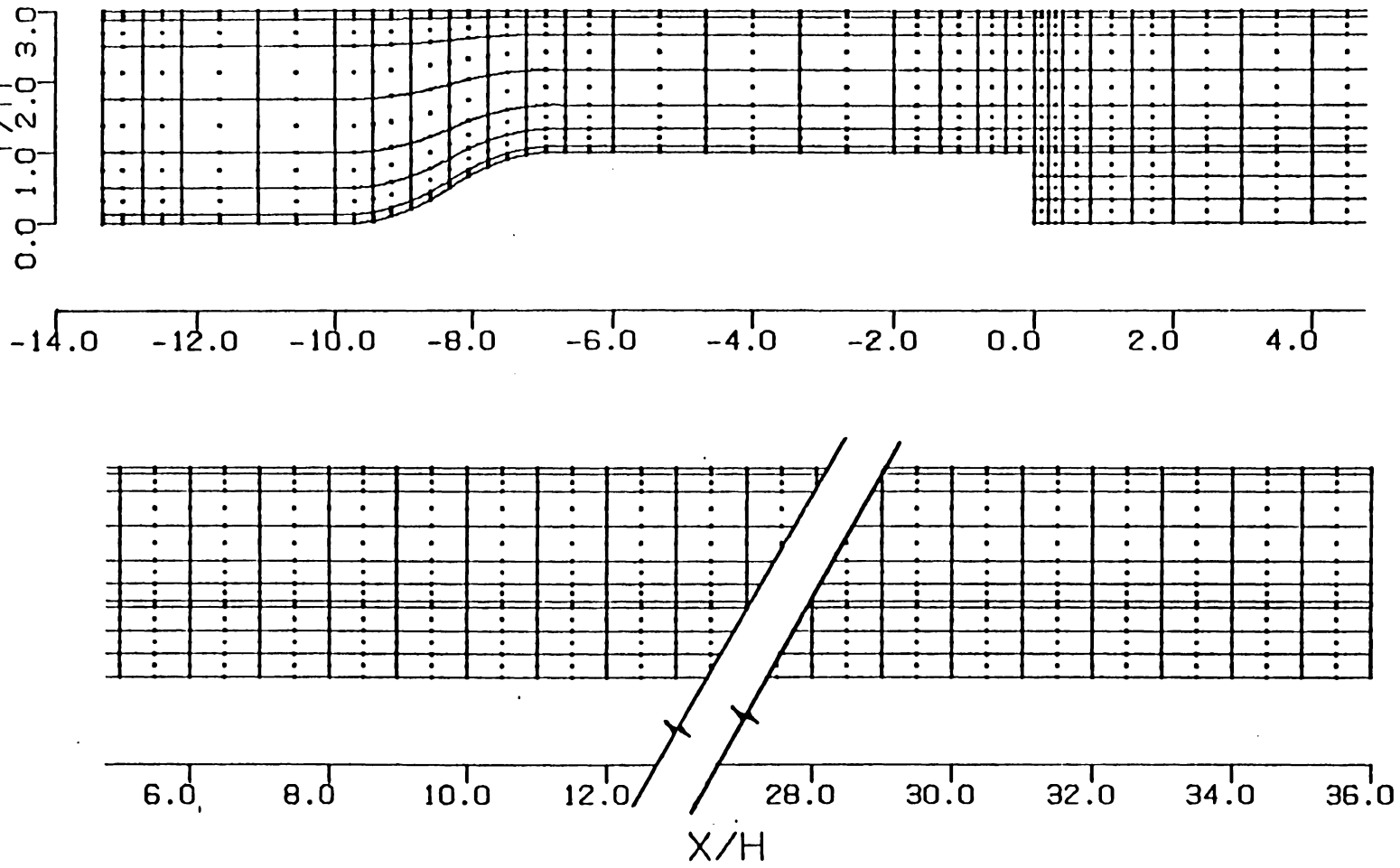

Fig. 3.37. Finite element mesh with 516 elements and 2199 nodal points for run 603.

The significant results of the 600 series of runs are shown in Figs. 3.38 through 3.40, where they are also compared to the results of the earlier analysis, run 404, in which the original inlet profile was used. As expected, and indeed hoped for, these figures clearly show that while the u-velocity components both upstream and in the vicinity of the fairing are noticeably different than those of run 404, all the results displayed in these figures at and downstream of the initial plane of experimental data are virtually indistiguishable. This is also illustrated in Table 3.6, which summarizes the computed u-velocity components for runs 404 and 601 through 603 at the streamwise location of the initial plane of experimental data. As can be seen by comparing the entries in this table, the maximum relative difference between the 600 series results and those of run 404 is only 1.9 percent. Thus, assuming the salient features of the actual inlet profile were within the range of the parameters tested, it can be concluded that the results and conclusions presented earlier in section 3.2.2 are unaffected by possible differences between the assumed and actual (unknown) inlet profiles.

3.2.3.2 Geometry of the Fairing

The 700 series of runs was made to assess the sensitivity of the flow near the step to the presumed details

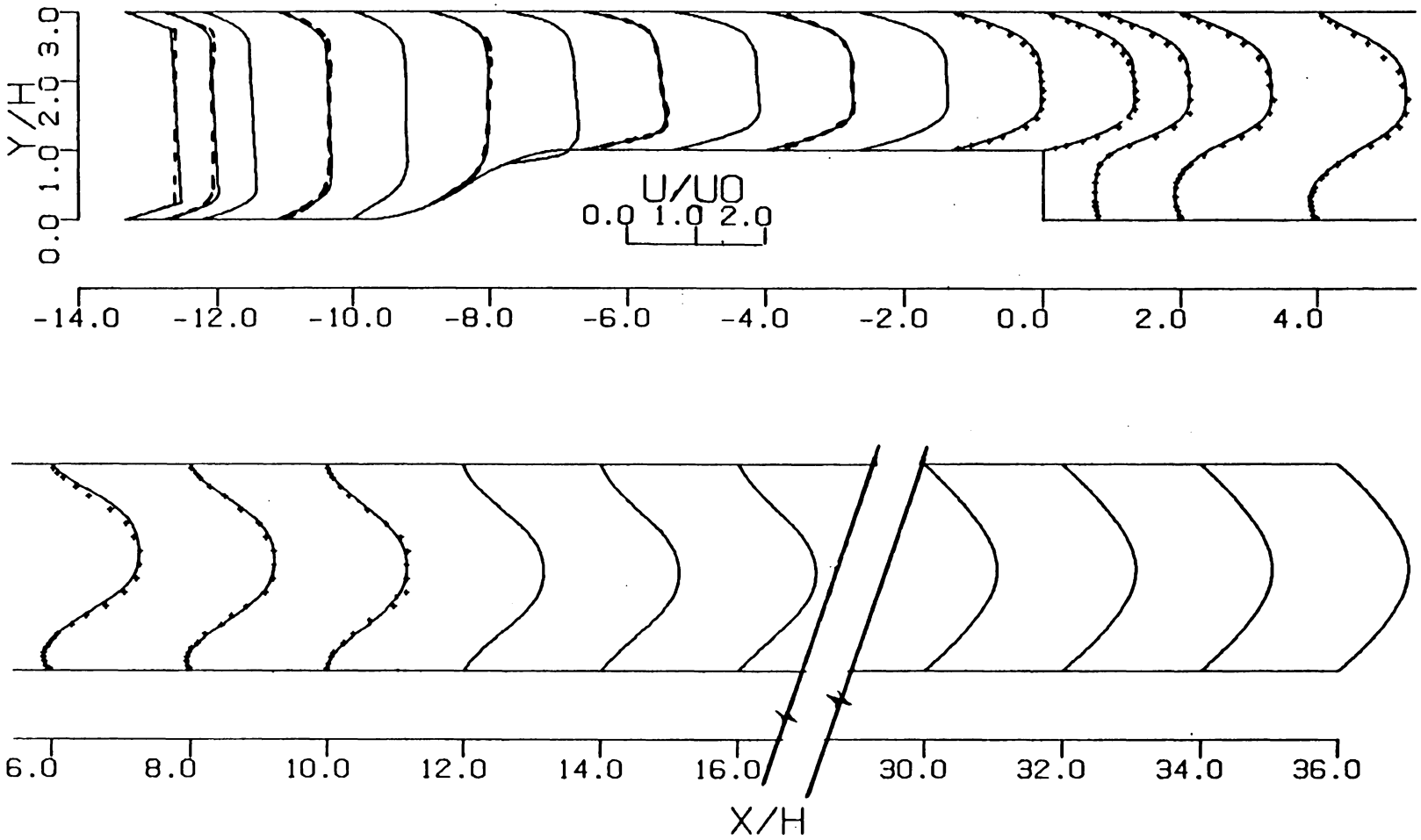

Fig. 3.38 U-velocity profiles from run 601. Inlet mass flow shifted towards tunnel floor. ---, run 404; +, Denham and Patrick.

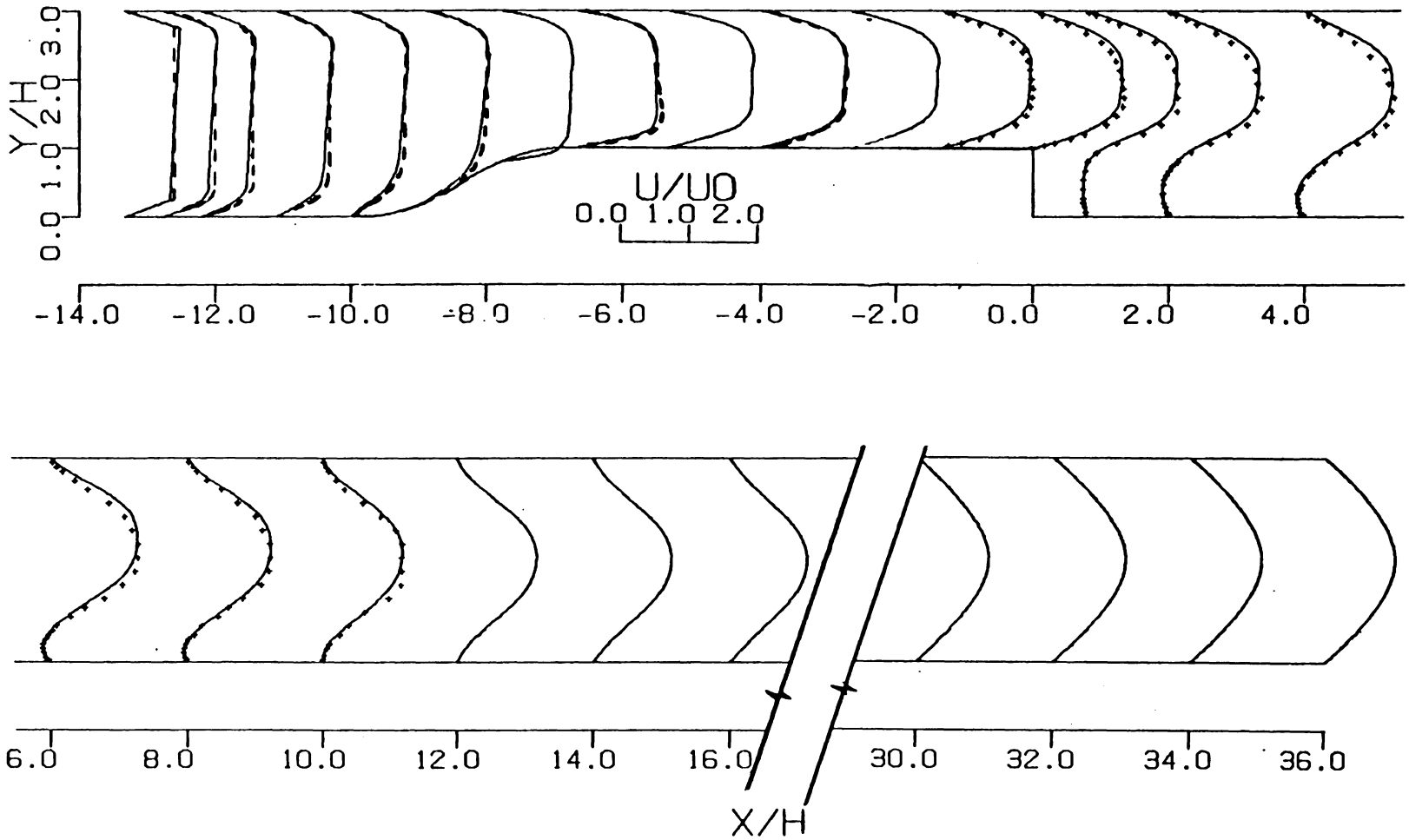

Fig. 3.39. U-velocity profiles from run 602. Inlet mass flow shifted towards top of tunnel. ---, run 404; +, Denham and Patrick.

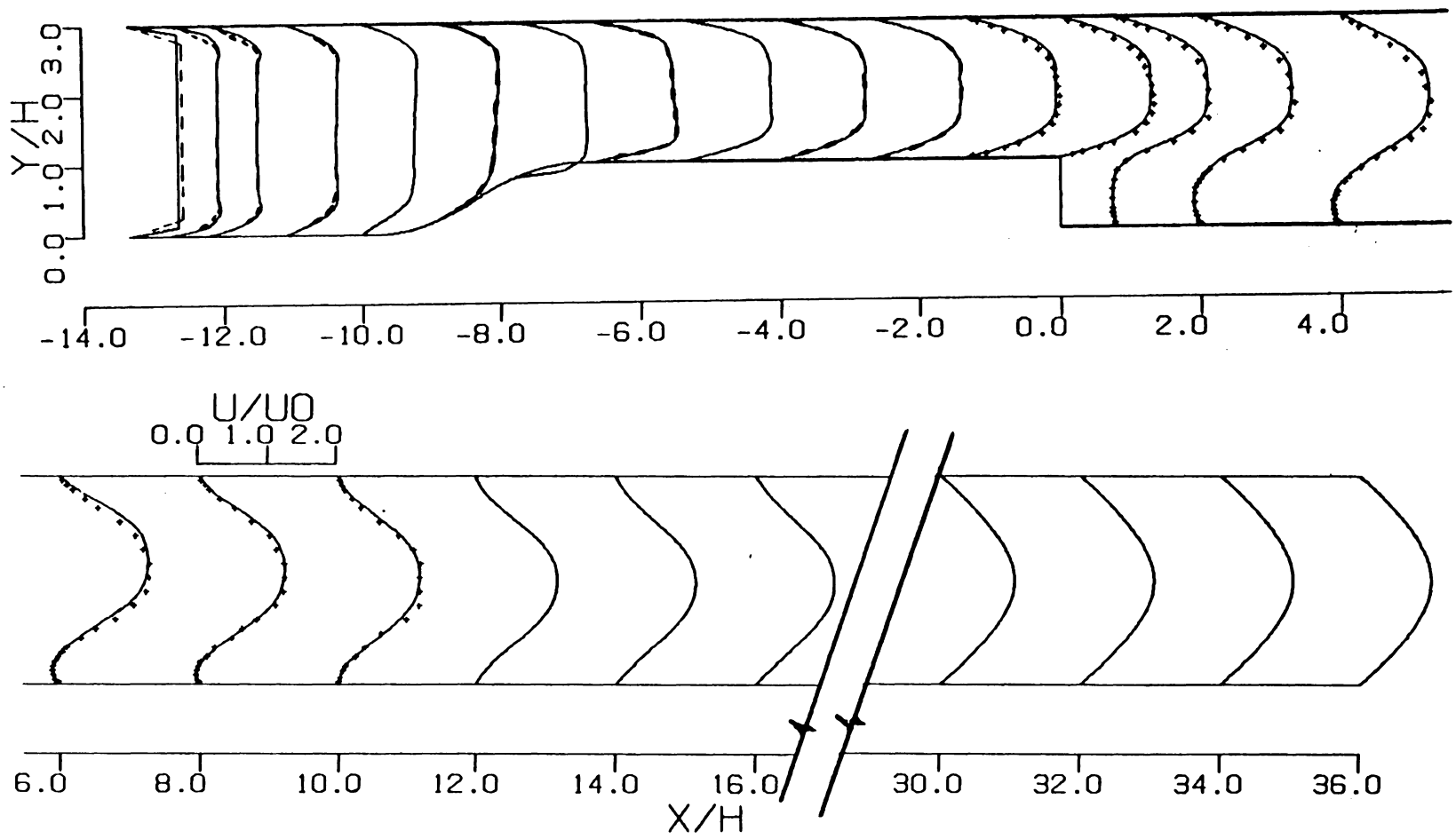

Fig. 3.40. U-velocity profile from run 603. Thinner boundary layers at the inlet. ---, run 404; +, Denham and Patrick.

Table 3.6. Comparison of u-velocities from runs 404, 601, 602 and 603 at x/h = - 1.333

$\frac{y}{h}$	$\frac{U_{404}}{U_o}$	$\frac{U_{601}}{U_o}$	Δ_{601}	$\frac{U_{602}}{U_o}$	Δ_{602}	$\frac{U_{603}}{U_o}$	Δ_{603}
1.000	0.000	0.000	0.0	0.000	0.0	0.000	0.0
1.083	0.308	0.313	1.6	0.303	1.6	0.309	0.3
1.167	0.574	0.584	1.7	0.565	1.6	---	---
1.250	0.796	0.810	1.8	0.782	1.7	---	---
1.333	0.973	0.990	1.7	0.956	1.7	0.976	0.3
1.500	1.919	1.211	1.7	1.171	1.7	1.193	0.2
1.667	1.276	1.244	1.4	1.259	1.3	1.275	0.1
1.917	1.293	1.298	0.0	1.288	0.4	1.288	0.4
2.167	1.285	1.276	0.1	1.295	0.8	1.281	0.3
2.417	1.241	1.222	1.5	1.260	1.5	1.241	0.0
2.667	0.979	0.961	1.8	0.996	1.7	0.983	0.4
2.750	0.802	0.787	1.9	0.816	1.7	---	---
2.833	0.574	0.563	1.9	0.584	1.7	---	---
2.917	0.304	0.299	1.6	0.309	1.6	0.306	0.6
3.000	0.000	0.000	0.0	0.000	0.0	0.000	0.0

Note: $\Delta_{xxx} \equiv [|U_{404} - U_{xxx}|/U_{404}] \times 100\%$

of the manner in which the step test section was faired into the floor of the tunnel. The two alternative geometries selected for this study are shown in Fig. 3.41. As is evident from this figure, the profiles for runs 701 and 702 were obtained by merely stretching and compressing the shape originally assumed.

All the runs in this series were made at Re = 229 using the inlet velocity profile used earlier in runs 401 through 504. The finite element grids for runs 701 and 702 are presented in Figs. 3.42 and 3.43, respectively. These grids are everywhere identical to that used earlier in run 404, the basis for comparison for this series of runs, except of necessity in the segment of the working section leading up to the constant area section that forms the step. The pertinent results of runs 701 and 702 are displayed and compared to those of run 404 and in Figs. 3.44 and 3.45, respectively. These comparisons clearly indicate that the alterations to the working section geometry described above do not propagate far enough downstream to affect the results either near or downstream of the step. This conclusion can also be drawn from the comparison of the computed nodal point velocities presented in the form of Table 3.7. As can be seen by comparing the corresponding entries in this table, the nodal velocities at x/h = - 1.333 do not vary by more than 1.3 percent.

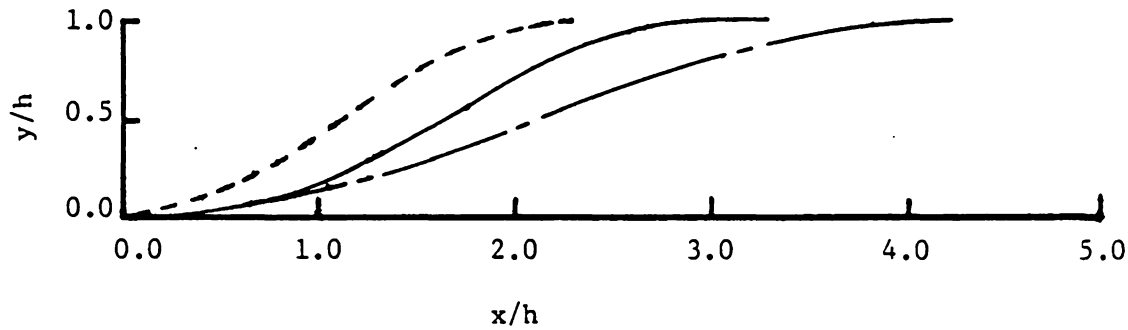

Fig. 3.41. Alternative transitions to the step.
——, run 404; —— - ——, run 702;
– – –, run 703.

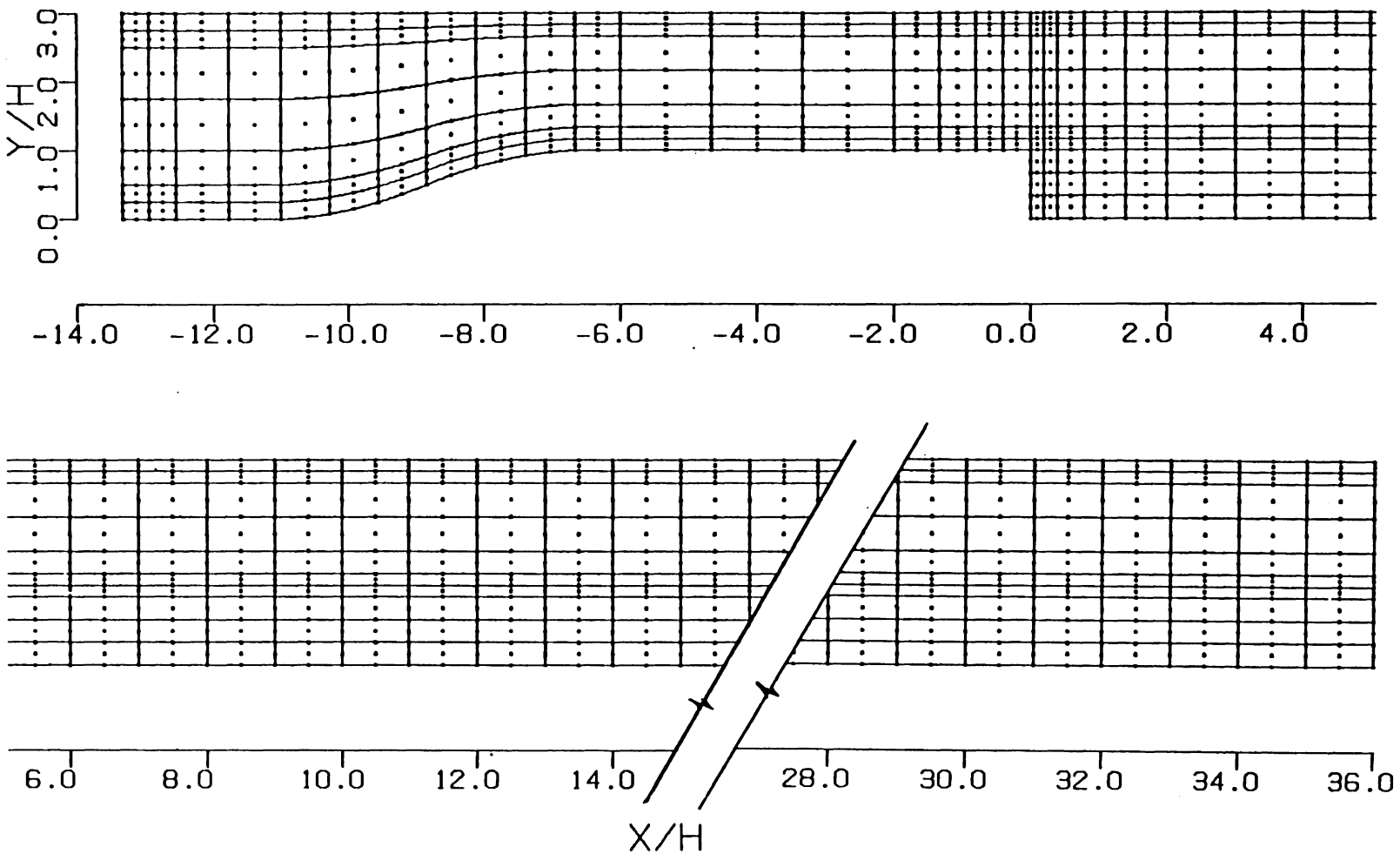

Fig. 3.42. Finite element mesh with 516 elements and 2199 nodal points for run 701. Lengthened transition to the step.

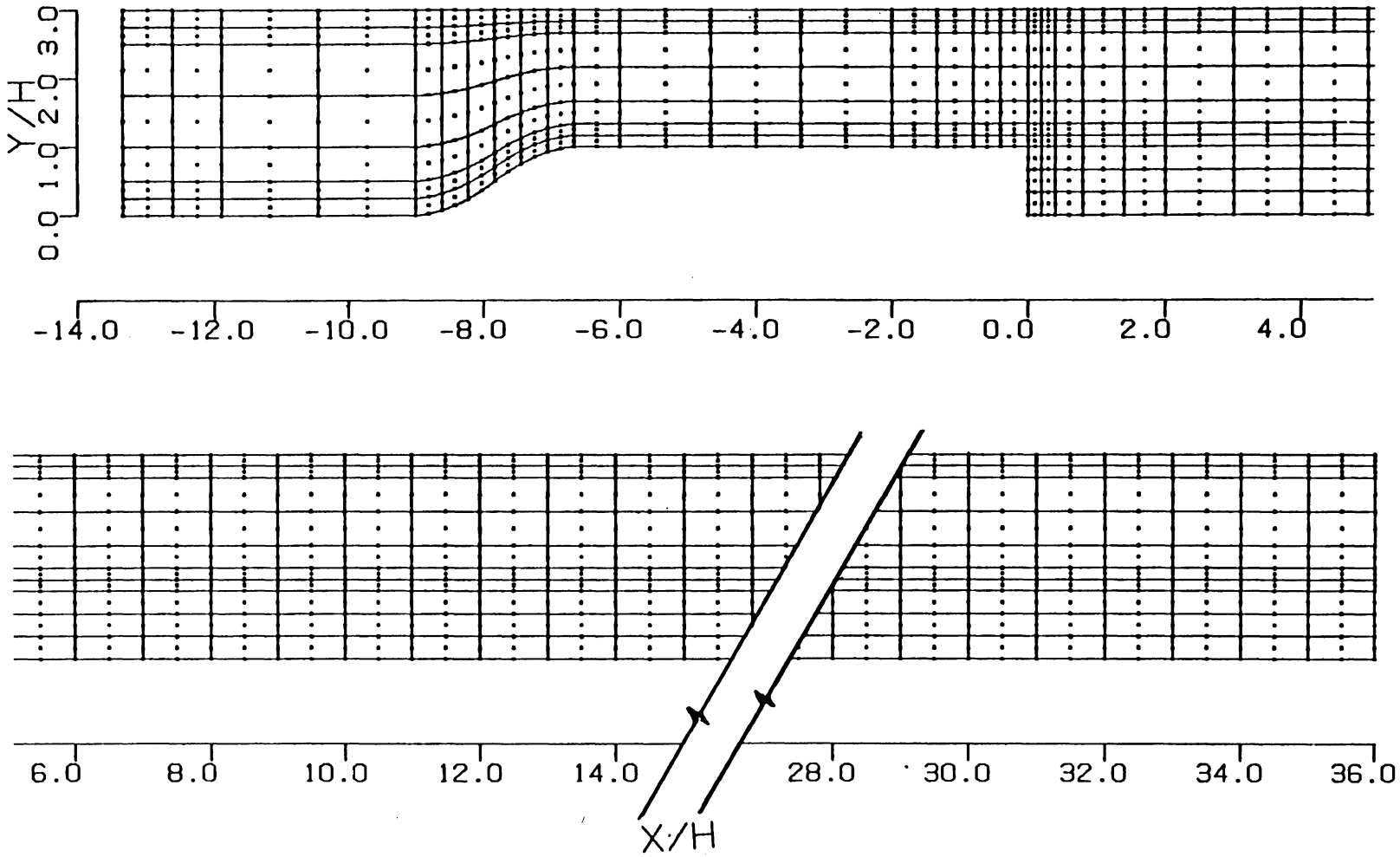

Fig. 3.43. Finite element mesh with 516 elements and 2199 nodal points for run 702. Shortened transition to the step.

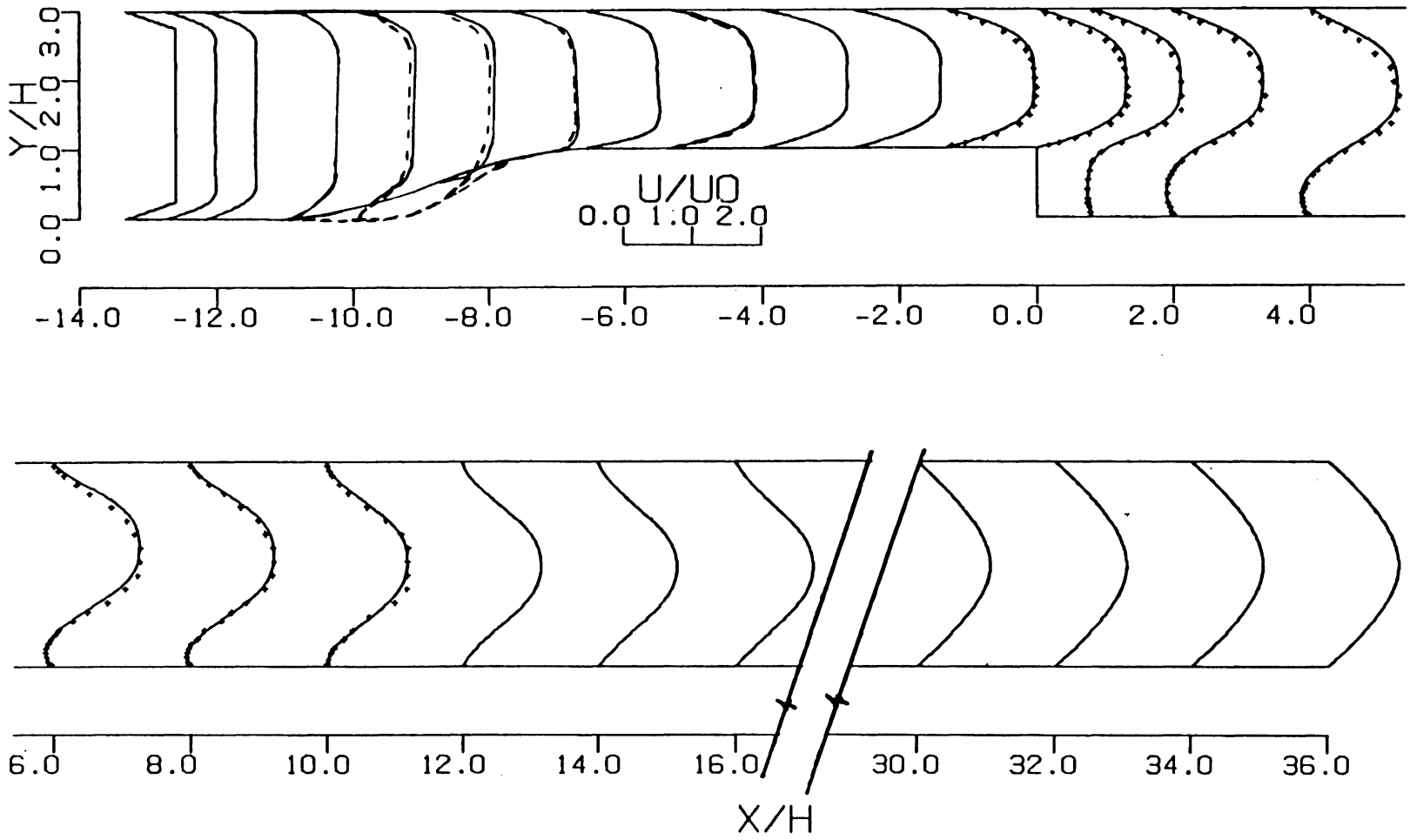

Fig. 3.44. U-velocity profiles from run 701. Effects of lenghtening the transition to the step. ---, run 404; +, Denham and Patrick.

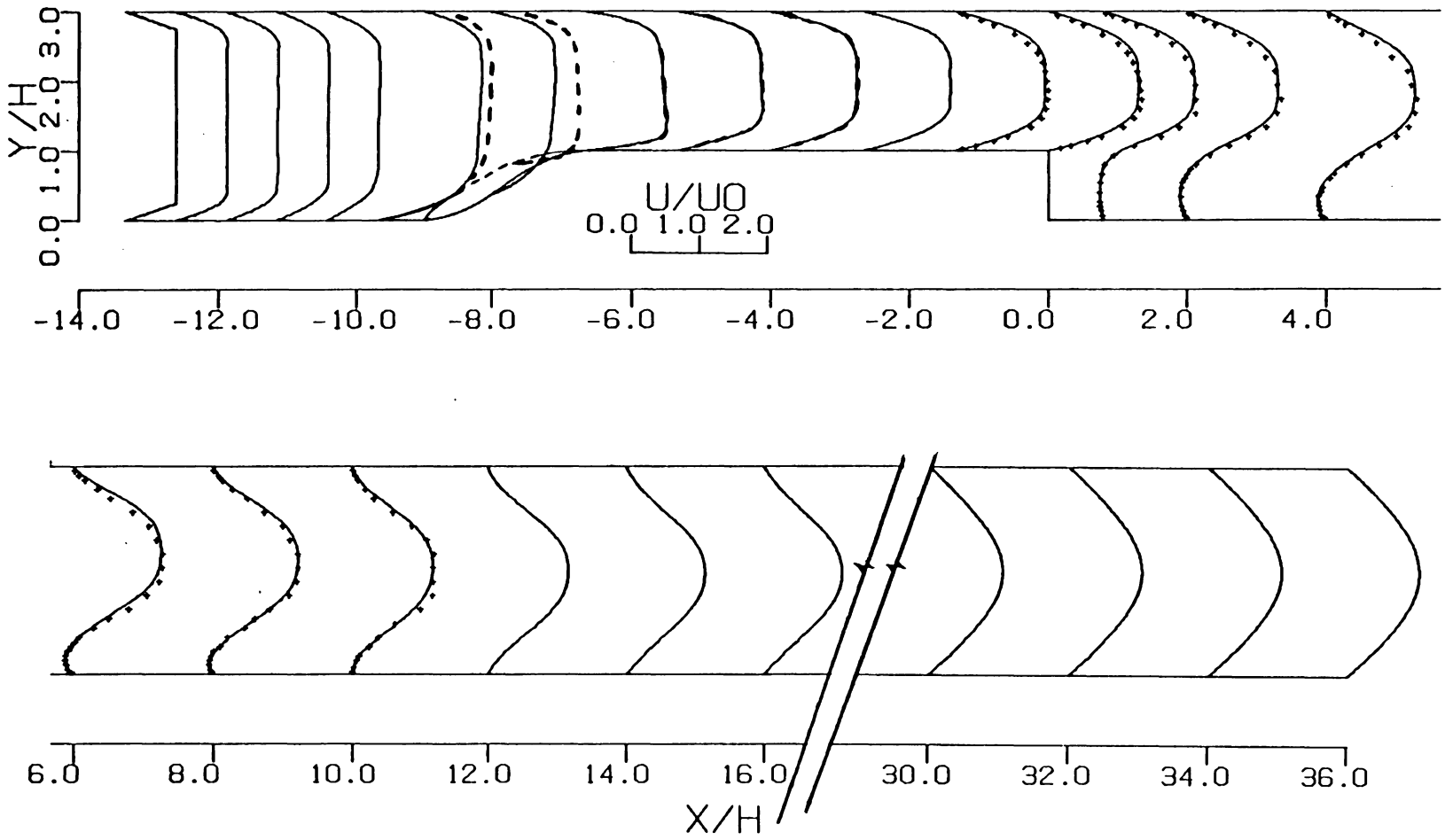

Fig. 3.45. U-velocity profiles from run 702. Effects of shortening the transition to the step: +, Denham and Patrick (7); ---, run 404.

Table 3.7 Comparison of computed u-velocity components from runs 404, 701, and 702 at x/h = -1.333

$\frac{y}{h}$	$\frac{U_{404}}{U_o}$	$\frac{U_{701}}{U_o}$	Δ_{701}	$\frac{U_{702}}{U_o}$	Δ_{702}
1.000	0.000	0.000	0.000	0.000	0.0
1.083	0.308	0.309	0.3	0.309	0.3
1.167	0.574	0.576	0.3	0.577	0.5
1.250	0.796	0.799	0.4	0.799	0.4
1.333	0.973	0.976	0.3	0.976	0.3
1.500	1.191	1.193	0.2	1.191	0.0
1.667	1.276	1.278	0.2	1.272	0.3
1.917	1.293	1.295	0.2	1.288	04
2.167	1.285	1.286	0.1	1.280	0.4
2.417	1.241	1.239	0.1	1.290	0.1
2.667	0.979	0.974	0.5	0.987	0.8
2.750	0.802	0.797	0.6	0.810	1.0
2.833	0.574	0.571	0.5	0.581	1.2
2.917	0.403	0.302	0.6	0.308	1.3
3.000	0.000	0.000	0.0	0.000	0.0

Note: $\Delta_{xxx} \equiv [|U_{404} - U_{xxx}|/U_{404}] \times 100\%$

4. SUMMARY

In Chapter 2, a finite element analysis was presented in which:

1. The weak or integral form of the governing equations was generated by the standard Bubnov-Galerkin method for mixed problems.
2. The finite dimensional subspace of velocity approximations was generated by a set of basis functions constructed from second order Lagrange interpolating polynomials.
3. The spatial variation of the pressure field on each element was represented in terms of a discontinuous, linear approximation.
4. The set of nonlinear, algebraic equations resulting from the spatial discretization of the field equations was linearized by employing a successive substitution method to bring the initial estimates inside the radius of convergence of a Newton-Raphson scheme, which was then used to accelerate the convergence.
5. The solution to the set of linear, algebraic equations produced at each iteration by either of the schemes just mentioned was obtained using the out-of-core, profile type solver by Hasbani and Engelman (40).

The method described above was used to predict the

confined, laminar flow over a backward facing step, and to determine the cause(s) and effects of the noticeable lack of development and skewness that characterized the experimental data both at and upstream of the step. The results of the various analyses presented in Chapter 3, together with the ensuing comparisons indicate that:

1. With the proper choice of basis functions, a conventional Galerkin scheme such as the one used here can yield results that are in as good and in many cases better agreement with the available experimental data than those of unconventional formulations that rely upon an infusion of artifical dissipation to enhance their numerical stability.
2. As suggested originally by Denham and Patrick (7), the skewness in their initial plane of data was indeed caused by the asymmetry of the contraction leading up to the step, rather than by some elliptic effect of the step itself.
3. For a given Reynolds number, the flow field downstream of the step is sensitive to the degree of development of the velocity field just upstream of the step. For example, it appears that enhancing the degree of development of the velocity field at the step increases the length

of the recirculating region behind it.

4. The flow field in the vicinity of the step does not appear to be overly sensitive to either the shape of the u-velocity profile at the inlet to the working section, or to the manner in which the step test section is faired into the floor of the tunnel. This latter observation is of course predicated upon the assumption that the transition is not so sharp as to induce separation.

REFERENCES

1. Shen, S., "Finite Element Methods in Fluid Mechanics," Ann. Rev. Fluid Mech., Vol. 9, 1977, pp. 421-445.

2. Martin, H. C., Proc. Conf. Matrix Methods in Structural Mechanics, AFFDL-TR-68-150, Wright Patterson Air Force Base, Dayton, Ohio, 1968, pp. 517-535.

3. Bredif, M., "Calculation of Laminar Flow Over a Step by a Finite Element Method Based on the Stream Function-Vorticity Formulation," Seminaire "Analyse Numerique de 1'Ecoulement Laminaire Derriere une Marche," Bievres, 1983.

4. Ecer, A., Rout, R. K., and Ward, P., "Investigation of Solution of Navier-Stokes Equations Using a Variational Formulation," International Journal for Numerical Methods in Fluids, Vol. 3, 1983, pp. 23-31.

5. Thomas, C. E., Morgan, K., and Taylor, C., "A Finite Element Analysis of Flow Over a Backward Facing Step," Computers and Fluids, Vol. 9, 1981, pp. 265-278.

6. Fortin, M., "Old and New Finite Elements for Incompressible Flows," International Journal for Numerical Methods in Fluids, Vol. 1, 1981, pp. 347-364.

7. Denham, M. K., and Patrick, M. A., "Laminar Flow Over a Downstream-Facing Step in a Two-Dimensional Flow Channel," Trans. Instn. Chem. Engrs., Vol. 52, 1974, pp. 361-367.

8. Ladyzhenskaya, O. A., The Mathematical Theory of Viscous Incompressible Flow, Rev. 2nd ed., Gordon and Breach, New York, 1969.

9. Teman, R., Navier-Stokes Equations, North-Holland, Amsterdam, 1979.

10. Girault, V., and Raviart, P., "Finite Element Approximations of the Navier-Stokes Equations," Lecture Notes in Mathematics, Vol. 749, Springer-Verlag, Berlin, 1979.

11. White, F. M., Viscous Fluid Flow, McGraw-Hill, New York, 1974.

12. Becker, E. B., Graham, F. C., and Oden, J. T., Finite

Elements, Vol. 1, Prentice-Hall, New Jersey, 1981.

13. Gresho, P. M., Lee, R. L., and Sani, R. L., "On the Time-Dependent Solution of the Incompressible Navier-Stokes Equations in Two and Three Dimensions," Lawrence Livermore Laboratory, UCRL-83282, 1979.

14. Sani, R. L., Gresho, P. M., Lee, R. L., and Griffiths, D. F., "The Cause and Cure (?) of the Spurious Pressures Generated by Certain FEM Solutions of the Incompressible Navier-Stokes Equations: Part 1," International Journal for Numerical Methods in Fluids, Vol. 1, 1981, pp. 17-43.

15. Reddy, J. N., "The Penalty Function Method in Mechanics: A Review of Recent Advances," ASME Applied Mechanics, Vol. 4., 1980.

16. Hughes, T. J. R., Liu, W. K., and Brooks, A., "Finite Element Analysis of Incompressible Viscous Flows by the Penalty Function Formulation," Journal of Computational Physics, Vol. 30, 1979, pp. 1-60.

17. Engelman, M. S. and Sani, R. L., "Finite-Element Simulation of an In-Package Pasteurization Process," Numerical Heat Transfer, Vol. 6, 1983, pp. 41-54.

18. Zienkiewicz, O. C., The Finite Element Method, 3rd ed., McGraw-Hill, New York, 1982.

19. Huyakorn, P., "Solution of Steady-State, Convective Transport Equations Using an Upwind Finite Element Scheme," Applied Mathematical Modeling, Vol. 1, 1977, pp. 187-195.

20. Heinrich, J., Huyakorn, P., Zienkiewicz, O., and Mitchell, A., "An Upwind Finite Element Scheme for Two Dimensional Convective Transport Equations," International Journal for Numerical Methods in Engineering, Vol. 11, 1977, pp. 131-143.

21. Gresho, P. M., and Lee, R. L., "Don't Suppress the Wiggles - They're Telling You Something!," Computers and Fluids, Vol. 9, 1981, pp. 223-253.

22. Taylor, C. and Hughes, T. G., Finite Element Programming of the Navier-Stokes Equations, Pineridge Press Limited, Swansea, U.K., 1981.

23. Prenter, P. M., Splines and Variational Methods, Wiley-Interscience, New York, 1975.

24. Babuska, I., "Error Bounds for Finite Element Methods," Numer. Math, Vol. 16, 1971, pp. 322-333.

25. Brezzi, F., "On the Existence, Uniqueness and Approximation of Adddle Point Problems Arising From Lagrangian Multipliers," RAIRO, Vol. 8, R-2, 1974, pp. 129-151.

26. Fix, G. J., Gunzburger, M. D., Nicolaides, R. A., and Peterson, J. S., "Mixed Finite Element Methods for Acoustics and Flow Problems," AIAA 5th Computational Fluids Dynamics Conference, Palo Alto, CA, 1981.

27. Gunzburger, M. D., and Peterson, J. S., "On Conforming Mixed Finite Element Methods for the Inhomogeneous Stationary Navier-Stokes Equations," Department of Mathematics and Statistics, University of Pittsburg, Technical Report ICMA-82-83, 1982.

28. Gunzburger, M. D., Nicolaides, R. A., and Peterson, J. S., "On Conforming Mixed Fiite Element Methods for Incompressible Viscous Flow Problems," Institute for Computer Applications in Science and Engineering, NASA Langley Research Center, Virginia, Report Number 81-23, 1981.

29. Sani, R. L., Gresho, P. M., Lee, R. L., Griffiths, D. F., and Engelman, M., "The Cause and Cure (?) of the Spurious Pressures Generated by Certain FEM Solutions of the Incompressible Navier-Stokes Equations: Part 2," International Journal for Numerical Methods in Fluids, Vol. 1, 1981, pp. 171-204.

30. Crouzeix, M. and Raviart, "Conforming and Non-Conforming Finite Element Methods for Solving the Stationary Stokes Equations," RAIRO, 7-R2, 1973, pp. 33-76.

31. Huyakorn, P. S., Taylor, R. L., Lee, R. L., and Gresho, P. M., "A Comparison of Various Mixed-Interpolation Finite Elements in the Velocity-Pressure Formulation of the Navier-Stokes Equations," Computers and Fluids, Vol. 6, 1978, pp. 25-35.

32. Gresho, P. M., Lee, R. L., Chan, S. T., and Leone, J. M., "A New Finite Element for Incompressible Boussinesq Fluids," Proc. Third International Conference on Finite Elements in Fluid Flow Problems, Baniff, Canada, June 10-13, 1980.

33. Leone, J. M., "Finite Element Simulations of Stratified Flow Over Simple Geometric Obstructions and Arbitrarily Complex Terrain," Ph.D. Thesis, Iowa State University, Ames, Iowa, 1980.

34. Sani, R. L., Gresho, P. M., and Lee, R. L., "On the Spurious Pressures Generated by Certain FEM Solutions of the Incompressible Navier-Stokes Equations," Proc. Third International Conference on Finite Elements in Flow Problems, Baniff, Canada, June 10-13, 1980.

35. Hinton, E. and Owen, D. R. J., "An Introduction to Finite Element Computations," Pineridge Press Limited, Swansea, U.K., 1981.

36. Bathe, K-J. and Wilson, E. L., "Numerical Methods in Finite Element Analysis," Prentice-Hall, New Jersey, 1976.

37. Heubner, K. H. and Thornton, E. A., "The Finite Element Method for Engineers," John Wiley & Sons, 2nd ed., 1982.

38. Irons, B. M., "Quadrature Rules for Brick Based Finite-Elements," International Journal for Numerical Methods in Engineering, Vol. 3, 1971.

39. Burden, R. L., Faires, J. D., and Reynolds, A. C., Numerical Analysis, 2nd ed., Prindle, Weber & Schmidt, Boston, Massachusetts, 1981.

40. Hasbani, Y. and Engelman, M., "Out-of-Core Solution of Linear Equations with Non-Symmetric Coefficient Matrix," Computers and Fluids, Vol. 7, 1979, pp. 13-31.

41. Meyer, C., "Solution of Equations; State of the Art," Journal of Structures Division, ASCE, Vol. 99, 1973, pp. 1507-1526.

42. Pelletier, D. H., "GENZD - A General Purpose Finite Element Mesh Generator for Two-Dimensional Geometries," Aerospace and Ocean Engineering Department, Virginia Polytechnic Institute and State University, Blacksburg, Virginia, Report. No. VPI-Aero-142, 1984.

43. Sampson, R. J., "SURFACE II Graphics Systems," Series on Spatial Analysis, Kansas Geological Survey, Lawrence, Kansas, 1978.

APPENDIX A

Tabulated Results of the Analysis of the Denham and Patrick (7) Step

A.1 Results of the Analysis at RE = 73 (Run 201)

NODE NUMBER	NODAL COORDINATES X/L	Y/L	VELOCITY COMPONENTS U/U0	V/V0	AVERAGE PRESSURES (P-P0)/(RHO0*U0**2)
1	-1.333D+00	3.000D+00	0.0	0.0	-2.077D-02
2	-1.333D+00	2.900D+00	3.500D-01	0.0	-2.137D-02
3	-1.333D+00	2.800D+00	6.000D-01	0.0	-2.368D-02
4	-1.333D+00	2.700D+00	8.600D-01	0.0	-2.764D-02
5	-1.333D+00	2.600D+00	1.020D+00	0.0	-3.223D-02
6	-1.333D+00	2.450D+00	1.250D+00	0.0	-4.109D-02
7	-1.333D+00	2.300D+00	1.400D+00	0.0	-4.863D-02
8	-1.333D+00	2.150D+00	1.480D+00	0.0	-5.867D-02
9	-1.333D+00	2.000D+00	1.500D+00	0.0	-6.841D-02
10	-1.333D+00	1.850D+00	1.440D+00	0.0	-7.795D-02
11	-1.333D+00	1.700D+00	1.330D+00	0.0	-8.689D-02
12	-1.333D+00	1.550D+00	1.150D+00	0.0	-9.291D-02
13	-1.333D+00	1.400D+00	9.000D-01	0.0	-9.990D-02
14	-1.333D+00	1.300D+00	6.900D-01	0.0	-1.021D-01
15	-1.333D+00	1.200D+00	5.000D-01	0.0	-1.029D-01
16	-1.333D+00	1.100D+00	2.500D-01	0.0	-1.030D-01
17	-1.333D+00	1.000D+00	0.0	0.0	-1.033D-01
137	0.0	3.000D+00	0.0	0.0	-9.125D-02
138	3.238D-17	2.900D+00	2.869D-01	-2.727D-03	-9.076D-02
139	-9.252D-18	2.800D+00	5.519D-01	-9.341D-03	-9.022D-02
140	1.388D-17	2.700D+00	7.868D-01	-1.755D-02	-9.074D-02
141	-6.476D-17	2.600D+00	9.863D-01	-2.570D-02	-9.109D-02
142	4.163D-26	2.450D+00	1.218D+00	-3.584D-02	-9.465D-02
143	-5.551D-17	2.300D+00	1.377D+00	-4.336D-02	-9.847D-02
144	-4.626D-18	2.150D+00	1.468D+00	-4.875D-02	-1.057D-01
145	4.163D-26	2.000D+00	1.492D+00	-5.215D-02	-1.130D-01
146	-4.626D-17	1.850D+00	1.450D+00	-5.298D-02	-1.220D-01
147	-6.014D-17	1.700D+00	1.346D+00	-5.217D-02	-1.311D-01
148	-4.626D-17	1.550D+00	1.179D+00	-4.799D-02	-1.398D-01
149	-4.626D-18	1.400D+00	9.494D-01	-4.280D-02	-1.487D-01
150	-4.626D-18	1.300D+00	7.657D-01	-3.564D-02	-1.540D-01
151	9.252D-18	1.200D+00	5.533D-01	-3.226D-02	-1.614D-01
152	-5.089D-17	1.100D+00	3.183D-01	-2.044D-02	-1.682D-01
153	0.0	1.000D+00	0.0	0.0	-1.773D-01
369	8.000D-01	3.000D+00	0.0	0.0	-1.004D-01
370	8.000D-01	2.900D+00	2.450D-01	-2.790D-03	-9.977D-02

371	8.000D-01	2.800D+00	4.845D-01	-1.002D-02	-9.917D-02
372	8.000D-01	2.700D+00	7.093D-01	-1.987D-02	-9.930D-02
373	8.000D-01	2.600D+00	9.106D-01	-3.116D-02	-9.937D-02
374	8.000D-01	2.450D+00	1.155D+00	-4.609D-02	-1.016D-01
375	8.000D-01	2.300D+00	1.329D+00	-6.002D-02	-1.042D-01
376	8.000D-01	2.150D+00	1.433D+00	-6.875D-02	-1.092D-01
377	8.000D-01	2.000D+00	1.471D+00	-7.690D-02	-1.144D-01
378	8.000D-01	1.850D+00	1.444D+00	-7.924D-02	-1.205D-01
379	8.000D-01	1.700D+00	1.354D+00	-8.088D-02	-1.266D-01
380	8.000D-01	1.550D+00	1.202D+00	-7.672D-02	-1.314D-01
381	8.000D-01	1.400D+00	9.886D-01	-7.031D-02	-1.359D-01
382	8.000D-01	1.300D+00	8.174D-01	-6.241D-02	-1.375D-01
383	8.000D-01	1.200D+00	6.324D-01	-5.126D-02	-1.391D-01
384	8.000D-01	1.100D+00	4.512D-01	-3.604D-02	-1.400D-01
385	8.000D-01	1.000D+00	2.932D-01	-1.836D-02	-1.409D-01
386	8.000D-01	9.000D-01	1.681D-01	-7.801D-04	-1.413D-01
387	8.000D-01	8.000D-01	7.570D-02	1.346D-02	-1.417D-01
388	8.000D-01	7.000D-01	1.078D-02	2.264D-02	-1.413D-01
389	8.000D-01	6.000D-01	-3.291D-02	2.659D-02	-1.408D-01
390	8.000D-01	5.000D-01	-5.956D-02	2.548D-02	-1.400D-01
391	8.000D-01	4.000D-01	-7.162D-02	2.108D-02	-1.393D-01
392	8.000D-01	3.000D-01	-7.094D-02	1.451D-02	-1.390D-01
393	8.000D-01	2.000D-01	-5.823D-02	7.625D-03	-1.388D-01
394	8.000D-01	1.500D-01	-4.770D-02	4.661D-03	-1.390D-01
395	8.000D-01	1.000D-01	-3.446D-02	2.204D-03	-1.391D-01
396	8.000D-01	5.000D-02	-1.857D-02	6.423D-04	-1.394D-01
485	2.000D+00	3.000D+00	0.0	0.0	-8.865D-02
486	2.000D+00	2.900D+00	1.847D-01	-2.432D-03	-8.809D-02
487	2.000D+00	2.800D+00	3.790D-01	-8.951D-03	-8.751D-02
488	2.000D+00	2.700D+00	5.756D-01	-1.886D-02	-8.726D-02
489	2.000D+00	2.600D+00	7.656D-01	-3.092D-02	-8.697D-02
490	2.000D+00	2.450D+00	1.018D+00	-4.988D-02	-8.761D-02
491	2.000D+00	2.300D+00	1.215D+00	-6.863D-02	-8.843D-02
492	2.000D+00	2.150D+00	1.347D+00	-8.267D-02	-9.065D-02
493	2.000D+00	2.000D+00	1.414D+00	-9.506D-02	-9.301D-02
494	2.000D+00	1.850D+00	1.417D+00	-1.006D-01	-9.616D-02
495	2.000D+00	1.700D+00	1.359D+00	-1.049D-01	-9.934D-02
496	2.000D+00	1.550D+00	1.240D+00	-1.016D-01	-1.023D-01
497	2.000D+00	1.400D+00	1.067D+00	-9.622D-02	-1.051D-01
498	2.000D+00	1.300D+00	9.267D-01	-8.804D-02	-1.064D-01

499	2.000D+00	1.200D+00	7.746D-01	-7.880D-02	-1.077D-01
500	2.000D+00	1.100D+00	6.188D-01	-6.689D-02	-1.084D-01
501	2.000D+00	1.000D+00	4.687D-01	-5.459D-02	-1.091D-01
502	2.000D+00	9.000D-01	3.307D-01	-4.172D-02	-1.093D-01
503	2.000D+00	8.000D-01	2.088D-01	-3.001D-02	-1.095D-01
504	2.000D+00	7.000D-01	1.055D-01	-1.973D-02	-1.093D-01
505	2.000D+00	6.000D-01	2.173D-02	-1.159D-02	-1.091D-01
506	2.000D+00	5.000D-01	-4.120D-02	-5.630D-03	-1.087D-01
507	2.000D+00	4.000D-01	-8.200D-02	-1.823D-03	-1.083D-01
508	2.000D+00	3.000D-01	-9.940D-02	1.012D-04	-1.081D-01
509	2.000D+00	2.000D-01	-9.202D-02	6.035D-04	-1.078D-01
510	2.000D+00	1.500D-01	-7.877D-02	5.244D-04	-1.078D-01
511	2.000D+00	1.000D-01	-5.905D-02	3.151D-04	-1.077D-01
512	2.000D+00	5.000D-02	-3.281D-02	1.322D-04	-1.078D-01
513	2.000D+00	-4.788D-16	0.0	0.0	-1.078D-01
601	4.000D+00	3.000D+00	0.0	0.0	-4.293D-02
602	4.000D+00	2.900D+00	1.139D-01	-1.224D-03	-4.259D-02
603	4.000D+00	2.800D+00	2.438D-01	-4.897D-03	-4.225D-02
604	4.000D+00	2.700D+00	3.865D-01	-1.101D-02	-4.186D-02
605	4.000D+00	2.600D+00	5.374D-01	-1.920D-02	-4.146D-02
606	4.000D+00	2.450D+00	7.646D-01	-3.517D-02	-4.064D-02
607	4.000D+00	2.300D+00	9.726D-01	-5.225D-02	-3.974D-02
608	4.000D+00	2.150D+00	1.141D+00	-7.016D-02	-3.843D-02
609	4.000D+00	2.000D+00	1.259D+00	-8.422D-02	-3.706D-02
610	4.000D+00	1.850D+00	1.318D+00	-9.666D-02	-3.541D-02
611	4.000D+00	1.700D+00	1.320D+00	-1.031D-01	-3.377D-02
612	4.000D+00	1.550D+00	1.264D+00	-1.069D-01	-3.217D-02
613	4.000D+00	1.400D+00	1.157D+00	-1.047D-01	-3.065D-02
614	4.000D+00	1.300D+00	1.060D+00	-1.013D-01	-2.978D-02
615	4.000D+00	1.200D+00	9.477D-01	-9.567D-02	-2.897D-02
616	4.000D+00	1.100D+00	8.234D-01	-8.836D-02	-2.833D-02
617	4.000D+00	1.000D+00	6.927D-01	-7.951D-02	-2.772D-02
618	4.000D+00	9.000D-01	5.609D-01	-6.967D-02	-2.725D-02
619	4.000D+00	8.000D-01	4.327D-01	-5.924D-02	-2.679D-02
620	4.000D+00	7.000D-01	3.127D-01	-4.857D-02	-2.642D-02
621	4.000D+00	6.000D-01	2.050D-01	-3.813D-02	-2.606D-02
622	4.000D+00	5.000D-01	1.134D-01	-2.828D-02	-2.574D-02
623	4.000D+00	4.000D-01	4.134D-02	-1.931D-02	-2.541D-02
624	4.000D+00	3.000D-01	-8.241D-03	-1.157D-02	-2.512D-02
625	4.000D+00	2.000D-01	-3.282D-02	-5.440D-03	-2.481D-02

626	4.000D+00	1.500D-01	-3.513D-02	-3.150D-03	-2.464D-02
627	4.000D+00	1.000D-01	-3.051D-02	-1.420D-03	-2.447D-02
628	4.000D+00	5.000D-02	-1.884D-02	-3.678D-04	-2.428D-02
629	4.000D+00	-4.267D-16	0.0	0.0	-2.409D-02
717	6.000D+00	3.000D+00	0.0	0.0	-1.152D-03
718	6.000D+00	2.900D+00	8.493D-02	-3.034D-04	-1.042D-03
719	6.000D+00	2.800D+00	1.819D-01	-1.390D-03	-9.421D-04
720	6.000D+00	2.700D+00	2.901D-01	-3.443D-03	-7.082D-04
721	6.000D+00	2.600D+00	4.074D-01	-6.662D-03	-5.142D-04
722	6.000D+00	2.450D+00	5.941D-01	-1.388D-02	3.626D-04
723	6.000D+00	2.300D+00	7.807D-01	-2.318D-02	1.299D-03
724	6.000D+00	2.150D+00	9.517D-01	-3.437D-02	3.404D-03
725	6.000D+00	2.000D+00	1.091D+00	-4.496D-02	5.627D-03
726	6.000D+00	1.850D+00	1.187D+00	-5.560D-02	9.001D-03
727	6.000D+00	1.700D+00	1.234D+00	-6.281D-02	1.247D-02
728	6.000D+00	1.550D+00	1.229D+00	-6.899D-02	1.631D-02
729	6.000D+00	1.400D+00	1.175D+00	-7.054D-02	2.008D-02
730	6.000D+00	1.300D+00	1.113D+00	-7.081D-02	2.235D-02
731	6.000D+00	1.200D+00	1.034D+00	-6.885D-02	2.457D-02
732	6.000D+00	1.100D+00	9.403D-01	-6.611D-02	2.631D-02
733	6.000D+00	1.000D+00	8.360D-01	-6.153D-02	2.802D-02
734	6.000D+00	9.000D-01	7.247D-01	-5.628D-02	2.920D-02
735	6.000D+00	8.000D-01	6.111D-01	-4.969D-02	3.035D-02
736	6.000D+00	7.000D-01	4.991D-01	-4.259D-02	3.106D-02
737	6.000D+00	6.000D-01	3.929D-01	-3.480D-02	3.174D-02
738	6.000D+00	5.000D-01	2.958D-01	-2.687D-02	3.212D-02
739	6.000D+00	4.000D-01	2.103D-01	-1.903D-02	3.249D-02
740	6.000D+00	3.000D-01	1.379D-01	-1.181D-02	3.276D-02
741	6.000D+00	2.000D-01	7.898D-02	-5.756D-03	3.303D-02
742	6.000D+00	1.500D-01	5.448D-02	-3.384D-03	3.319D-02
743	6.000D+00	1.000D-01	3.321D-02	-1.558D-03	3.335D-02
744	6.000D+00	5.000D-02	1.507D-02	-4.067D-04	3.356D-02
745	6.000D+00	-2.914D-16	0.0	0.0	3.377D-02
833	8.000D+00	3.000D+00	0.0	0.0	2.447D-02
834	8.000D+00	2.900D+00	8.345D-02	1.633D-04	2.445D-02
835	8.000D+00	2.800D+00	1.732D-01	4.862D-04	2.442D-02
836	8.000D+00	2.700D+00	2.690D-01	7.376D-04	2.450D-02
837	8.000D+00	2.600D+00	3.705D-01	6.195D-04	2.455D-02
838	8.000D+00	2.450D+00	5.308D-01	-5.518D-04	2.501D-02
839	8.000D+00	2.300D+00	6.935D-01	-3.263D-03	2.547D-02

840	8.000D+00	2.150D+00	8.490D-01	-7.320D-03	2.672D-02
841	8.000D+00	2.000D+00	9.841D-01	-1.247D-02	2.799D-02
842	8.000D+00	1.850D+00	1.089D+00	-1.791D-02	3.015D-02
843	8.000D+00	1.700D+00	1.153D+00	-2.316D-02	3.235D-02
844	8.000D+00	1.550D+00	1.173D+00	-2.754D-02	3.499D-02
845	8.000D+00	1.400D+00	1.149D+00	-3.065D-02	3.761D-02
846	8.000D+00	1.300D+00	1.109D+00	-3.193D-02	3.925D-02
847	8.000D+00	1.200D+00	1.052D+00	-3.232D-02	4.088D-02
848	8.000D+00	1.100D+00	9.805D-01	-3.202D-02	4.221D-02
849	8.000D+00	1.000D+00	8.974D-01	-3.080D-02	4.354D-02
850	8.000D+00	9.000D-01	8.056D-01	-2.887D-02	4.448D-02
851	8.000D+00	8.000D-01	7.090D-01	-2.608D-02	4.541D-02
852	8.000D+00	7.000D-01	6.106D-01	-2.270D-02	4.599D-02
853	8.000D+00	6.000D-01	5.133D-01	-1.873D-02	4.655D-02
854	8.000D+00	5.000D-01	4.192D-01	-1.451D-02	4.686D-02
855	8.000D+00	4.000D-01	3.291D-01	-1.024D-02	4.716D-02
856	8.000D+00	3.000D-01	2.431D-01	-6.298D-03	4.734D-02
857	8.000D+00	2.000D-01	1.604D-01	-3.030D-03	4.752D-02
858	8.000D+00	1.500D-01	1.199D-01	-1.763D-03	4.761D-02
859	8.000D+00	1.000D-01	7.973D-02	-8.060D-04	4.770D-02
860	8.000D+00	5.000D-02	3.980D-02	-2.021D-04	4.781D-02
861	8.000D+00	-3.331D-16	0.0	0.0	4.792D-02

A.2 Results of the Analysis at Re = 125 (Run 301)

NODE NUMBER	NODAL COORDINATES X/L	Y/L	VELOCITY COMPONENTS U/U0	V/V0	AVERAGE PRESSURES (P-P0)/(RHO0*U0**2)
1	-1.333D+00	3.000D+00	0.0	0.0	-2.133D-02
2	-1.333D+00	2.917D+00	2.000D-01	0.0	-2.120D-02
3	-1.333D+00	2.833D+00	4.400D-01	0.0	-1.804D-02
4	-1.333D+00	2.750D+00	6.620D-01	0.0	-1.447D-02
5	-1.333D+00	2.667D+00	8.300D-01	0.0	-1.250D-02
6	-1.333D+00	2.417D+00	1.211D+00	0.0	-1.316D-02
7	-1.333D+00	2.167D+00	1.368D+00	0.0	-1.572D-02
8	-1.333D+00	1.917D+00	1.389D+00	0.0	-1.850D-02
9	-1.333D+00	1.667D+00	1.315D+00	0.0	-1.852D-02
10	-1.333D+00	1.500D+00	1.165D+00	0.0	-1.501D-02
11	-1.333D+00	1.333D+00	9.200D-01	0.0	-1.236D-02
12	-1.333D+00	1.250D+00	7.230D-01	0.0	-1.003D-02
13	-1.333D+00	1.167D+00	5.530D-01	0.0	-4.727D-03
14	-1.333D+00	1.083D+00	3.350D-01	0.0	-4.722D-06
15	-1.333D+00	1.000D+00	0.0	0.0	3.028D-04
91	0.0	3.000D+00	0.0	0.0	-3.010D-02
92	-3.238D-17	2.917D+00	2.225D-01	-8.314D-04	-3.003D-02
93	-2.776D-17	2.833D+00	4.324D-01	-2.682D-03	-2.992D-02
94	-6.014D-17	2.750D+00	6.265D-01	-5.354D-03	-3.022D-02
95	9.252D-18	2.667D+00	8.015D-01	-8.687D-03	-3.009D-02
96	-9.252D-18	2.417D+00	1.188D+00	-1.670D-02	-3.474D-02
97	-3.701D-17	2.167D+00	1.367D+00	-2.334D-02	-4.026D-02
98	-6.939D-17	1.917D+00	1.401D+00	-2.183D-02	-5.030D-02
99	-3.701D-17	1.667D+00	1.324D+00	-2.483D-02	-6.059D-02
100	-2.776D-17	1.500D+00	1.181D+00	-1.942D-02	-6.849D-02
101	1.850D-17	1.333D+00	9.346D-01	-2.332D-02	-7.667D-02
102	1.388D-17	1.250D+00	7.634D-01	-1.727D-02	-8.028D-02
103	-3.701D-17	1.167D+00	5.599D-01	-2.018D-02	-8.482D-02
104	2.313D-17	1.083D+00	3.171D-01	-1.150D-02	-8.928D-02
105	3.701D-17	1.000D+00	0.0	0.0	-9.244D-02
217	8.000D-01	3.000D+00	0.0	0.0	-3.688D-02
218	8.000D-01	2.917D+00	2.031D-01	-1.245D-03	-3.670D-02
219	8.000D-01	2.833D+00	4.008D-01	-4.525D-03	-3.650D-02
220	8.000D-01	2.750D+00	5.882D-01	-9.175D-03	-3.665D-02
221	8.000D-01	2.667D+00	7.620D-01	-1.463D-02	-3.637D-02
222	8.000D-01	2.417D+00	1.155D+00	-2.889D-02	-4.017D-02

223	8.000D-01	2.167D+00	1.354D+00	-3.926D-02	-4.470D-02
224	8.000D-01	1.917D+00	1.397D+00	-4.341D-02	-5.305D-02
225	8.000D-01	1.667D+00	1.321D+00	-4.488D-02	-6.115D-02
226	8.000D-01	1.500D+00	1.186D+00	-4.420D-02	-6.555D-02
227	8.000D-01	1.333D+00	9.467D-01	-4.028D-02	-6.966D-02
228	8.000D-01	1.250D+00	7.873D-01	-3.658D-02	-7.041D-02
229	8.000D-01	1.167D+00	6.091D-01	-3.009D-02	-7.145D-02
230	8.000D-01	1.083D+00	4.322D-01	-1.975D-02	-7.205D-02
231	8.000D-01	1.000D+00	2.793D-01	-7.153D-03	-7.277D-02
232	8.000D-01	8.333D-01	7.642D-02	1.693D-02	-7.314D-02
233	8.000D-01	6.667D-01	-2.101D-02	2.864D-02	-7.322D-02
234	8.000D-01	5.000D-01	-6.189D-02	2.638D-02	-7.235D-02
235	8.000D-01	3.333D-01	-6.534D-02	1.619D-02	-7.157D-02
236	8.000D-01	1.667D-01	-4.319D-02	5.210D-03	-7.173D-02
237	8.000D-01	-7.078D-16	0.0	0.0	-7.193D-02
301	2.000D+00	3.000D+00	0.0	0.0	-3.255D-02
302	2.000D+00	2.917D+00	1.634D-01	-1.473D-03	-3.232D-02
303	2.000D+00	2.833D+00	3.328D-01	-5.475D-03	-3.208D-02
304	2.000D+00	2.750D+00	5.028D-01	-1.160D-02	-3.207D-02
305	2.000D+00	2.667D+00	6.681D-01	-1.919D-02	-3.176D-02
306	2.000D+00	2.417D+00	1.075D+00	-3.998D-02	-3.402D-02
307	2.000D+00	2.167D+00	1.309D+00	-5.810D-02	-3.691D-02
308	2.000D+00	1.917D+00	1.377D+00	-6.538D-02	-4.294D-02
309	2.000D+00	1.667D+00	1.320D+00	-7.007D-02	-4.890D-02
310	2.000D+00	1.500D+00	1.205D+00	-6.712D-02	-5.258D-02
311	2.000D+00	1.333D+00	1.001D+00	-6.275D-02	-5.599D-02
312	2.000D+00	1.250D+00	8.700D-01	-5.703D-02	-5.703D-02
313	2.000D+00	1.167D+00	7.256D-01	-5.005D-02	-5.811D-02
314	2.000D+00	1.083D+00	5.775D-01	-4.148D-02	-5.871D-02
315	2.000D+00	1.000D+00	4.366D-01	-3.216D-02	-5.936D-02
316	2.000D+00	8.333D-01	1.991D-01	-1.376D-02	-5.962D-02
317	2.000D+00	6.667D-01	3.007D-02	-2.807D-04	-5.975D-02
318	2.000D+00	5.000D-01	-7.327D-02	5.907D-03	-5.927D-02
319	2.000D+00	3.333D-01	-1.129D-01	5.862D-03	-5.882D-02
320	2.000D+00	1.667D-01	-8.810D-02	2.440D-03	-5.878D-02
321	2.000D+00	-7.702D-16	0.0	0.0	-5.879D-02
385	4.000D+00	3.000D+00	0.0	0.0	-1.228D-03
386	4.000D+00	2.917D+00	1.001D-01	-1.155D-03	-1.023D-03
387	4.000D+00	2.833D+00	2.152D-01	-4.448D-03	-8.123D-04
388	4.000D+00	2.750D+00	3.426D-01	-9.648D-03	-6.568D-04

389	4.000D+00	2.667D+00	4.786D-01	-1.633D-02	-3.873D-04
390	4.000D+00	2.417D+00	8.787D-01	-4.257D-02	-5.618D-04
391	4.000D+00	2.167D+00	1.173D+00	-6.664D-02	-9.236D-04
392	4.000D+00	1.917D+00	1.307D+00	-8.420D-02	-2.629D-03
393	4.000D+00	1.667D+00	1.306D+00	-9.129D-02	-4.389D-03
394	4.000D+00	1.500D+00	1.236D+00	-9.213D-02	-5.634D-03
395	4.000D+00	1.333D+00	1.096D+00	-8.866D-02	-6.815D-03
396	4.000D+00	1.250D+00	1.003D+00	-8.436D-02	-7.267D-03
397	4.000D+00	1.167D+00	8.952D-01	-7.925D-02	-7.709D-03
398	4.000D+00	1.083D+00	7.765D-01	-7.230D-02	-7.992D-03
399	4.000D+00	1.000D+00	6.532D-01	-6.471D-02	-8.303D-03
400	4.000D+00	8.333D-01	4.066D-01	-4.699D-02	-8.395D-03
401	4.000D+00	6.667D-01	1.886D-01	-3.045D-02	-8.400D-03
402	4.000D+00	5.000D-01	1.940D-02	-1.626D-02	-8.039D-03
403	4.000D+00	3.333D-01	-8.121D-02	-6.436D-03	-7.653D-03
404	4.000D+00	1.667D-01	-9.300D-02	-1.402D-03	-7.404D-03
405	4.000D+00	-8.327D-16	0.0	0.0	-7.189D-03
469	6.000D+00	3.000D+00	0.0	0.0	3.686D-02
470	6.000D+00	2.917D+00	6.084D-02	-5.394D-04	3.697D-02
471	6.000D+00	2.833D+00	1.367D-01	-2.184D-03	3.706D-02
472	6.000D+00	2.750D+00	2.265D-01	-4.791D-03	3.720D-02
473	6.000D+00	2.667D+00	3.288D-01	-8.474D-03	3.727D-02
474	6.000D+00	2.417D+00	6.753D-01	-2.767D-02	3.834D-02
475	6.000D+00	2.167D+00	9.897D-01	-4.906D-02	3.960D-02
476	6.000D+00	1.917D+00	1.192D+00	-7.018D-02	4.253D-02
477	6.000D+00	1.667D+00	1.261D+00	-7.980D-02	4.562D-02
478	6.000D+00	1.500D+00	1.234D+00	-8.502D-02	4.809D-02
479	6.000D+00	1.333D+00	1.149D+00	-8.350D-02	5.036D-02
480	6.000D+00	1.250D+00	1.086D+00	-8.229D-02	5.140D-02
481	6.000D+00	1.167D+00	1.009D+00	-7.952D-02	5.238D-02
482	6.000D+00	1.083D+00	9.189D-01	-7.574D-02	5.317D-02
483	6.000D+00	1.000D+00	8.198D-01	-7.060D-02	5.401D-02
484	6.000D+00	8.333D-01	6.011D-01	-5.847D-02	5.502D-02
485	6.000D+00	6.667D-01	3.819D-01	-4.359D-02	5.593D-02
486	6.000D+00	5.000D-01	1.877D-01	-2.850D-02	5.636D-02
487	6.000D+00	3.333D-01	4.542D-02	-1.481D-02	5.677D-02
488	6.000D+00	1.667D-01	-2.228D-02	-4.321D-03	5.707D-02
489	6.000D+00	-8.431D-16	0.0	0.0	5.741D-02
553	8.000D+00	3.000D+00	0.0	0.0	6.818D-02
554	8.000D+00	2.917D+00	4.798D-02	-7.124D-05	6.820D-02

555	8.000D+00	2.833D+00	1.073D-01	-3.808D-04	6.821D-02
556	8.000D+00	2.750D+00	1.775D-01	-9.697D-04	6.828D-02
557	8.000D+00	2.667D+00	2.579D-01	-2.072D-03	6.822D-02
558	8.000D+00	2.417D+00	5.450D-01	-9.999D-03	6.920D-02
559	8.000D+00	2.167D+00	8.403D-01	-2.205D-02	7.031D-02
560	8.000D+00	1.917D+00	1.076D+00	-3.586D-02	7.420D-02
561	8.000D+00	1.667D+00	1.196D+00	-4.549D-02	7.840D-02
562	8.000D+00	1.500D+00	1.205D+00	-5.058D-02	8.213D-02
563	8.000D+00	1.333D+00	1.159D+00	-5.163D-02	8.565D-02
564	8.000D+00	1.250D+00	1.115D+00	-5.210D-02	8.730D-02
565	8.000D+00	1.167D+00	1.059D+00	-5.120D-02	8.890D-02
566	8.000D+00	1.083D+00	9.909D-01	-5.003D-02	9.025D-02
567	8.000D+00	1.000D+00	9.120D-01	-4.762D-02	9.168D-02
568	8.000D+00	8.333D-01	7.290D-01	-4.192D-02	9.341D-02
569	8.000D+00	6.667D-01	5.323D-01	-3.295D-02	9.500D-02
570	8.000D+00	5.000D-01	3.439D-01	-2.307D-02	9.555D-02
571	8.000D+00	3.333D-01	1 867D-01	-1.252D-02	9.605D-02
572	8.000D+00	1.667D-01	7.213D-02	-3.763D-03	9.629D-02
573	8.000D+00	-8.223D-16	0.0	0.0	9.658D-02
637	1.000D+01	3.000D+00	0.0	0.0	8.933D-02
638	1.000D+01	2.917D+00	5.099D-02	1.678D-04	8.931D-02
639	1.000D+01	2.833D+00	1.092D-01	5.564D-04	8.928D-02
640	1.000D+01	2.750D+00	1.743D-01	1.026D-03	8.930D-02
641	1.000D+01	2.667D+00	2.462D-01	1.403D-03	8.923D-02
642	1.000D+01	2.417D+00	4.979D-01	9.248D-04	8.975D-02
643	1.000D+01	2.167D+00	7.679D-01	-2.718D-03	9.029D-02
644	1.000D+01	1.917D+00	1.002D+00	-8.238D-03	9.267D-02
645	1.000D+01	1.667D+00	1.141D+00	-1.475D-02	9.524D-02
646	1.000D+01	1.500D+00	1.168D+00	-1.787D-02	9.769D-02
647	1.000D+01	1.333D+00	1.143D+00	-2.033D-02	1.000D-01
648	1.000D+01	1.250D+00	1.110D+00	-2.112D-02	1.011D-01
649	1.000D+01	1.167D+00	1.066D+00	-2.153D-02	1.022D-01
650	1.000D+01	1.083D+00	1.010D+00	-2.167D-02	1.031D-01
651	1.000D+01	1.000D+00	9.437D-01	-2.138D-02	1.041D-01
652	1.000D+01	8.333D-01	7.866D-01	-1.964D-02	1.054D-01
653	1.000D+01	6.667D-01	6.122D-01	-1.623D-02	1.065D-01
654	1.000D+01	5.000D-01	4.377D-01	-1.147D-02	1.069D-01
655	1.000D+01	3.333D-01	2.774D-01	-6.173D-03	1.073D-01
656	1.000D+01	1.667D-01	1.332D-01	-1.801D-03	1.074D-01
657	1.000D+01	-6.869D-16	0.0	0.0	1.076D-01

A.3 Results of the Analysis at Re = 191 (Run 302)

NODE NUMBER	NODAL COORDINATES X/L	Y/L	VELOCITY COMPONENTS U/U0	V/V0	AVERAGE PRESSURES (P-P0)/(RHO0*U0**2)
1	-1.333D+00	3.000D+00	0.0	0.0	-1.356D-01
2	-1.333D+00	2.917D+00	1.640D-01	0.0	-1.352D-01
3	-1.333D+00	2.833D+00	4.350D-01	0.0	-1.318D-01
4	-1.333D+00	2.750D+00	6.460D-01	0.0	-1.277D-01
5	-1.333D+00	2.667D+00	8.400D-01	0.0	-1.244D-01
6	-1.333D+00	2.417D+00	1.218D+00	0.0	-1.213D-01
7	-1.333D+00	2.167D+00	1.380D+00	0.0	-1.206D-01
8	-1.333D+00	1.917D+00	1.426D+00	0.0	-1.210D-01
9	-1.333D+00	1.667D+00	1.365D+00	0.0	-1.198D-01
10	-1.333D+00	1.500D+00	1.265D+00	0.0	-1.166D-01
11	-1.333D+00	1.333D+00	1.030D+00	0.0	-1.141D-01
12	-1.333D+00	1.250D+00	8.300D-01	0.0	-1.130D-01
13	-1.333D+00	1.167D+00	6.050D-01	0.0	-1.117D-01
14	-1.333D+00	1.083D+00	3.400D-01	0.0	-1.106D-01
15	-1.333D+00	1.000D+00	0.0	0.0	-1.105D-01
91	0.0	3.000D+00	0.0	0.0	-1.241D-01
92	-3.238D-17	2.917D+00	2.189D-01	-1.673D-04	-1.242D-01
93	-2.776D-17	2.833D+00	4.292D-01	-4.527D-04	-1.242D-01
94	-6.014D-17	2.750D+00	6.283D-01	-1.352D-03	-1.245D-01
95	9.252D-18	2.667D+00	8.098D-01	-3.533D-03	-1.245D-01
96	-9.252D-18	2.417D+00	1.201D+00	-8.590D-03	-1.280D-01
97	-3.701D-17	2.167D+00	1.380D+00	-1.307D-02	-1.322D-01
98	-6.939D-17	1.917D+00	1.430D+00	-1.173D-02	-1.391D-01
99	-3.701D-17	1.667D+00	1.378D+00	-1.483D-02	-1.460D-01
100	-2.776D-17	1.500D+00	1.266D+00	-1.025D-02	-1.517D-01
101	1.850D-17	1.333D+00	1.026D+00	-1.626D-02	-1.577D-01
102	1.388D-17	1.250D+00	8.419D-01	-1.085D-02	-1.603D-01
103	-3.701D-17	1.167D+00	6.166D-01	-1.531D-02	-1.637D-01
104	2.313D-17	1.083D+00	3.440D-01	-7.254D-03	-1.668D-01
105	3.701D-17	1.000D+00	0.0	0.0	-1.683D-01
217	8.000D-01	3.000D+00	0.0	0.0	-1.283D-01
218	8.000D-01	2.917D+00	2.098D-01	-7.642D-04	-1.282D-01
219	8.000D-01	2.833D+00	4.136D-01	-2.818D-03	-1.282D-01
220	8.000D-01	2.750D+00	6.064D-01	-5.692D-03	-1.284D-01
221	8.000D-01	2.667D+00	7.843D-01	-9.159D-03	-1.282D-01
222	8.000D-01	2.417D+00	1.180D+00	-1.842D-02	-1.313D-01

223	8.000D-01	2.167D+00	1.373D+00	-2.440D-02	-1.349D-01
224	8.000D-01	1.917D+00	1.427D+00	-2.723D-02	-1.412D-01
225	8.000D-01	1.667D+00	1.376D+00	-2.771D-02	-1.472D-01
226	8.000D-01	1.500D+00	1.265D+00	-2.844D-02	-1.506D-01
227	8.000D-01	1.333D+00	1.029D+00	-2.625D-02	-1.539D-01
228	8.000D-01	1.250D+00	8.539D-01	-2.451D-02	-1.544D-01
229	8.000D-01	1.167D+00	6.471D-01	-2.029D-02	-1.552D-01
230	8.000D-01	1.083D+00	4.368D-01	-1.202D-02	-1.556D-01
231	8.000D-01	1.000D+00	2.602D-01	-9.568D-04	-1.561D-01
232	8.000D-01	8.333D-01	5.095D-02	1.978D-02	-1.564D-01
233	8.000D-01	6.667D-01	-2.921D-02	2.806D-02	-1.564D-01
234	8.000D-01	5.000D-01	-5.794D-02	2.372D-02	-1.558D-01
235	8.000D-01	3.333D-01	-5.483D-02	1.378D-02	-1.553D-01
236	8.000D-01	1.667D-01	-3.362D-02	4.241D-03	-1.554D-01
237	8.000D-01	-7.078D-16	0.0	0.0	-1.556D-01
301	2.000D+00	3.000D+00	0.0	0.0	-1.267D-01
302	2.000D+00	2.917D+00	1.804D-01	-1.184D-03	-1.266D-01
303	2.000D+00	2.833D+00	3.649D-01	-4.380D-03	-1.265D-01
304	2.000D+00	2.750D+00	5.469D-01	-9.089D-03	-1.265D-01
305	2.000D+00	2.667D+00	7.198D-01	-1.470D-02	-1.263D-01
306	2.000D+00	2.417D+00	1.128D+00	-2.923D-02	-1.287D-01
307	2.000D+00	2.167D+00	1.348D+00	-4.055D-02	-1.314D-01
308	2.000D+00	1.917D+00	1.415D+00	-4.494D-02	-1.367D-01
309	2.000D+00	1.667D+00	1.375D+00	-4.749D-02	-1.420D-01
310	2.000D+00	1.500D+00	1.273D+00	-4.617D-02	-1.452D-01
311	2.000D+00	1.333D+00	1.061D+00	-4.271D-02	-1.482D-01
312	2.000D+00	1.250D+00	9.112D-01	-3.879D-02	-1.490D-01
313	2.000D+00	1.167D+00	7.401D-01	-3.285D-02	-1.499D-01
314	2.000D+00	1.083D+00	5.637D-01	-2.552D-02	-1.503D-01
315	2.000D+00	1.000D+00	4.012D-01	-1.700D-02	-1.508D-01
316	2.000D+00	8.333D-01	1.511D-01	-1.288D-03	-1.509D-01
317	2.000D+00	6.667D-01	-3.637D-03	8.788D-03	-1.510D-01
318	2.000D+00	5.000D-01	-8.625D-02	1.110D-02	-1.507D-01
319	2.000D+00	3.333D-01	-1.086D-01	7.984D-03	-1.504D-01
320	2.000D+00	1.667D-01	-7.744D-02	2.841D-03	-1.504D-01
321	2.000D+00	-7.702D-16	0.0	0.0	-1.505D-01
385	4.000D+00	3.000D+00	0.0	0.0	-1.046D-01
386	4.000D+00	2.917D+00	1.198D-01	-1.286D-03	-1.044D-01
387	4.000D+00	2.833D+00	2.569D-01	-4.875D-03	-1.043D-01
388	4.000D+00	2.750D+00	4.062D-01	-1.057D-02	-1.042D-01

389	4.000D+00	2.667D+00	5.611D-01	-1.771D-02	-1.040D-01
390	4.000D+00	2.417D+00	9.852D-01	-4.012D-02	-1.054D-01
391	4.000D+00	2.167D+00	1.263D+00	-5.959D-02	-1.073D-01
392	4.000D+00	1.917D+00	1.374D+00	-6.982D-02	-1.117D-01
393	4.000D+00	1.667D+00	1.367D+00	-7.547D-02	-1.160D-01
394	4.000D+00	1.500D+00	1.298D+00	-7.400D-02	-1.189D-01
395	4.000D+00	1.333D+00	1.143D+00	-7.102D-02	-1.217D-01
396	4.000D+00	1.250D+00	1.032D+00	-6.604D-02	-1.227D-01
397	4.000D+00	1.167D+00	9.014D-01	-6.027D-02	-1.236D-01
398	4.000D+00	1.083D+00	7.563D-01	-5.280D-02	-1.242D-01
399	4.000D+00	1.000D+00	6.083D-01	-4.463D-02	-1.248D-01
400	4.000D+00	8.333D-01	3.303D-01	-2.692D-02	-1.251D-01
401	4.000D+00	6.667D-01	1.067D-01	-1.217D-02	-1.253D-01
402	4.000D+00	5.000D-01	-5.068D-02	-2.523D-03	-1.250D-01
403	4.000D+00	3.333D-01	-1.298D-01	1.460D-03	-1.247D-01
404	4.000D+00	1.667D-01	-1.154D-01	1.136D-03	-1.246D-01
405	4.000D+00	-8.327D-16	0.0	0.0	-1.246D-01
469	6.000D+00	3.000D+00	0.0	0.0	-7.127D-02
470	6.000D+00	2.917D+00	6.612D-02	-9.434D-04	-7.115D-02
471	6.000D+00	2.833D+00	1.535D-01	-3.721D-03	-7.104D-02
472	6.000D+00	2.750D+00	2.599D-01	-8.164D-03	-7.094D-02
473	6.000D+00	2.667D+00	3.825D-01	-1.412D-02	-7.077D-02
474	6.000D+00	2.417D+00	7.854D-01	-3.929D-02	-7.085D-02
475	6.000D+00	2.167D+00	1.115D+00	-6.323D-02	-7.106D-02
476	6.000D+00	1.917D+00	1.292D+00	-8.225D-02	-7.220D-02
477	6.000D+00	1.667D+00	1.340D+00	-9.010D-02	-7.339D-02
478	6.000D+00	1.500D+00	1.309D+00	-9.271D-02	-7.427D-02
479	6.000D+00	1.333D+00	1.212D+00	-9.100D-02	-7.512D-02
480	6.000D+00	1.250D+00	1.139D+00	-8.768D-02	-7.548D-02
481	6.000D+00	1.167D+00	1.045D+00	-8.407D-02	-7.584D-02
482	6.000D+00	1.083D+00	9.338D-01	-7.781D-02	-7.610D-02
483	6.000D+00	1.000D+00	8.113D-01	-7.107D-02	-7.636D-02
484	6.000D+00	8.333D-01	5.441D-01	-5.335D-02	-7.647D-02
485	6.000D+00	6.667D-01	2.898D-01	-3.620D-02	-7.651D-02
486	6.000D+00	5.000D-01	7.570D-02	-1.992D-02	-7.624D-02
487	6.000D+00	3.333D-01	-6.740D-02	-8.115D-03	-7.592D-02
488	6.000D+00	1.667D-01	-1.035D-01	-1.830D-03	-7.570D-02
489	6.000D+00	-8.431D-16	0.0	0.0	-7.551D-02
553	8.000D+00	3.000D+00	0.0	0.0	-3.921D-02
554	8.000D+00	2.917D+00	3.406D-02	-4.442D-04	-3.915D-02

555	8.000D+00	2.833D+00	8.732D-02	-1.808D-03	-3.910D-02
556	8.000D+00	2.750D+00	1.592D-01	-3.943D-03	-3.902D-02
557	8.000D+00	2.667D+00	2.486D-01	-7.038D-03	-3.902D-02
558	8.000D+00	2.417D+00	5.895D-01	-2.492D-02	-3.819D-02
559	8.000D+00	2.167D+00	9.297D-01	-4.552D-02	-3.720D-02
560	8.000D+00	1.917D+00	1.172D+00	-6.701D-02	-3.430D-02
561	8.000D+00	1.667D+00	1.285D+00	-7.657D-02	-3.118D-02
562	8.000D+00	1.500D+00	1.291D+00	-8.300D-02	-2.843D-02
563	8.000D+00	1.333D+00	1.242D+00	-8.219D-02	-2.586D-02
564	8.000D+00	1.250D+00	1.197D+00	-8.211D-02	-2.460D-02
565	8.000D+00	1.167D+00	1.134D+00	-8.005D-02	-2.341D-02
566	8.000D+00	1.083D+00	1.056D+00	-7.723D-02	-2.239D-02
567	8.000D+00	1.000D+00	9.634D-01	-7.256D-02	-2.131D-02
568	8.000D+00	8.333D-01	7.386D-01	-6.170D-02	-2.000D-02
569	8.000D+00	6.667D-01	4.944D-01	-4.643D-02	-1.880D-02
570	8.000D+00	5.000D-01	2.601D-01	-3.096D-02	-1.834D-02
571	8.000D+00	3.333D-01	7.544D-02	-1.654D-02	-1.789D-02
572	8.000D+00	1.667D-01	-2.166D-02	-4.935D-03	-1.767D-02
573	8.000D+00	-8.223D-16	0.0	0.0	-1.741D-02
637	1.000D+01	3.000D+00	0.0	0.0	-1.274D-02
638	1.000D+01	2.917D+00	2.425D-02	-4.917D-05	-1.273D-02
639	1.000D+01	2.833D+00	6.387D-02	-2.691D-04	-1.273D-02
640	1.000D+01	2.750D+00	1.185D-01	-6.914D-04	-1.269D-02
641	1.000D+01	2.667D+00	1.877D-01	-1.564D-03	-1.277D-02
642	1.000D+01	2.417D+00	4.668D-01	-8.740D-03	-1.202D-02
643	1.000D+01	2.167D+00	7.831D-01	-2.015D-02	-1.120D-02
644	1.000D+01	1.917D+00	1.058D+00	-3.347D-02	-7.455D-03
645	1.000D+01	1.667D+00	1.218D+00	-4.256D-02	-3.326D-03
646	1.000D+01	1.500D+00	1.255D+00	-4.761D-02	6.966D-04
647	1.000D+01	1.333D+00	1.240D+00	-4.872D-02	4.504D-03
648	1.000D+01	1.250D+00	1.211D+00	-4.968D-02	6.410D-03
649	1.000D+01	1.167D+00	1.169D+00	-4.894D-02	8.269D-03
650	1.000D+01	1.083D+00	1.112D+00	-4.842D-02	9.902D-03
651	1.000D+01	1.000D+00	1.041D+00	-4.627D-02	1.164D-02
652	1.000D+01	8.333D-01	8.580D-01	-4.179D-02	1.386D-02
653	1.000D+01	6.667D-01	6.429D-01	-3.331D-02	1.591D-02
654	1.000D+01	5.000D-01	4.192D-01	-2.416D-02	1.660D-02
655	1.000D+01	3.333D-01	2.245D-01	-1.344D-02	1.723D-02
656	1.000D+01	1.667D-01	8.329D-02	-4.156D-03	1.739D-02
657	1.000D+01	-6.869D-16	0.0	0.0	1.761D-02

A.4 Results of the Analysis at Re = 229 (Run 303)

NODE NUMBER	NODAL COORDINATES X/L	Y/L	VELOCITY COMPONENTS U/U0	V/V0	AVERAGE PRESSURES (P-P0)/(RHO0*U0**2)
1	-1.333D+00	3.000D+00	0.0	0.0	-1.115D-01
2	-1.333D+00	2.917D+00	2.200D-01	0.0	-1.114D-01
3	-1.333D+00	2.833D+00	4.600D-01	0.0	-1.104D-01
4	-1.333D+00	2.750D+00	6.620D-01	0.0	-1.093D-01
5	-1.333D+00	2.667D+00	8.500D-01	0.0	-1.080D-01
6	-1.333D+00	2.417D+00	1.174D+00	0.0	-1.093D-01
7	-1.333D+00	2.167D+00	1.282D+00	0.0	-1.122D-01
8	-1.333D+00	1.917D+00	1.313D+00	0.0	-1.138D-01
9	-1.333D+00	1.667D+00	1.310D+00	0.0	-1.132D-01
10	-1.333D+00	1.500D+00	1.250D+00	0.0	-1.099D-01
11	-1.333D+00	1.333D+00	1.080D+00	0.0	-1.076D-01
12	-1.333D+00	1.250D+00	8.700D-01	0.0	-1.069D-01
13	-1.333D+00	1.167D+00	6.450D-01	0.0	-1.065D-01
14	-1.333D+00	1.083D+00	3.500D-01	0.0	-1.061D-01
15	-1.333D+00	1.000D+00	0.0	0.0	-1.061D-01
91	0.0	3.000D+00	0.0	0.0	-1.193D-01
92	-3.238D-17	2.917D+00	2.311D-01	-5.134D-04	-1.193D-01
93	-2.776D-17	2.833D+00	4.481D-01	-1.710D-03	-1.193D-01
94	-6.014D-17	2.750D+00	6.467D-01	-3.300D-03	-1.195D-01
95	9.252D-18	2.667D+00	8.208D-01	-5.829D-03	-1.196D-01
96	-9.252D-18	2.417D+00	1.162D+00	-1.134D-02	-1.224D-01
97	-3.701D-17	2.167D+00	1.288D+00	-1.422D-02	-1.256D-01
98	-6.939D-17	1.917D+00	1.323D+00	-1.169D-02	-1.312D-01
99	-3.701D-17	1.667D+00	1.319D+00	-1.421D-02	-1.368D-01
100	-2.776D-17	1.500D+00	1.257D+00	-9.131D-03	-1.421D-01
101	1.850D-17	1.333D+00	1.058D+00	-1.592D-02	-1.477D-01
102	1.388D-17	1.250D+00	8.805D-01	-1.037D-02	-1.502D-01
103	-3.701D-17	1.167D+00	6.504D-01	-1.511D-02	-1.535D-01
104	2.313D-17	1.083D+00	3.643D-01	-6.266D-03	-1.564D-01
105	3.701D-17	1.000D+00	0.0	0.0	-1.577D-01
217	8.000D-01	3.000D+00	0.0	0.0	-1.238D-01
218	8.000D-01	2.917D+00	2.173D-01	-9.456D-04	-1.238D-01
219	8.000D-01	2.833D+00	4.263D-01	-3.416D-03	-1.237D-01
220	8.000D-01	2.750D+00	6.199D-01	-6.696D-03	-1.239D-01
221	8.000D-01	2.667D+00	7.926D-01	-1.044D-02	-1.238D-01
222	8.000D-01	2.417D+00	1.144D+00	-1.935D-02	-1.264D-01

223	8.000D-01	2.167D+00	1.286D+00	-2.383D-02	-1.294D-01
224	8.000D-01	1.917D+00	1.324D+00	-2.547D-02	-1.344D-01
225	8.000D-01	1.667D+00	1.317D+00	-2.538D-02	-1.393D-01
226	8.000D-01	1.500D+00	1.254D+00	-2.710D-02	-1.425D-01
227	8.000D-01	1.333D+00	1.057D+00	-2.529D-02	-1.456D-01
228	8.000D-01	1.250D+00	8.901D-01	-2.425D-02	-1.462D-01
229	8.000D-01	1.167D+00	6.783D-01	-2.053D-02	-1.470D-01
230	8.000D-01	1.083D+00	4.528D-01	-1.270D-02	-1.474D-01
231	8.000D-01	1.000D+00	2.615D-01	-1.571D-03	-1.479D-01
232	8.000D-01	8.333D-01	4.430D-02	1.926D-02	-1.481D-01
233	8.000D-01	6.667D-01	-3.015D-02	2.710D-02	-1.481D-01
234	8.000D-01	5.000D-01	-5.555D-02	2.245D-02	-1.476D-01
235	8.000D-01	3.333D-01	-5.066D-02	1.281D-02	-1.472D-01
236	8.000D-01	1.667D-01	-3.015D-02	3.887D-03	-1.473D-01
237	8.000D-01	-7.078D-16	0.0	0.0	-1.474D-01
301	2.000D+00	3.000D+00	0.0	0.0	-1.227D-01
302	2.000D+00	2.917D+00	1.850D-01	-1.242D-03	-1.226D-01
303	2.000D+00	2.833D+00	3.735D-01	-4.597D-03	-1.225D-01
304	2.000D+00	2.750D+00	5.568D-01	-9.527D-03	-1.225D-01
305	2.000D+00	2.667D+00	7.269D-01	-1.522D-02	-1.224D-01
306	2.000D+00	2.417D+00	1.099D+00	-2.897D-02	-1.245D-01
307	2.000D+00	2.167D+00	1.270D+00	-3.825D-02	-1.270D-01
308	2.000D+00	1.917D+00	1.317D+00	-4.115D-02	-1.315D-01
309	2.000D+00	1.667D+00	1.311D+00	-4.355D-02	-1.359D-01
310	2.000D+00	1.500D+00	1.255D+00	-4.355D-02	-1.389D-01
311	2.000D+00	1.333D+00	1.081D+00	-4.117D-02	-1.417D-01
312	2.000D+00	1.250D+00	9.390D-01	-3.805D-02	-1.426D-01
313	2.000D+00	1.167D+00	7.661D-01	-3.242D-02	-1.434D-01
314	2.000D+00	1.083D+00	5.801D-01	-2.529D-02	-1.439D-01
315	2.000D+00	1.000D+00	4.068D-01	-1.649D-02	-1.443D-01
316	2.000D+00	8.333D-01	1.458D-01	-2.567D-04	-1.445D-01
317	2.000D+00	6.667D-01	-7.677D-03	9.993D-03	-1.446D-01
318	2.000D+00	5.000D-01	-8.589D-02	1.193D-02	-1.443D-01
319	2.000D+00	3.333D-01	-1.045D-01	8.355D-03	-1.440D-01
320	2.000D+00	1.667D-01	-7.290D-02	2.919D-03	-1.440D-01
321	2.000D+00	-7.702D-16	0.0	0.0	-1.441D-01
385	4.000D+00	3.000D+00	0.0	0.0	-1.026D-01
386	4.000D+00	2.917D+00	1.208D-01	-1.348D-03	-1.025D-01
387	4.000D+00	2.833D+00	2.603D-01	-5.127D-03	-1.023D-01
388	4.000D+00	2.750D+00	4.116D-01	-1.119D-02	-1.023D-01

389	4.000D+00	2.667D+00	5.667D-01	-1.881D-02	-1.021D-01
390	4.000D+00	2.417D+00	9.690D-01	-4.054D-02	-1.038D-01
391	4.000D+00	2.167D+00	1.206D+00	-5.831D-02	-1.060D-01
392	4.000D+00	1.917D+00	1.285D+00	-6.577D-02	-1.103D-01
393	4.000D+00	1.667D+00	1.293D+00	-7.162D-02	-1.147D-01
394	4.000D+00	1.500D+00	1.262D+00	-7.101D-02	-1.178D-01
395	4.000D+00	1.333D+00	1.144D+00	-7.007D-02	-1.208D-01
396	4.000D+00	1.250D+00	1.046D+00	-6.565D-02	-1.219D-01
397	4.000D+00	1.167D+00	9.216D-01	-6.038D-02	-1.231D-01
398	4.000D+00	1.083D+00	7.758D-01	-5.297D-02	-1.237D-01
399	4.000D+00	1.000D+00	6.233D-01	-4.450D-02	-1.245D-01
400	4.000D+00	8.333D-01	3.331D-01	-2.568D-02	-1.248D-01
401	4.000D+00	6.667D-01	1.033D-01	-9.965D-03	-1.251D-01
402	4.000D+00	5.000D-01	-5.607D-02	-2.200D-04	-1.248D-01
403	4.000D+00	3.333D-01	-1.348D-01	3.003D-03	-1.245D-01
404	4.000D+00	1.667D-01	-1.177D-01	1.757D-03	-1.245D-01
405	4.000D+00	-8.327D-16	0.0	0.0	-1.244D-01
469	6.000D+00	3.000D+00	0.0	0.0	-7.217D-02
470	6.000D+00	2.917D+00	6.249D-02	-1.032D-03	-7.206D-02
471	6.000D+00	2.833D+00	1.479D-01	-4.093D-03	-7.195D-02
472	6.000D+00	2.750D+00	2.537D-01	-9.050D-03	-7.187D-02
473	6.000D+00	2.667D+00	3.762D-01	-1.571D-02	-7.170D-02
474	6.000D+00	2.417D+00	7.721D-01	-4.252D-02	-7.208D-02
475	6.000D+00	2.167D+00	1.078D+00	-6.618D-02	-7.269D-02
476	6.000D+00	1.917D+00	1.217D+00	-8.328D-02	-7.461D-02
477	6.000D+00	1.667D+00	1.259D+00	-9.033D-02	-7.655D-02
478	6.000D+00	1.500D+00	1.253D+00	-9.356D-02	-7.802D-02
479	6.000D+00	1.333D+00	1.190D+00	-9.407D-02	-7.945D-02
480	6.000D+00	1.250D+00	1.134D+00	-9.132D-02	-8.012D-02
481	6.000D+00	1.167D+00	1.056D+00	-8.888D-02	-8.079D-02
482	6.000D+00	1.083D+00	9.541D-01	-8.266D-02	-8.130D-02
483	6.000D+00	1.000D+00	8.371D-01	-7.624D-02	-8.184D-02
484	6.000D+00	8.333D-01	5.656D-01	-5.669D-02	-8.221D-02
485	6.000D+00	6.667D-01	3.012D-01	-3.820D-02	-8.247D-02
486	6.000D+00	5.000D-01	7.534D-02	-1.976D-02	-8.222D-02
487	6.000D+00	3.333D-01	-7.934D-02	-6.983D-03	-8.189D-02
488	6.000D+00	1.667D-01	-1.186D-01	-1.255D-03	-8.165D-02
489	6.000D+00	-8.431D-16	0.0	0.0	-8.148D-02
553	8.000D+00	3.000D+00	0.0	0.0	-4.350D-02
554	8.000D+00	2.917D+00	2.640D-02	-5.166D-04	-4.345D-02

555	8.000D+00	2.833D+00	7.319D-02	-2.083D-03	-4.340D-02
556	8.000D+00	2.750D+00	1.399D-01	-4.461D-03	-4.333D-02
557	8.000D+00	2.667D+00	2.259D-01	-7.843D-03	-4.333D-02
558	8.000D+00	2.417D+00	5.627D-01	-2.806D-02	-4.255D-02
559	8.000D+00	2.167D+00	8.939D-01	-4.972D-02	-4.162D-02
560	8.000D+00	1.917D+00	1.109D+00	-7.208D-02	-3.897D-02
561	8.000D+00	1.667D+00	1.206D+00	-8.000D-02	-3.615D-02
562	8.000D+00	1.500D+00	1.221D+00	-8.730D-02	-3.361D-02
563	8.000D+00	1.333D+00	1.197D+00	-8.706D-02	-3.122D-02
564	8.000D+00	1.250D+00	1.170D+00	-8.807D-02	-2.996D-02
565	8.000D+00	1.167D+00	1.125D+00	-8.675D-02	-2.878D-02
566	8.000D+00	1.083D+00	1.064D+00	-8.489D-02	-2.771D-02
567	8.000D+00	1.000D+00	9.865D-01	-8.051D-02	-2.657D-02
568	8.000D+00	8.333D-01	7.766D-01	-7.024D-02	-2.509D-02
569	8.000D+00	6.667D-01	5.317D-01	-5.324D-02	-2.375D-02
570	8.000D+00	5.000D-01	2.836D-01	-3.579D-02	-2.319D-02
571	8.000D+00	3.333D-01	7.898D-02	-1.943D-02	-2.266D-02
572	8.000D+00	1.667D-01	-3.243D-02	-5.874D-03	-2.242D-02
573	8.000D+00	-8.223D-16	0.0	0.0	-2.215D-02
637	1.000D+01	3.000D+00	0.0	0.0	-1.990D-02
638	1.000D+01	2.917D+00	1.484D-02	-7.971D-05	-1.989D-02
639	1.000D+01	2.833D+00	4.626D-02	-3.633D-04	-1.988D-02
640	1.000D+01	2.750D+00	9.404D-02	-8.236D-04	-1.985D-02
641	1.000D+01	2.667D+00	1.576D-01	-1.749D-03	-1.994D-02
642	1.000D+01	2.417D+00	4.278D-01	-9.660D-03	-1.919D-02
643	1.000D+01	2.167D+00	7.366D-01	-2.201D-02	-1.836D-02
644	1.000D+01	1.917D+00	9.967D-01	-3.600D-02	-1.448D-02
645	1.000D+01	1.667D+00	1.145D+00	-4.451D-02	-1.019D-02
646	1.000D+01	1.500D+00	1.183D+00	-4.955D-02	-5.998D-03
647	1.000D+01	1.333D+00	1.185D+00	-5.043D-02	-2.018D-03
648	1.000D+01	1.250D+00	1.170D+00	-5.187D-02	7.518D-05
649	1.000D+01	1.167D+00	1.144D+00	-5.124D-02	2.115D-03
650	1.000D+01	1.083D+00	1.105D+00	-5.138D-02	4.008D-03
651	1.000D+01	1.000D+00	1.051D+00	-4.936D-02	6.024D-03
652	1.000D+01	8.333D-01	8.957D-01	-4.594D-02	8.807D-03
653	1.000D+01	6.667D-01	6.928D-01	-3.719D-02	1.143D-02
654	1.000D+01	5.000D-01	4.625D-01	-2.790D-02	1.240D-02
655	1.000D+01	3.333D-01	2.508D-01	-1.575D-02	1.325D-02
656	1.000D+01	1.667D-01	9.345D-02	-5.007D-03	1.343D-02
657	1.000D+01	-6.869D-16	0.0	0.0	1.367D-02

The vita has been removed from the scanned document

A FINITE ELEMENT, NAVIER-STOKES STUDY OF THE CONFINED, LAMINAR FLOW OVER A DOWNSTREAM FACING STEP

by

Philip A. Treventi

(ABSTRACT)

The two-dimensional, confined, laminar flow over a downstream facing step was studied using a finite element, Navier-Stokes equation solver. The weak form of the stationary, incompressible Navier-Stokes equations in primitive variable form was obtained using the conventional Galerkin technique for mixed problems. Biquadratic Lagrange interpolating polynomials were used to construct the basis functions that generated the finite-dimensional subspace containing the approximate solutions to the velocity field, while the pressure field was represented by a discontinuous, piecewise-linear approximation. This particular combination of solution subspaces was previously shown in a mathematically rigorous fashion to yield stable, consistent solutions to the Navier-Stokes equations.

The results of the computations were benchmarked against the experimental data of Denham and Patrick, and also compared to earlier calculations by Ecer and Thomas, both of whom utilized alternative, unconventional formulations. These comparisons indicate that with the proper

choice of basis functions, a conventional Galerkin scheme can yield results that are in as good and in many cases better agreement with the available experimental data than those of unconventional schemes that rely upon an infusion of artificial dissipation to enhance their numerical stability.

The computational algorithm was also used to ascertain the cause of the noticeable lack of development and skewness that characterized the experimental data of Denham and Patrick both at and upstream of the step. The results of this study indicated that as suspected by Denham and Patrick, the skewness as well as the lack of development of the velocity profiles near the step were caused by the geometry of the test apparatus upstream of the step rather than by the presence of the step itself.

The numerical experiments conducted here have been carefully documented so as to facilitate future comparisons intended to assess the relative efficiency of the present method of computation.